2017

# THE ROLE OF GLN146 TO THE STABILITY AND ACTIVITY OF MANGANESE SUPEROXIDE DISMUTASE

Ting Wang
*University of Kentucky*, twa700@yahoo.com
Digital Object Identifier: https://doi.org/10.13023/ETD.2017.049

STUDENT AGREEMENT:

I represent that my thesis or dissertation and abstract are my original work. Proper attribution has been given to all outside sources. I understand that I am solely responsible for obtaining any needed copyright permissions. I have obtained needed written permission statement(s) from the owner(s) of each third-party copyrighted matter to be included in my work, allowing electronic distribution (if such use is not permitted by the fair use doctrine) which will be submitted to UKnowledge as Additional File.

I hereby grant to The University of Kentucky and its agents the irrevocable, non-exclusive, and royalty-free license to archive and make accessible my work in whole or in part in all forms of media, now or hereafter known. I agree that the document mentioned above may be made available immediately for worldwide access unless an embargo applies.

I retain all other ownership rights to the copyright of my work. I also retain the right to use in future works (such as articles or books) all or part of my work. I understand that I am free to register the copyright to my work.

REVIEW, APPROVAL AND ACCEPTANCE

The document mentioned above has been reviewed and accepted by the student's advisor, on behalf of the advisory committee, and by the Director of Graduate Studies (DGS), on behalf of the program; we verify that this is the final, approved version of the student's thesis including all changes required by the advisory committee. The undersigned agree to abide by the statements above.

Ting Wang, Student

Dr. Anne-Frances Miller, Major Professor

Dr. Mark Lovell, Director of Graduate Studies

# THE ROLE OF GLN146 TO THE STABILITY AND ACTIVITY OF MANGANESE SUPEROXIDE DISMUTASE

---

DISSERTATION

---

A dissertation submitted in partial fulfillment of the
requirements for the degree of Doctor of Philosophy in the
College of Art and Science
at the University of Kentucky

By
Ting Wang
Lexington, Kentucky

Director: Dr. Anne-Frances Miller, Professor of
Chemistry
Lexington, Kentucky
2017

ABSTRACT OF DISSERTATION

# THE ROLE OF GLN146 IN THE STABILITY AND ACTIVITY OF MANGANESE SUPEROXIDE DISMUTASE

Gln146 is a highly conserved outer-sphere amino acid residue at the active site of MnSOD. It serves as a hydrogen bond donor to both the solvent molecules at the active site and Tyr 34, the conserved "gateway" amino acid residue. This dissertation develops our understanding of the effect of amino acid Gln146 at the second shell of the active site of metalloprotein MnSOD in facilitating metal binding, the modulation of redox potential, and the optimization of catalytic activity and structure stability. Different from the wild-type MnSOD, Q146E is always purified as a completely apo-protein with zero active metal ion and non-catalytic activity. But unlike apoMn-SOD, Q146E as an apo-protein exhibits extraordinarily conformational restricted protein structure. Because of the hyper-thermal stability of Q146E-apoMn-SOD, the protein itself loses its ability to form an "open" state which is responsible for the metal binding and protein maturation of apoMn-SOD. Increased thermal stability of protein structure also can be found in other mutants at the same position Gln146, Q146X-MnSOD (X=A, C, N or S), in addition to decreased catalytic activity, low $Mn^{3+}$/Mn ratio and the reduction potential of the activity site. Thus Gln146 is very effective in facilitating metal binding by destabilizing protein structure.

KEYWORDS: manganese superoxide dismutase, metal binding, protein stability, protein melting, reduction potential, Electron Paramagnetic Resonance

Ting Wang

Dec 27, 2016

# THE ROLE OF GLN146 IN THE STABILITY AND ACTIVITY OF MANGANESE SUPEROXIDE DISMUTASE

By

Ting Wang

Dr. Anne-Frances Miller

Director of Dissertation

Dr. Mark Lovell

Director of Graduate Studies

Dec 5, 2016

**Acknowledgements**

On the adventure of pursuing my chemistry PhD, the road is full of difficulties and challenges, not only for a period of intense learning in the scientific area, but also on a personal level. As the finishing touch on my dissertation, I would like to write this note of thanks to appreciate the people who have supported and helped me so much throughout this special journey.

I would like to express my sincere appreciation to my advisor Dr. Anne-Frances Miller for the role she has played in my academic and personal development. She has shown continuously and persuasively a spirit of excitement, enthusiasm and genius in regard to research, scholarship and teaching. I am deeply impressed with her diligent and energetic working as a female chemistry professor, which positively influenced me a lot. Without her supervision, encouragement and constant help, this dissertation would not have been possible.

I would like to thank my committee members (alphabetic order), Dr. Edith P. Glazer, Dr. Folami T. Ladipo, Dr. Stephen Testa, and Dr. Trevor P. Creamer, for their time serving on my committee and their valuable guidance and attributes. Their ideas and suggestion on my research areas always inspired me to learn and develop new thoughts on research.

I would like to express thanks to the group members of Dr. Yinan Wei's lab and Dr. Trevor P. Creamer's lab, for their generous of sharing with me the lab instruments collecting valuable data sets.

I would like to give my special thanks to all the group members in Miller's lab at UK for their wonderful personality and collaboration. They are very active, kind and supportive in setting up a friendly lab environment for research and studies. They provide tremendous help during my time at UK.

My PhD would not have been possible without the support and encouragement from my friends. All the memories are full of joy, uncountable meaningful conservations and positive encouragements. Without them, I would have given up thousands of times. They help me find the true strength of my heart.

Last but not least, the endless gratitude goes to my whole family for their sympathetic ear to tolerate my nerdy talk and their wise counsel in my life. They are always there for me. I would particularly like to single out my grandmother for her unconditional love and encouragement.

## Table of Contents

## List of Tables

## List of Figures

# Chapter 1 Introduction

## 1.1 The important role of SOD

Every cell needs consistent energy to support its activities through the last second of its life, such as cell growth, division, differentiation and apoptosis. The significant rise of atmospheric $O_2$ gave rise to the high energy yields of aerobic metabolism by reduction of oxygen, typically via the electron transfer system supported by mitochondrial membranes.[1] Naturally one to two percent of total cellular oxygen consumption is allocated to toxic oxygen metabolites generating reactive oxygen species such as $O_2^{\cdot-}$, $OH^{\cdot}$ and $H_2O_2$, known as the by-product of cellular aerobic metabolism.[1-2] Other sources of deleterious ROS include radiation (e.g., UV light) and electron transfer to $O_2$ under the environment of toxic chemicals (e.g., paraquat) and drugs (e.g., adriamycin, bleomycin).[2] Superoxide is generally the ROS formed, and its spontaneous reactions produce a variety of others.[3] To prevent vital biological macromolecules including lipids, proteins and nucleic acids from damaging reactions with ROS, antioxidant catalysts and reactions that could consume or transform ROS are of great importance to the extension of length of cell life.[4]

Superoxide dismutase (SOD) is an oxidoreductase, in that it oxidizes one substrate and reduces another alternately. Oxidoreductases account for 3.2 percent of human total proteins grouped by function[3] (e.g., dehydrogenase, transferase). The SOD activity of erythrocuprein and its physiological importance in scavenging ROS was first discovered and characterized by McCord and Fridovich in 1969.[7] Dismutases are a special subset that would reduce a second molecule of the same substrate as was subject to oxidation. Totally two molecules of the toxic substrate are consumed per turnover.[6] The importance of

enzymatic antioxidant defenses has been underscored by the fact that none of aerobic organism has yet been found to lack at least one form of superoxide dismutase. Indeed, most aerobes possess several.[5]

Distinguished by protein folding structure and the redox-active metal ions at their active sites, there are three different families of SOD proteins: cooper and zinc-containing SOD (Cu,ZnSOD), nickel-containing SOD (NiSOD) and the family of iron or manganese containing SODs (Fe/Mn-SOD) (Figure 1-1).[8] One of these families, Manganese superoxide dismutase, MnSOD, and iron superoxide dismutase, FeSOD, are expressed in both prokaryotic and eukaryotic cells and functions to protect the cells against ROS.[9] Specifically FeSOD is found in prokaryotes, protists and the chloroplasts of plants whereas MnSOD is mostly found in prokaryotes and the matrix of mitochondria.[8, 10]

With catalase and peroxidases, SOD provides an elaborate antioxidant defense system to detoxify malicious radicals arising from aerobic respirations. The overall mechanism by which SOD catalyzes the disproportionation of superoxide ($O_2^{\cdot -}$) to hydrogen peroxide ($H_2O_2$) and oxygen ($O_2$) is shown in equations (1.1 and 1.2) as follows, where M represents redox active metal ion, Mn ion or Fe ion, and E represents the SOD protein. The total reaction cycles involves alternating between reduction of the $M^{3+}$ SOD and oxidation of $M^{2+}$ SOD. Subsequently the reactive hydrogen peroxide ($H_2O_2$) is converted to water ($H_2O$) by glutathione peroxidase, or to oxygen ($O_2$) and water ($H_2O_2$) by catalase.

$$E - M^{3+}(OH^-) + O_2^{\cdot -} + H^+ \rightarrow E - M^{2+}(H_2O) + O_2 \quad (1.1)$$

$$E - M^{2+}(H_2O) + O_2^{\cdot -} + H^+ \rightarrow E - M^{3+}(OH^-) + H_2O_2 \quad (1.2)$$

Because as much as 90% of cellular ROS is generated in mitochondria, the eukaryotic mitochondrial MnSOD is critically demanded for mitigation of endogenous oxidative stress in this organelle.[2, 11] Previous research shows that lacking of MnSOD in mammalian cells would give rise to an extensive range of oxidative stress damage to the cardiovascular system, the brain, and the nervous system, resulting in dilated cardiomyopathy, hepatic lipid accumulation, mitochondrial defects and early neonatal death and much more.[1, 9, 12] Severely, complete depletion of cellular MnSOD enzymatic activity by homozygous MnSOD gene deletion, mice was only being able to develop embryonically[12] and the life span of *Drosophila* models was found drastically decreased.[13] On the other hand, overexpression of MnSOD in mice and *Drosophila* models leads to an increased lifespan.[13] Some other diseases are associated with production of Fe-substituted MnSOD, FesubMn-SOD, bearing the nonnative metal ion Fe at its active site instead of Mn ion. Studies found that more than 90 % of its enzymatic activity has been compromised because of metal mis-coordinations.[14]

## 1.2 Metallation process of SOD

Metalloproteins correspond to as much as 25% of all structurally well-characterized proteins.[15] Some half of these metalloproteins perform indispensable catalytic roles in lots of cellular activities such as DNA biosynthesis,[16] detoxification,[6] energy metabolism[14 17] and the stress response et al.[18] In many cases of metalloprotein-related disease or toxicity, a non-native metal ion was found substituting for the native metal ion. Depending on the

identity of the metal ion bound, this kind of substitution alters the redox behavior of the protein system.[19]

The mechanisms of metal incorporation for MnSOD are still under development and only poorly understood, as well as the majority of those metalloproteins.[20] In our project, understanding how the cognate metal ion is delivered to a correct target SOD is an interesting biological topic, in addition to being an important step for the maturation of the metalloprotein.

The proteins of MnSOD and FeSOD are closely homologous to one another with the same overall folding and extensive amino acid sequence conservation (Figure 1-1).[21] The active site of MnSODs and FeSODs (Mn/FeSODs, collectively) contains a single metal ion located between the N- and C-terminal domains and coordinated by four amino acid side chains (those of His-26, His-81, Asp-167, His-181 in *Escherichia coli* MnSOD) (Figure 1-2). Beyond the metal ion's coordination sphere, a hydrogen bond network extends from a metal-bound solvent molecule via a set of amino acid side chains which have been totally conserved,[22] to the dimer interface (Figure 1-1 and Figure 1-2). [23]

Catalysis of disproportionation of superoxide by SOD requires a redox-active transition metal ion at the active site that can accept and release an electron alternately.[24] Despite the high degree of homology between FeSOD and MnSOD at the levels of primary, secondary and tertiary structure and particularly their virtually identical metal binding sites (Figure 1-3),[21a, 25] the full catalytic function is generally only achieved when its specific cognate metal ion is bound at the active site.[10] Although a few anaerobic organisms are

evolved with a special SODs which are known as 'cambialistic' SODs (Fe/MnSOD), which is capable to perform activity with either metal ion.

Mis-incorporation of iron into *E. coli* MnSOD or vice versa *in vivo* was first noticed by Beyer and Fridovich.[26] It is not an abnormal that a metalloeznyme is willing to bind different kind of metal ions other than its native metal ion, because analysis of protein structures reveals that structure or amino acid sequence is not the most important determinant factor of protein metal selection.[3] A metallochaperone was discovered to participate in metal ion delivery to eukaryotic (Cu, Zn)SOD.[27] Meanwhile the bioavailability of manganese *versus* iron in culture environment is reported as the key in determining the identity of metal ion at the active site of MnSOD in bacterial cells.[26, 28] The availability of metal ions differs a lot in different cellular compartments and organelles regulated by numerous complex mechanisms.[29] In *E. coli*, the iron ion tends to be accumulated up to 10–100 times higher concentration than that of manganese ion. The total cellular free iron is maintained at a concentration of approximately 100 μM and that of free manganese at approximately 10 μM.[18b] When *E. coli* cell is grown in medium supplemented with iron salts and manganese salts, dimeric MnSOD protein is found taking either Mn ion or Fe ion indiscriminately, and typically purified as a mixture of species with different stoichiometries of Fe and Mn ion bound (e.g. $Mn_2$, (Mn, Fe), $Fe_2$, and half-apo dimer, Fe or Mn).[26, 30]

There have been two different methods to introduce metal ion to the active site of MnSOD, chemical or temperature induced. One is that the replacement of the active site metal ion could be achieved by steps of unfolding MnSOD by applying guanidinium

hydrochloride (GumHCl), chelating of the native metal ion, and refolding MnSOD in the presence of the substituent metal ion.[19c, 31] Also a thermally triggered re-activation of MnSOD apo-protein *in vitro* by incubating protein with Mn salts at elevated temperature has been demonstrated.[32] A detailed analysis of the temperature dependence of metal uptake by apoMn-SOD revealed a steep onset of metal assimilation in a narrow temperature range, resembling the cooperative melting curves of proteins or nucleic acids.[33] The temperature dependence of metal uptake by apoMn-SOD suggests a temperature dependent state transition of the apoMn-SOD protein for metallation process. Elevated temperature was needed to enable the protein to traverse an activation energy barrier from a low-temperature "closed" state to a high-temperature "open" state competent for rapid metal ion uptake. At low temperature the apo-SOD is trapped in a so-called "closed" state, unable to take up metal ions.[32b, 32c, 34]

Two alternative mechanisms had been first proposed involved in protein metallation: subunit dissociation[35] and domain separation.[35b, 36] However analysis of the apoMn-SOD mutants indicated that neither complete subunit dissociation nor domain separation is required for metal ion uptake.[37] ApoMn-SOD can still take up metal ions in its high-temperature "open" state even when a disulfide linkage is engineered at its domain interface or between the subunits.[38] As a result complete dissociation of subunits or domains, or unfolding, had been proved not to be necessary but only a subtle reorientation of amino acid side chains involving interactions between subunits or domains was needed in order for metal ion binding to occur (i.e.Glu170, His171, His30 and Tyr34).[35a, 38] For example under high temperature ~60 ℃ the "gateway" residues (ie. His30 and Tyr34) at the domain interface opens the "gateway" funnel at the domain interface and exposes the

hydrophilic metal ion-binding residues by partially separating the domains.[33, 38] Under normal conditions, these two residues restrict afflux of substrate and product at the active metal site of MnSOD (Figure 1-2).[37] These two residues are also known sterically constricting the funnel which is linking the active site to bulk solvent or substrate molecule.

### 1.3 Redox potential tuning by MnSOD

Fundamentally the reduction potential ($E°$) determines the chemistry that the bound metal ion of the metalloprotein could perform, because the $E^o$ of a reaction represents the free energy of the process of per electron gained (equation 1.3) where $F$ is Faraday's constant and n is the total number of electrons transferred in the reaction.

$$\Delta G^{\circ} = -nFE_m \qquad (1.3)$$

Reactions with a negative Gibbs free energy ($\Delta G$) or a positive redox potential ($E°$) are considered as thermodynamically favorable (exogenous).[39]

For the process of disproportionation of superoxide ($O_2^{\cdot-}$) into dioxygen ($O_2$) and hydrogen peroxide ($H_2O_2$), superoxide dismutase SOD proteins play an indispensable role in adjusting the redox potential of the redox active metal ion and render the reactions thermodynamically favorable for both oxidation and reduction of superoxide ($O_2^{\cdot-}$) (equations 1.1 and 1.2). In order to enable the alternation between reducing $O_2^{\cdot-}$ to $H_2O_2$ and also oxidizing $O_2^{\cdot-}$ to $O_2$, the reduction potential of SOD must be in between of the potentials of the two half reactions (Figure 1-4).[10, 40] Moreover, to achieve the optimum turnover rate the reduction potential of the catalytic metal ion in SOD had better be near the average of the two half reactions (~ 0.36 V).[41]

The $E^o$s of the two half reactions for disproportionation superoxide ($O_2^{\cdot-}$) into dioxygen ($O_2$) and hydrogen peroxide ($H_2O_2$) are -0.619 V and 0.89 V respectively (Table 1-1). The $E°$ of the $Mn^{3+}/Mn^{2+}$ couple of $Mn(H_2O)_6$ is near 1.41 V *vs*. NHE (normal hydrogen electrode). Reduction of superoxide ($O_2^{\cdot-}$) to hydrogen peroxide ($H_2O_2$), by $Mn^{2+}(H_2O)_6$ is associated with a negative reduction potential ~ -0.52V too low to reduce superoxide ($O_2^{\cdot-}$) to $H_2O_2$ thermodynamically. However interactions between the Mn ion and the two solvent molecules and amino acid residues at active site of the MnSOD protein tunes the reduction potential of the $Mn^{3+}/Mn^{2+}$ couple to an appropriately intermediate $E°$ of 0.29 V.[42] Consequently the $E^o$ of the bound manganese ion fits in between of the potentials of the two half reactions, ideally close to the optimum midpoint near ~0.36 V. The bound manganese ion of MnSOD is therefore almost optimally tuned to support the accepted mechanism of alternating reduction and oxidation of superoxide.

Although overall structures of FeSOD and MnSOD are essentially superimposable (Figure 1-1 and Figure 1-3), considering the different intrinsic reduction potentials of their native metal ions, these two SOD proteins, FeSOD and MnSOD, must be able apply very different redox tuning upon their cognate metal ions in order to have the appropriate reduction potentials that are close enough to the average of the two half reactions (~ 0.3 V) in both cases.[41] For the best activity, both of them must depress the $E°$ of the metal ion at the catalytic site to different extend. The MnSOD protein must depress the $E°$ of $Mn^{3+/2+}$ by approximately half a volt more than the midpoint potential depression applied to $Fe^{3+/2+}$ by FeSOD protein (Figure 1-4),[10, 43] because of the different electron configurations of the d- orbital of the metal ion $Mn^{3+/2+}$ and $Fe^{3+/2+}$. For the free hexa-aquo ions, the reduction midpoint potentials for $Mn^{3+/2+}$ and $Fe^{3+/2+}$ are reported to be 1.5 and 0.77 V *vs.* NHE,

respectively.[44] The electronic configuration of high-spin $Fe^{3+}$ is $d^5$, thus upon reduction one of the d orbitals must accommodate a second electron. This situation is critically different from the case of high-spin $d^4$ $Mn^{3+}$ who owns a vacant d orbital that is readily to be able to accept a d electron with little electrostatic repulsion towards existing electrons. Thus $d^5$ $Fe^{3+}$ is less oxidizing than $d^4$ $Mn^{3+}$ under the same charge.

As stated previously, MnSOD and FeSOD are highly homologous in term of their structures and metal-ligating amino acids, including His 26, 81, 171 and Asp167 (Figure 1-3). Their active sites are relatively non-selective when binding divalent metal ions. For example, the catalytic site of MnSOD would take up Fe, Co or Zn, in addition to Mn, particularly when the manganese ion is scarce in the growth medium.[25a, 26, 42a] As listed in Table 1-2, with a non-native metal at the active site, very little catalytic activity is discovered.[26] For metal-substituated enzymes, the different electronic configurations of Fe and Mn ion combining with the distinct midpoint potential tuning applied by the apoFe-SOD and apoMn-SOD proteins would yield inappropriate reduction midpoint potentials as explored by Vance, Xie, Yikilmaz,, Miller (Figure 1-4).[31, 45] The manganese substituted iron superoxide dismutase, MnsubFe-SOD, exhibits a reduction midpoint potential ($E°$), almost 700 mV higher than that of MnSOD.[45b] In agree with the estimated reduction midpoint potential, the MnsubFe-SOD combination is in the reduced state ($Mn^{2+}$) as isolated whereas the native MnSOD is isolated predominantly as the oxidized state ($Mn^{3+}$).[25a, 42b] Accordingly the iron-substituted manganese superoxide dismutase, FesubMn-SOD, exhibits a $E°$, -0.24V, which is some 300 mV lower than that of FeSOD.[42a]

Besides the inappropriate redox potential tuning on non-native metal ion, based on pH titrations, EPR spectroscopy and X-ray crystallography, the loss of catalytic activity could also due to a competitive inhibitor. The substitution of Fe ion for Mn ion at MnSOD active site resulted increased tendency for the metal ion to bind a second equivalent of $OH^-$, a competitive inhibitor, particularly at higher pH.[19c, 46]

## 1.4 Research motivation and outline

The ligands in the first coordination shell of the redox active metal ion of metalloprotein directly determine the coordination geometry of active site.[47] In addition to the inner sphere ligands, the second shell sphere is also known as affecting the metal site's structure and catalytic functions significantly.[43] The second sphere residues influence the polarity of the adjacent environment, participate in the hydrogen bond network and involve in electrostatic interactions that would modify the ligand $pK_A$s which consequently modulate the metal ion reduction midpoint potential ($E°$). And the second sphere residues are known as very critical in facilitating proton transfer, substrate binding and product releasing at active site.[32a, 35b, 37, 48]

At the second shell of the catalytic site of MnSOD, Gln146 is believed to be the central control of the hydrogen bonding network as its carboxamide group $-NH_2$ forms one hydrogen bond with the coordinated solvent molecule at the first shell,[42] and another hydrogen bond with the hydroxyl of Tyr34 nearby. Tyr34 is hydrogen-bonded via a water molecule to the side chain of His30 nearby (Figure 1-2). Tyr34 and His30 are called the "gateway" amino acid residues since they are at the neck of a funnel controlling substrate access to the active site, and are also known as facilitating the thermally triggered metal

uptake by MnSOD.[38] Mutation of Gln146 of *E. coli* MnSOD will alter the strength and polarity of the hydrogen-bonding network,[45] which in turn can be reflected by the redox potential of the metal ion.

Several studies demonstrated that well-conserved residues at the outer sphere of active site are critical for catalytic function and the metal ion specificity of the SOD proteins.[25a, 37, 48] Some studies[42b, 49] revealed that Gln146 is one of those amino acid residues that maintain both the enzymatic activity and metal ion specificity for SODs. By site directed mutagenesis, the reduction potential tuning, metal ion specificity and catalytic activity related with Gln146 has been studied by several groups.[45b, 50] The Gln146 is conserved among amino acid residues of *E. coli* MnSOD and structurally equivalent to Gln69 of FeSOD and Gln143 of human MnSOD.[19c, 42b, 43] As a well-conserved residue in the second sphere of FeSOD's active site, substitution of Gln69 in FeSOD with His or Glu exerted dramatic redox tuning over the $E^o$ of the metal ion.[45b] Our lab prior work on FeSOD found that mutation of Gln69 to Glu causes a > 660 mV increase in the $E°$ of bound Fe.[45] Considering the $E^o$ depression applied to metal ion at active site by the MnSOD protein (more than 1 volts) and the $E^o$ increase produced by mutation of Gln69 to Glu in FeSOD (~ 660 mV) together, we propose that mutation of Gln146 to Glu will exert a significant influence on the $E^o$ of MnSOD. Furthermore we hypothesize that although the reduction potential of $Fe^{3+}/Fe^{2+}$ at FesubMn-SOD was too low to perform both half of the reactions (equations 1.1 and 1.2), the $E^o$ of mutant Q146E-FesubMn-SOD should be right in between of the two half-reactions' $E°_s$, and Q146E substitution could enable FesubMn-SOD to be active with an appropriate $E^o$.

However very few information had been learned from the Q146E-Mn-SOD or Q146E-FesubMn-SOD for so many years, because Q146E was only reported as an apo-protein as isolated in the literature paper.[50b] The metal content of Q146E is so low as zero such that it is impossible to estimate its catalytic activity not to mention its redox potential. Thus, instead of investigating the redox potential tuning by Q146E substitution, practically our research is devoted to understanding Glu146's effect on the metal binding process with a hope of improving metal ion binding ability of Q146E-apoMn-SOD.

Chapter 2 proposed a simplified purification methods we apply to MnSOD overexpressed by *Ox326-A* cells. First we characterized the relationship between protein yield and IPTG induction time. Second a modified purification method was developed since the target protein was exported into the growth medium by the cell line *Ox326*. Finally, the isolated protein was characterized with respect to its catalytic activity and metal ion content.

Chapter 3 describes the studies following the producing and characterizing the desired mutant Q146E-apoMn-SOD. First we compared the features of the ultraviolent absorption spectra, the metal ion content and the catalytic activity of *E. coli* MnSOD and its mutant Q146E as isolated and after metal reconstitution. Second the thermal stability of WT-holoMn-SOD, apoMn-SOD and Q146E-apoMn-SOD were assessed via their melting temperatures determined via the temperature dependences of their far-UV CD spectra. Furthermore, to explore metal ion binding to Q146E-apoMn-SOD, protein refolding with metal ion by cooling down from their melting temperature for WT-holoMn-SOD, WT-apoMn-SOD and Q146E-apoMn-SOD were monitored by far-UV CD spectra. Last we

compared the different metal binding behaviors between wild-type apoMn-SOD and mutant Q146E to reveal the function of Gln146 for metalation process by MnSOD.

Chapter 4 seeks to extend our understanding of Gln146 in the MnSOD protein by introducing a series of amino acid substitutions in place of Gln146. Ala, Cys, Asn, Ser, Tyr were introduced at position 146 to test how the length, proton affinity, size and charge of the side chain affect the catalytic and stability of MnSOD. All the mutant protein were first characterized with respect to catalytic activity and metal content. The features of their optical spectra were also compared. The thermal stability of the mutants were estimated by their melting curve via far-UV CD. Low-temperature electron paramagnetic resonance (EPR) was used to estimate their midpoint reduction potential and probe the coordination geometry of the metal ion bound to the activity site of each of the mutants.

Chapter 5 reviews the work developed in the previous chapters and identifies important opportunities created for future research on this topic.

Table 1-1: Standard Reduction Potentials of Oxidation and Reduction of Superoxide ($O_2^{\cdot-}$)

| reaction | $E^o$ (redox potential, V) *vs* NHE |
|---|---|
| $O_2 + e^- \rightarrow O_2^{\cdot-}$ | -0.169 |
| $O_2^{\cdot-} + e^- + 2H^+ \rightarrow H_2O_2$ | 0.89 |
| $Mn^{3+} + e^- \rightarrow Mn^{2+}$ | 1.41 |
| $Mn^{3+} + O_2^{\cdot-} \rightarrow Mn^{2+} + O_2$ | 1.579 |
| $Mn^{2+} + O_2^{\cdot-} + 2H^+ \rightarrow H_2O_2 + Mn^{3+}$ | -0.52 |
| $SOD \cdot Mn^{3+} + e^- \rightarrow SOD \cdot Mn^{2+}$ | 0.29 |
| $SOD \cdot Mn^{3+} + O_2^{\cdot-} \rightarrow SOD \cdot Mn^{2+} + O_2$ | 0.459 |
| $SOD \cdot Mn^{2+} + O_2^{\cdot-} + 2H^+ \rightarrow H_2O_2 + SOD \cdot Mn^{3+}$ | 0.70 |

NHE = Normal hydrogen electrode. The standard state used here is unit pressure. Potentials are vs NHE and those of superoxide's reaction are from published papers.[42, 51]

Table 1-2: Superoxide dismutase activity supported by each of Fe or Mn

| SOD protein | Fe-supported activity(unit/mg protein) | Mn-supported activity (unit/mg protein) |
|---|---|---|
| ***E. coli*** **(Fe)SOD**[42a] | 7000 | 10 |
| ***E. coli*** **manganese specific SOD (Mn)SOD**[31, 52] | 10 | 7000 |

The activity of SOD was measured using the standard assay of McCord and Fridovitch[7] and corrected for sub-stoichiometric metal incorporation. Superoxide dismutase activity is supported by each of Fe or Mn when bound to each of the (Fe)SOD or (Mn)SOD proteins of *E. coli*.

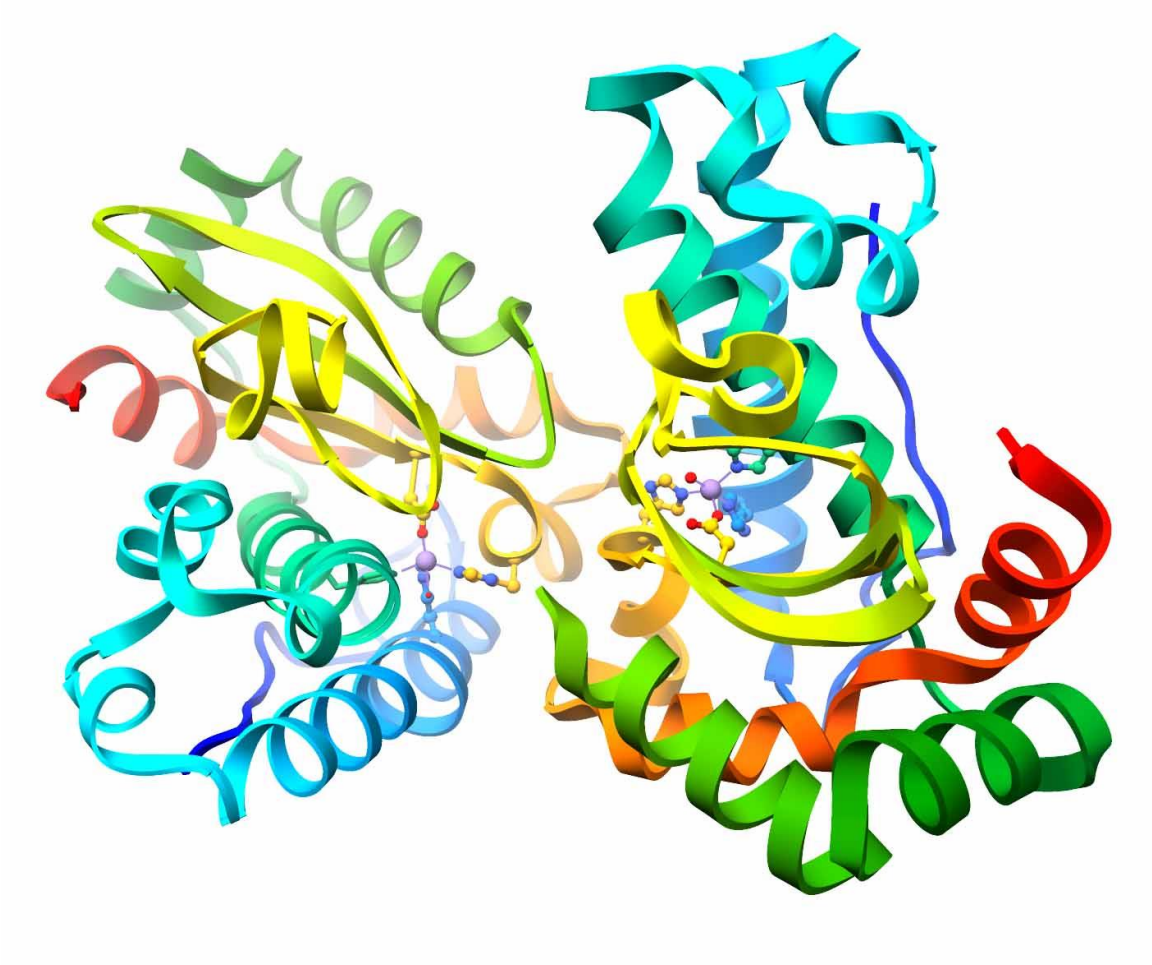

Figure 1-1: 3D ribbon structure of *E. coli* MnSOD.

The structure is based on the structure published by Lah *et al*[23] (PDB code: 1ISB), produced by Miller using Chimera.[53] The protein is a homodimer of identical 22 kDa monomers. The active metal ion is shown as a violet sphere lying between the N-terminal domain (composed of α- helices) and the C-terminal domain (composed of α-helices and a β-sheet). The side chains of amino acid residues that coordinate the metal ion are shown in ball and stick format with N and O atoms colored according to the CPK convention. These are three histidine, one aspartate (His26, His81, Asp167, and His181) and a solvent molecule. The ribbons are colored blue to red to indicate the course of the peptide from the N-terminus to the C terminus.

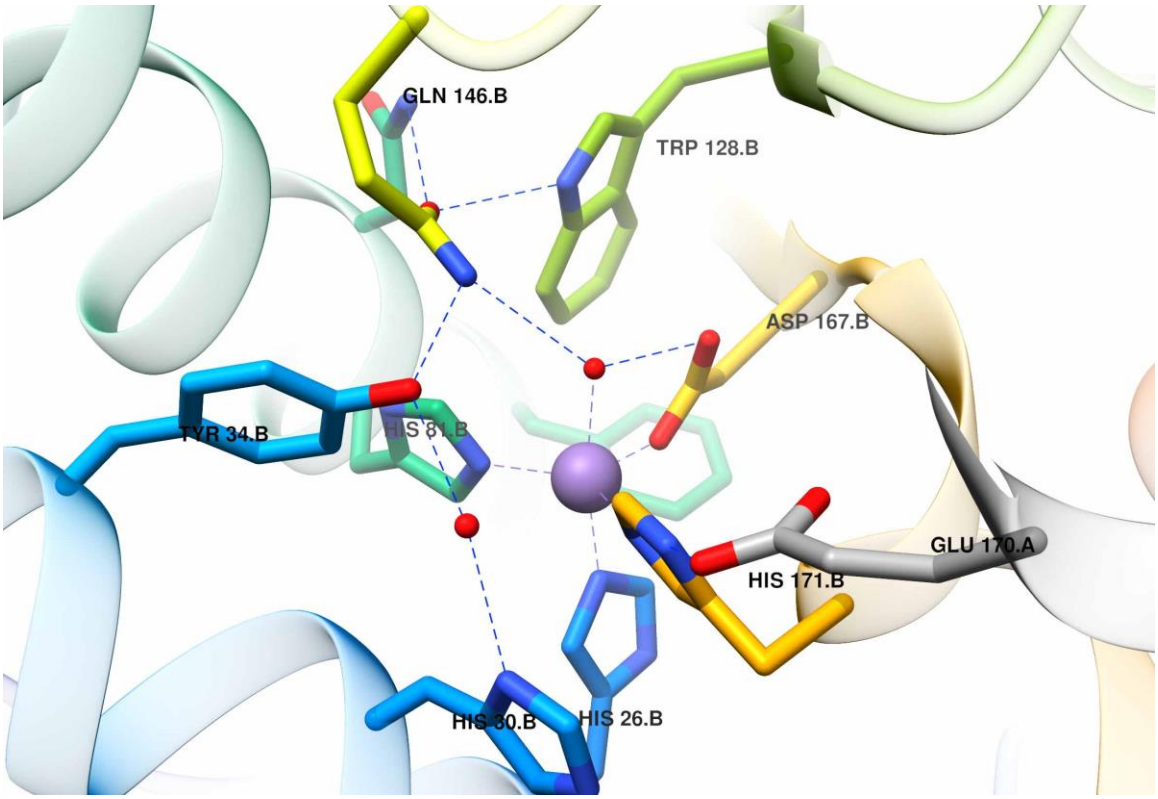


Figure 1-2: Cartoon view of metal binding site of MnSOD.

3D structure is based on the published SOD structure 1D5N.pdb.[48] The figure was generated by Miller using Chimera.[10] Numbering is based on the *E. coli* MnSOD.[53,54,55] The redox active metal ion $Mn^{3+/2+}$ is depicted as a violet ball trigonal bipyramidally coordinated by the side chains, three His, one Asp (His26, His81, Asp167, His181) and a solvent molecule to form a coordination polyhedron at first shell.[7] A hydrogen bond network also extends from the metal bound solvent molecule to amino acid side chains Tyr34, Gln146, Asn80 and Trp128 and His30 at the dimer interface.

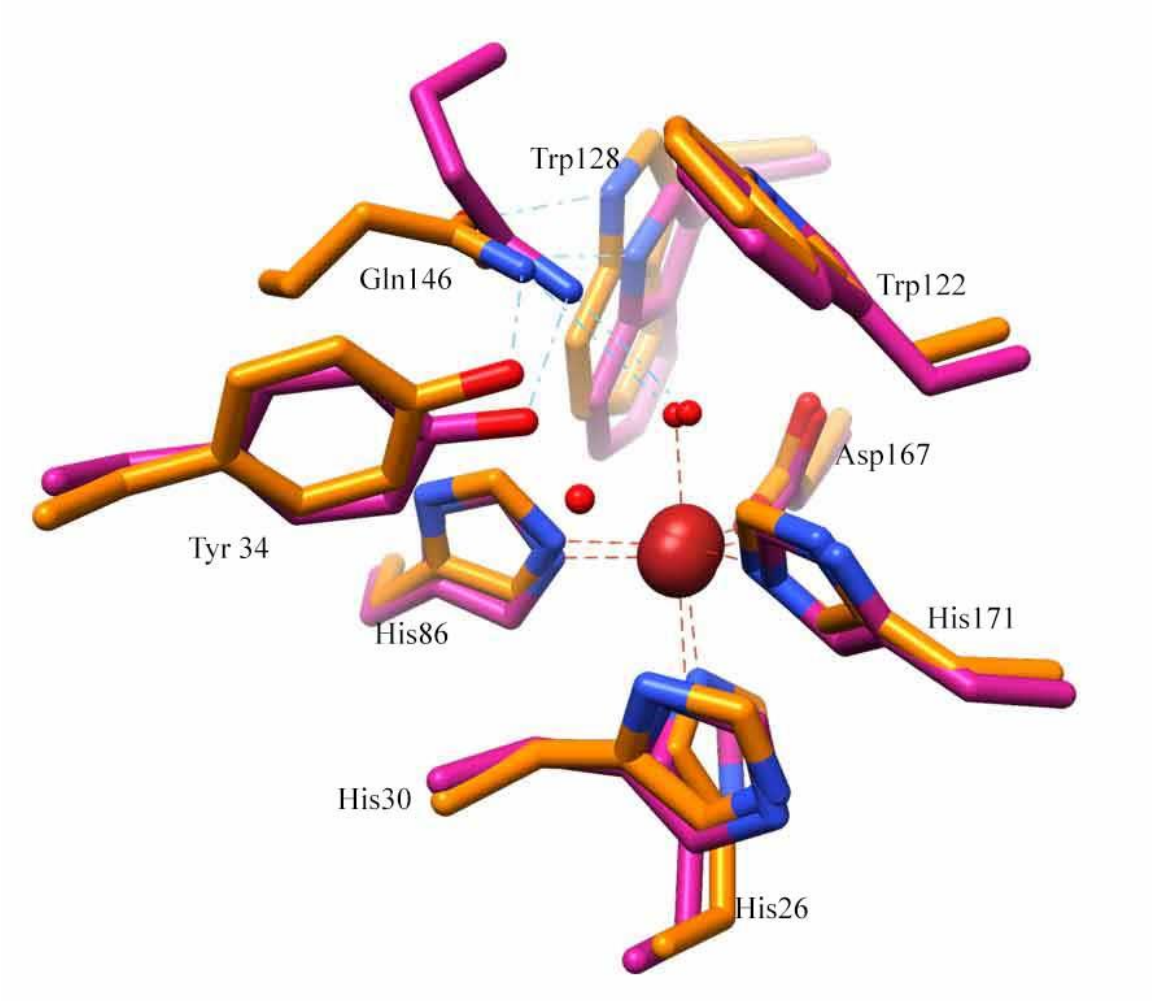


Figure 1-3: Overlay of the active site of *E. coli* FeSOD (orange skeleton) and MnSOD (magenta skeleton).

The structure is based on structure published by Lah et al,[23] 1ISB for FeSOD and 1MMM for MnSOD.[25a] Figure was generated by Miller, using Chimera.[10] Numbering of amino acid is based on the *E.* coli FeSOD and MnSOD.[53,54,55] Redox active metal ion is shown as a rust-colored sphere coordinated by the side chains of three His, one Asp (His26, His81, Asp167, His181) and a solvent molecule giving a trigonal bipyramidal coordination polyhedron.[7, 21a, 54] A hydrogen bond network (aqua) also extends from metal bound solvent molecule to amino acid side chains Try34, Gln69, Asn74 and Trp122 at the dimer interface.

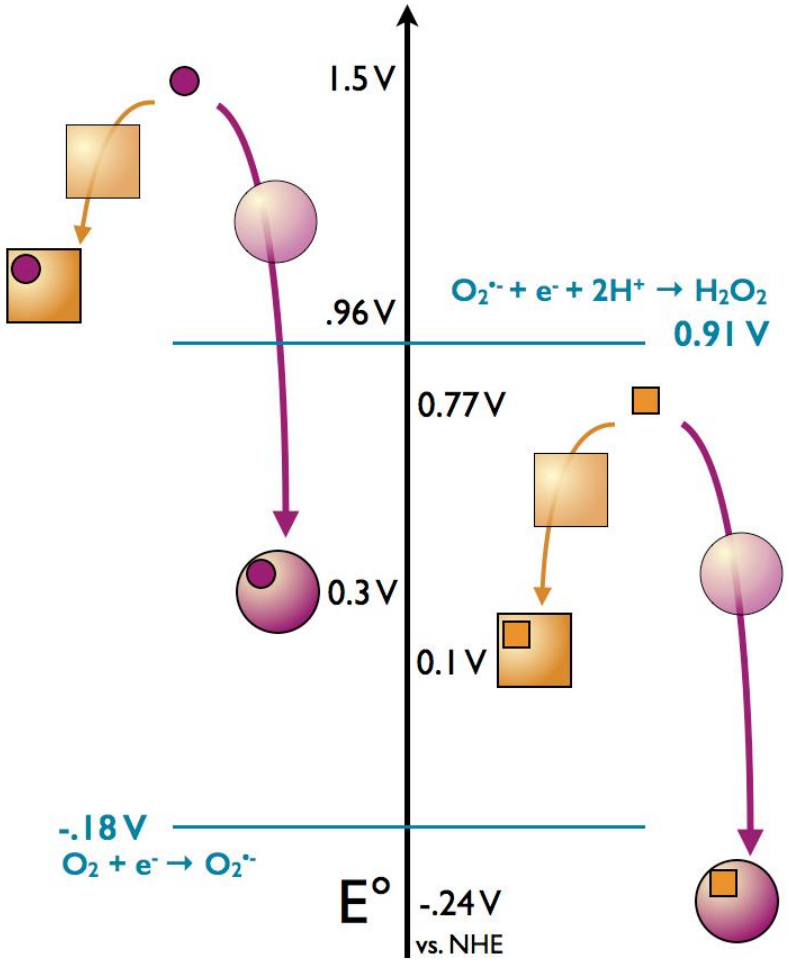


Figure 1-4: The cartoon model for different redox potentials tuning.

The cartoon is used to demonstrate the different redox potentials tuning of the catalytic metal ion $Fe^{3+/2+}$(orange square) and $Mn^{3+/2+}$ (purple circle) applied by iron specific superoxide dismutase (FeSOD) (yellow square) or manganese specific superoxide dismutase (MnSOD) (violet circle). Apo-protein are symbols, yellow square for apoFe-SOD, voilet circle for apoMn-SOD, without the metal ion at the center. Potentials are *vs* NHE and marked on the vertical axis. Those of superoxide's reactions are from Sawyer and Valentine.[51] NHE = Normal hydrogen electrode. Figure was generated by the courtesy of Miller.[10]

# Chapter 2 Overexpression, Purification and Characterization of *E.coli* MnSOD in *Ox326-A* cells

## 2.1 Introduction

As one of the essential proteins for aerobic organisms, superoxide dismutase (SOD) is an oxidoreductase that catalyzes the disproportionation of superoxide radicals ($O_2^{\cdot -}$) into hydrogen peroxide ($H_2O_2$) and dioxygen ($O_2$) preventing the cellular accumulation of superoxide. Four types of superoxide dismutase were identified, on the basis of their metal cofactor: the manganese-containing (MnSOD), the iron-containing (FeSOD), the copper-zinc-containing (CuZnSOD) and the nickel-containing SOD (NiSOD).[8] The alignment of the amino acid sequences and the crystal structures of FeSODs and MnSODs reveals considerable homology, the same folding structure including the same ligand set for the metal ion at active site.[55] Thus FeSODs and MnSODs are considered as a single family evolving from a common ancestor.[5]

Given their structural similarity, it is not a surprise to find that FeSODs and MnSODs can unselectively coordinate metal ion at active site, either Fe or Mn. Mis-incorporation of iron ion into *E. coli* MnSOD or vice versa *in vivo* was first noticed by Beyer and Fridovich.[26] Some members of the family of Fe- and MnSODs could even be active with either Fe or Mn as the metal cofactor, referred to as cambialistic SODs.[56] But most SODs are much more catalytic active with either only Fe or Mn (metal-ion specific activity). In order to profiles metalloprotein SODs, as a beginning preparation, developing an efficient method would be very necessary for overexpression and isolation metallized homogeneous protein with high catalytic activity and metal content.

As traditional method, after completion of IPTG induction, the cells are typically lysed by enzymatic treatment or mechanical disruption to liberate the desired protein. Although this method are used extensively to cracking cell and releasing proteins, the protein is contaminated by the undesired cellular content like the bulk of endogenous proteins and nucleic acids. The traditional purification method requires a lot of chromatographic steps to isolate the pure protein and takes a lot of time and materials.

Here the duration for IPTG induction and the following protein purification was studied on *Escherichia coli* MnSOD protein. Both the overexpression level and catalytic activity of MnSOD increases with longer IPTG induction time. Furthermore, we observed the secretion of MnSOD into the bacterial growth medium upon long hours of IPTG induction. SDS-PAGE analysis of supernatants of bacterial broth separating from bacterial cells showed that secreted MnSOD accumulates as we extending the induction times. Thereby MnSOD purified from secreted content has higher metal ion content than that of proteins retained intracellularly, when using an *E. coli Ox326-A* ($Sod^-$) expression system. The higher yield (~100 mg MnSOD per liter of cell culture) and higher quality of secreted MnSOD isolated from the supernatant, in combination with the ease and speed with which it can be purified, recommend our proposed harvesting and purification method as a practical improvement over the conventional method.

## 2.2 Materials and methods:

The SOD-deficient *E. coli* strain (*ΔsodAsodB*) *Ox326-A* was the generous gift from Prof. Steinman.[57] The wild-type MnSOD gene from *E. coli* on the pET21 derivative pAK0[1]

[1] Karapetyan, A. & Miller, A.-F., unpublished.

was transformed into the *Ox326-A* cell line and stored as a 20 % glycerol stock in Luria-Bertani medium with 50 µg/mL kanamycin and 50 µg/mL ampicillin at -80 ºC. All cell growth media used in this research were supplemented with 50 µg/mL kanamycin and 50 µg/mL ampicillin in order to keep positive colonies for the pAk0/Ox326-A strain and eliminate other contamination.

Xanthine Oxidase, bovine heart cytochrome c and nitroblue tetrazolium were products of Sigma chemical Co. The resin G-25, DE-52 and CM-52 were products of Whatman. Protein molecular weight standards were obtained from Bio-Rad Laboratories. All other chemicals were of highest available quality and all operations utilized water from a Millipore plus QPAK® purification system.

MnSOD was overexpressed from *Ox326-A Escherichia coli (E. coli)* which is a double deletion strain lacking the chromosomal genes for both FeSOD and MnSOD (ΔsodAsodB). *Ox326-A* was transformed with the sodA gene-bearing plasmid pET21 pAK0. The pAK0/*Ox326-A* cells in a glycerol stock were streaked onto an LB amp/kana plate and incubated at 37 ℃ for 12 - 15 h. A single colony was picked from that plate and inoculated 3 ml of LB (Luria Bertani) medium at 37°C 220 rpm for 12 – 15 h. Next 1 ml of the 3ml LB cell culture was then transferred to 100 ml M9 medium and incubated for another 12-15 h at 37°C 220 rpm. Finally, 20 ml of the 100 ml M9 medium cell culture were transferred to 2 L of M9 medium. This 2 L cell culture was incubated at 37 °C 220 rpm. Until the optical density of the 2 L culture reached an $OD_{600}$ of 0.5 - 0.7, Mn-nitrilotriaacetate (Mn-NTA) and IPTG was added to a final concentration of 10 µM and 50 µg/mL respectively, to trigger MnSOD protein overexpression. The cell culture in M9

continued incubating with Mn-NTA and IPTG for another 12-16 hours, at 37 °C and 220 rpm until the cell density reached an OD600 of ~ 2.3. In order to prolong the log phase for cell culture growth and extend time for correct protein folding and metal binding, selected cultures experienced low-temperature interval by cooling in the refrigerator at 4 ℃ for approximately 12 hours before returning to the shaker incubator at 37 °C and 220 rpm. This was repeated once or twice, as profiled in Figure 2-4.

Two different purification methods were compared for obtaining pure MnSOD protein. The conventional procedure 2.2.1 describes the purification of MnSOD from cells harvested at the end of the cultures growth, whereas our new procedure 2.2.2 exploits purification method based on our finding that MnSOD protein was secreted into the medium.

### 2.2.1 Purification of MnSOD retained in the harvested cell pellet

Cells were harvested by centrifugation at 4 °C, 8000 rpm for 20 min. The cell pellet was washed using wash buffer (5mM potassium phosphate, pH 7.4) and stored at -20 $^{0}$C until needed. Upon thawing the frozen cell pellet on ice for approximately 30 min, the cells were suspended in cell suspension buffer (50 mM potassium phosphate, 1 mM EDTA, 0.5% NaCl, 0.5% KCl, pH 7.4) to which was added lysozyme (10 mg/gram cell pellet). After homogenizing the cell pellet to a smooth slurry, add protease inhibitor, 0.2 mg/ml (AEBSF, 4-(2-aminoethyl) benzenesulfonyl fluoride hydrochloride), along with 0.1 mM $CaCl_2$. Cells were ruptured by passage through a French press or Parr cell disruptor 4 – 5 times at 12000 – 15000 PSI. Then cell debris were separated from soluble proteins by centrifugation at 63000 xg 4℃ for 30 min.

The supernatant (≈ soluble protein) was transferred to a beaker on ice. Solid KCl was added gradually to the soluble protein solution to a final concentration of 0.1 M, while stirring continuously. The solution was then incubated in 50 ℃ water bath for 3 min to precipitate less thermally stable proteins. The solution was cooled by placing the beaker on an ice bath without stirring for another 15 min. After cooling down, ammonium chloride was added as the solid to produce 0.17-0.20 g/ml while stirring on ice over an interval of at least 15 min. All the precipitate mostly proteins was removed by centrifugation at 63000 xg 4 ℃ for 30 min. The soluble protein remaining in the solution was concentrated using an Amicon® ultra-30 centrifugal filter device with a 30,000 NMWL cut-off (Normal Molecular Weight Limit), centrifuging at 4000 xg 4 ℃ for 20 min several times till the total volume of the protein solution was reduced to 3 - 5 ml.

In the conventional chromatography method, the 3 – 5 ml concentrated protein solution was loaded onto a G -25 sephadex column (5 cm × 40 cm) pre- equilibrated with 2-3 volumes of 5 mM potassium phosphate, pH 7.4, and eluted with 5 mM potassium phosphate, pH 7.4. The elution fraction was collected and its absorbance at 280 nm was monitored to identify protein-containing parts ($\varepsilon 280 = 86600\ M^{-1}cm^{-1}$ for MnSOD dimers[10]). Protein-containing fractions were then pooled and dialyzed overnight at 4 ℃ against 12 L 5 mM potassium phosphate, pH 7.4. The resin column was washed with 5 mM potassium phosphate, pH 7.4 until the absorbance at 280 nm indicated no protein remaining on the column. Finally for resin storage the column was washed with 2-3 column volumes of 500 mM potassium phosphate, pH 7.4.

After dialysis overnight, the desalted protein solution was concentrated to 3-5 ml using an Amicon® ultra -30 centrifugal filter device. The concentrated protein was loaded onto a anion exchange DE-52 column (5 cm × 45 cm) pre-equilibrated with 2-3 column volumes of 5 mM potassium phosphate, pH 7.4 and eluted using a linear gradient of total 500 ml 5 mM – 200 mM potassium phosphate, pH 7.4. The elution was collected while monitored of absorbance at 280 nm ($\varepsilon 280 = 86600\ M^{-1}cm^{-1}$ for MnSOD dimers[10]). Based on the absorbance at 280 nm, the fractions containing MnSOD were further analyzed by SDS-PAGE. Those fractions containing MnSOD were pooled first and concentrated to 3-5 mL using an Amicon® ultra -30 centrifugal filter device. When the absorbance at 280 nm indicated no further protein eluting at this ionic strength, the column was washed with 2-3 column volumes of 500 mM potassium phosphate, pH 7.4.

Concentrated protein solution was loaded on a G-25 desalting column equilibrated with 5 mM potassium acetate buffer pH 5.5 and eluted with the same buffer. Protein-containing fractions were identified again based on their absorbance at 280 nm and pooled and concentrated to 3-5 mL using an Amicon® ultra -30 centrifugal filter device. After concentration, protein solution was loaded on a CM-52 cation exchange column (5 cm × 40 cm) pre-equilibrated with 2-3 column volumes of 5 mM potassium acetate, pH 5.5. MnSOD was eluted using 5 mM potassium acetate, pH 5.5, as the flow-through, monitored via absorbance at 280 nm ($\varepsilon 280 = 86600\ M^{-1}cm^{-1}$ for MnSOD dimers[10]). Based on the absorbance at 280 nm the fractions containing protein were identified. When the absorbance at 280 nm indicated no further protein eluting at this ionic strength, the CM-52 column was washed with 2-3 column volumes of 500 mM potassium acetate pH 5.5. The peak fractions containing MnSOD were further analyzed and verified by SDS-PAGE.

Those containing MnSOD and free of other proteins were pooled and concentrated to 3-5 mL using an Amicon® ultra -30 centrifugal filter device. The MnSOD pooled from the elution fractions of the CM-52 column were further concentrated to a final MnSOD concentration of ~ 1 mM and stored at 4 ℃ in the refrigerator.

### 2.2.2 Simplified purification of MnSOD secreted to the medium

Because considerable quantities of MnSOD were secreted into the growth medium during the extended cell growth, we developed a simplified purification method directing at the secreted protein in the medium. After the cell pellet had been collected from a 2 L cell culture by centrifugation as described traditional purification method, the supernatant was concentrated using a pressurized membrane filtration assembly (Advantec MFS Inc,) with a Millipore 100 KDa NMWL (Normal Molecular Weight Limit) cutoff, ultracel regenerated cellulose ultrafiltration discs, by applying an air pressure at ~ 50 psi until the total volume of the supernatant was reduced to ~100 ml. Remove the possible cell debris and other impurities of the ~100 ml supernatant by centrifugation 63000 xg for 30 min at 4 ℃. Under ~ 50 psi air pressure, continue concentration of supernatant to ~ 30 mL using a pressurized membrane filtration assembly (Advantec MFS Inc,) with a Millipore 30 KDa NMWL (Normal Molecular Weight Limit) cutoff. Again remove the cell debris and precipitate remaining in the supernatant from soluble proteins by centrifugation at 63000 xg for 30 min at 4 ℃. Further concentration of solution to 10-15 mL was achieved using an Amicon® ultra -30 centrifugal filter device at 4000 xg 20 min 4 ℃ several times. Add EDTA to the protein solution to a final concentration of 1 mM to eliminate the external unspecific metal binding. The concentrated supernatant was then transferred to a dialysis

bag and dialyzed at 4 ℃ overnight against 12 L of 5 mM potassium phosphate, pH 7.4. The next day, supernatant protein was further concentrated to 3-5 mL using an Amicon® ultra -30 centrifugal filter device with a 30,000 NMWL (Normal Molecular Weight Limit), by centrifuging at 4000 xg 4 °C for 20 min intervals. Concentrated 3 - 5 ml protein supernatant was loaded on a sephadex G-25 desalting column pre-equilibrated with 2-3 column volumes of 5 mM potassium phosphate, pH 7.4. The protein was eluted with 5 mM potassium phosphate, pH 7.4. Fractions were collected and characterized with respect to absorbance at 280 nm. The peak fractions at 280nm containing MnSOD protein were further analyzed and verified by SDS-PAGE. Those fractions containing MnSOD but no other proteins were pooled and concentrated to ~ 1 mM and stored at 4 ℃ in the refrigerator.

Optical absorption spectra were obtained with a Hewlett Packard model 8453 diode array spectrophotometer. Protein concentrations were determined using molar absorptivity at 280 nm, with extinction coefficients of 86600 $M^{-1}$ $cm^{-1}$, 91900 $M^{-1}$ $cm^{-1}$, and 89500 $M^{-1}$ $cm^{-1}$ per dimer for MnSOD, FesubMn-SOD, and apoMn-SOD, respectively.[58]

Superoxide dismutase specific activity was assayed following the method of McCord and Fridovich.[7]

For qualitative assessment on the enzymatic activity of samples, the activity assay was performed by native electrophoresis on 12 % polyacrylamide gels combining the activity staining. The activity was visualized on non-denaturing polyacrylamide electrophoretic gels by the method of Beauchamp and Fridovich.[59] The details is described in the method of polyacrylamide gel electrophoresis.

To run the SDS polyacrylamide gel electrophoresis, 1 ml of each sample was collected from the cell culture at its indicated time. Samples were centrifuged at 12,000 xg for 2 min. After removing the supernatant, add 150 µl SDS-PAGE sample buffer and 50 µl 4x SDS loading buffer to each cell pellet. If needed, save 200 µl of the supernatant in a clean Eppendorf tube and add 120 µl SDS-PAGE sample buffer and 80 µl 4x SDS loading buffer. After vortex mixing, samples were pretreated by heating at 90 - 95 ℃ for 10 min and cooled on ice bath for another 5 min before loading 20 ul of each sample on the 12 % SDS gel. Run the electrophoresis at 100 V for about 1 hours to separate the proteins by size. Protein bands on the gel were stained with Coomaissie Brilliant Blue R250.

Specific activity was assessed qualitatively by resolving SOD using nondenaturing PAGE (polyacrylamide gel electrophoresis) and staining using nitroblue tetrazolium (NBT) and riboflavin.[7,59] Nondenaturing PAGE was carried out with 4 – 12 % polyacrylamide gel in a Tris-HCl/glycine buffer at pH 8.3.[60] Each gel was loaded with ~50 µg of protein and electrophoresed for 2-3 hours at 100 volts. The assay was conducted by soaking the gel in 0.3 mM NBT 30 mint and then 28 µM riboflavin 30 min in dark before irradiating with UV light for 20-30 min. In this assay, SOD activity manifests itself as an absence of the purple color that results from the reaction of photochemically-produced superoxide with NBT to form blue formazan when irradiating with UV. As a control, to demonstrate the identity and purity of protein samples, a duplicate gel was run in parallel but stained with Coomassie brilliant blue R250 and de-stained by 10 % acetic acid, 50 % methanol and 40 % $H_2O$ to reveal the location of protein bands.

Metal content was determined by ICP-OES (Inductively Coupled Plasma – Optical Emission Spectrometry)[61] at Environmental Research and Testing Lab located in the room 316 of Raymond Building in College of Engineering College at University of Kentucky. In order to account for possible contamination from the water as well as human error, triplicate samples of protein solution, a water blank and a series of duplicate standardized Mn ion solutions at different concentrations were prepared in parallel. 1 ml 0.1 M Nitric acid ($HNO_3$) was slowly added to each 1 ml protein sample (a 1:1 volume ratio) and the mixture was incubated on ice for 10 -15 min. Each solution then was centrifuged at 13,000 rpm for 2 min to remove precipitated proteins and other impurities. To have enough volume of solution for instrument, the supernatant were diluted by addition of 8 ml of distilled water before being fed into the plasma. The light emitted by Mn atoms was detected at its characteristic wavelength of 257.61 nm, 259.37 nm and 260.568 nm, by the optical spectrometer. The light emitted by Fe atoms was detected at the characteristic wavelength of 238.204 nm, 259.94 nm and 261.187 nm. A standard curve was constructed based on the duplicate standard samples and used to determine the concentrations of Mn and Fe ion of protein samples.

## 2.3 Results and discussion

### 2.3.1 Expression of MnSOD protein

Because m9 medium is a minimal medium requiring bacteria produce amino acids and other essential complex molecules on their own, bacteria grow much slower than they do in rich LB or defined medium. IPTG was added to the 2 L cell growth at 27 h when the cell density at $OD_{600}$ reached 0.5 – 0.7 during exponential growth phase. To identify MnSOD protein induced by IPTG, 1 ml worth of cells were collected approximately every

single hour along the IPTG induction and subjected to SDS-PAGE. Figure 2-1 demonstrates overexpression of MnSOD by *Ox326-A* cell upon the addition of IPTG (Isopropyl β-D-1-thiogalactopyranoside**)**. MnSOD protein is clearly evident as indicated by the target band on the SDS-gel in the red rectangle. The band of the target protein MnSOD on the SDS-gel starts at 29 h, 2 hours after IPTG induction, indicating that cells generated a lot of MnSOD which is an expected results for a much shorter period of time of other IPTG induced protein overexpression in the rich medium.[62]

### 2.3.2 Extension of growth period

To extend the time period of protein expression in the minimal medium m9 substantially, a 4 ℃ cooling interval was introduced at the process of cell cultivation as profiled in Figure 2-2, instead of keeping the growing temperature constantly at 37 ℃. As shown in Figure 2-3, this method is effective for the growth of cell culture, OD600 reflected that the desired bacteria grew continuously after experiencing cold shock, although the cooling interval makes the growing time longer than normal.

In Figure 2-4 we showed the yield and quality of MnSOD protein expressed by *Ox326-A* growing for three different length of period time and cooling interval, 30 hours, 37 hours and 55 hours. MnSOD produced over 37 h and 55 h displayed average catalytic activities of 10 – 15,000 U per mg protein or 10 – 13000 U per manganese site versus 10 – 13, 000 U per mg protein or 6 – 8000 U per manganese site upon 30 h cell growth. MnSOD from longer hour growth of more mature cultures, 37 h and 55h, displayed better catalytic activity determined via the xanthine/xanthine oxidase cytochrome c assay[63] and meanwhile the cell density did not decline as culture aging up to 50 hours (Figure 2-3).

The total yield of MnSOD also increased with the extension of the culture time, an average of ~ 5.5 mg/L MnSOD for 30 h, ~ 7.5 mg/L for 37 h and ~ 7.9 mg/L for 55 h culture time. Although the mechanism for MnSOD cellular maturation is not well investigated and understood so far, in the following cell growth, we decided to introduce the cooling interval once to cell culture, slowing down the growth rate and extending the time interval for protein synthesis because it could improve the yield and quality of MnSOD protein.

### 2.3.3 Protein secretion

The Mn-nitrilotriaacetate (Mn-NTA) was added to the medium for a second time at a final concentration 10 μM about 3- 4 hours after IPTG induction, to make sure the bioavailability of Mn ion. As the time interval for cell growth was extended substantially, we found that the medium of the cell culture turned from light transparent to light grape purple in color after about 40 hour growth (Figure 2-5).

To test the productivity of MnSOD protein by *Ox-326A* at the extended hours, the cell protein was analyzed by SDS-PAGE as shown in Figure 2-6. The results confirmed that the predicted 22 KD MnSOD was present upon the IPTG induction. We also had expected that the intensity of MnSOD protein band on the SDS-PAGE would become stronger along IPTG induction, since the cell density OD600 was increasing all the time (Figure 2-4). In Figure 2-6 the corresponding background proteins in the lanes were increased as expected, but the yield of MnSOD protein retained in cells diminished when the hours for cell growth went up to 40 h as identified in the red rectangle. It is very clear that under IPTG induction the amount of MnSOD retaining in the cells at 40 h was less than that retaining in cells at 34 h (Figure 2-6). This reflected that the amount of internal

cellular MnSOD was actually decreased when IPTG induction time intervals was extended above 40 hours.

Because the color of the supernatant of cell culture, light purple, was very suspiciously close to the color of $Mn^{3+}$ -SOD protein, the supernatant was subjected to the analysis by SDS-PAGE (Figure 2-7). Here we collected cell pellets and equal aliquots of supernatant at 26 h (without IPTG), 32 h, 34 h and 50 h (with IPTG) and loaded onto a SDS gel. The results in Figure 2-7 confirmed that an 22 KD protein band started showing up in the supernatant sample after 34 h instead the corresponding protein in the cell pellet was decreased simultaneously.

After harvesting the cells pellet, the supernatant of cell culture was saved and subjected to a simplified protein purification protocol, as described in the methods section 2.2.2. The purity of protein purified by this method was analyzed by SDS-PAGE (Figure 2-8) and the corresponding activity was analyzed by non-denaturing PAGE (Figure 2-9). Both gels reveals a distinct band of protein as MnSOD in the supernatant after the IPTG induction based on its catalytic activity and relative mobility. The clarified culture supernatant contained only traces of other proteins, the MnSOD is almost pure in the supernatant even before applied to the simplified purification method (Figure 2-8 & Figure 2-9). The overall quality of the MnSOD purified from the clarified culture supernatant is comparable to that obtained from the cell pellet following the traditional method with respect of catalytic activity, metal content and purity (Table 2-1 & Figure 2-10). Thus we conclude that MnSOD protein could be secreted into the cell medium. Combining all the

results above, we propose that upon IPTG induction the MnSOD overexpressed by *Ox326-A* could be released into the medium with extra hours of cell growth.

### 2.3.4 Culture condition investigation

In Table 2-2, we summarized the MnSOD purified from the cell pellet or supernatant with or without adding manganese for a second time after IPTG induction. All the MnSOD from the cell pellet displayed similar catalytic activity (11 – 13000 U/mg protein) and metal content (1.1 -1.4 Mn/dimer protein). The MnSOD with much better metal incorporation in the MnSOD (~1.8 Mn/dimer protein) is purified from the clarified cell supernatant. The manganese binding to MnSOD increases when extracellular manganese availability is abundant in the medium. The protein released by cell secretion is comparable to the protein purified from traditional chromatographic method considering the steps of cell lysis, French press, and enzymatic lysis.

Although the mechanism for MnSOD metallation and maturation is not well investigated and understood so far, MnSOD protein is expected to achieve a fully functional structure if it binds Mn properly.[10] The *E. coli* MnSOD was naturally expressed as a mixture of manganese and iron ion bounded at active site and the abundant extracellular iron ion could lead to iron insertion in the protein.[28, 64] Our results reflect that using of the clarified supernatant could provide a good starting point for preparation of MnSOD. This would save time on many steps of the traditional purification protocol but would only be useful if the secreted MnSOD is replete with Mn and retains high specific activity as our results (Figure 2-9 and 2-10). Thus taking advantage of the clarified cell supernatant provides a highly cost-effective new source of MnSOD, saving considerable

time by eliminating the need for enzymatic treatment, mechanical cell rupture, heat cut, the ammonium sulfate cut, chemical reagents, and time for chromatography and dialysis.

### 2.3.5 Integrity of cell membrane

Some studies on intact cells have demonstrated that the repeated cycles of freezing and thawing would disrupt the membranes and cause the formation of transient pores.[65] Subsequently up to 50 % of highly expressed recombinant proteins could be released from the cytoplasm.[66] Because a lot of MnSOD protein has been found in the cell medium at longer hour cell culture, to further investigate the cellular mechanism underlying MnSOD overexpression and exporting, we tested the integrity of cell membranes of *Ox326-A* cells by applying freezing stress to the cell pellet. If had the cell membranes been corrupted at the long growth hours, the freezing and thawing should have no affecting on the protein releasing.

Upon harvesting the cell pellet, to apply the freezing and thawing cycle, the cell was first rinsed by the cell suspension buffer, frozen at -20 °C overnight for ~ 8 hours and thawed in cell suspension buffer (5 mM phosphate buffer pH 7.4) till the next day. In Figure 2-11 we quantified the amount of MnSOD protein in the cell suspension buffer after cell experiencing freezing and thawing cycle zero, once, twice, third times. In Figure 2-12, the protein in the cell suspension buffer upon freezing and thawing was analyzed by SDS-PAGE, revealing a very clear band of protein as MnSOD by its relative mobility. Before experiencing the freezing and thawing steps there is only a small trace of MnSOD found in the cell suspension buffer. MnSOD protein was found in the cell suspension buffer upon exerting the freezing and thawing cycle to the *Ox326*. Compared with non-freezing and

thawing, substantial amount of MnSOD protein was found in the cell suspension buffer after freezing and thawing. It is clear that the cell membrane of *Ox326-A* is still functioning and cytosolic MnSOD in the cell can be released by applying freezing and thawing cycles.

### 2.3.6 Conclusion

Superoxide dismutases are typically soluble secreted and are also found localized in a number of subcellular compartments, such as mitochondrial intermembrane space,[67] the periplasmic spaces,[68] extracellular matrix.[69] In the SOD-deficient *E. coli* strain (ΔsodAsodB) *Ox326-A* the chromosomal *sod* genes were entirely deleted.[57] Hence this strain differs from the normal wild-type *E. coli* by being highly sensitive to oxidative stress, having an extended doubling time and weak defenses toward pathogens,[57] especially in minimal medium such as m9.[70] From the results above, the cell membrane and cell wall of *Ox326-A* apparently were not able to maintain all the overexpressed cytoplasmic MnSOD after long hour aerobic growth and the excessive MnSOD protein was able to escape from the cell into the growth media. However by introduce freezing and thawing to the cell, the cells releasing the MnSOD protein in good yield validates the integrity of cell membrane. Cellular condition can critically affect MnSOD overexpression and hence the location of the target proteins. The physiological structure of cell membrane might experience some alternation during the extended incubation time interval. To clarify the reason behind the MnSOD secretion and generalize the simplified purification procedure to a variety of different proteins, we should test the MnSOD overexpression under different cell lines system to see which properties of cell lines is critical in releasing the MnSOD into the growth media. Also we should try expression different kind of proteins in *Ox326-A* to find out if the identity the proteins or other factors involved in the secretion.

Inevitably, there are a number of uncertainties and limitations with our simplified purification system since the specific alternation of the physiological properties of the cell during the long hour overexpression are still unknown. But our simplified method overcomes the main limitation for obtaining enough target protein MnSOD in the m9 medium. M9 is convenient and universal because it is known as a minimal medium with many fewer complex ingredients provided and more produced by the cells. Thus it can be a useful medium for uniform isotopic labeling. By extending the incubation time for cell growth and increasing the manganese concentration during protein synthesis in the medium, collecting the protein in the supernatant is a highly time-efficient method sufficient to separate highly expressed proteins. We were able to enhance both the yield and quality of MnSOD for the other analysis and save considerable cost of the reagents and materials by the traditional chromatographic purification method.

Table 2-1: Comparison of catalytic activity, metal content and A260/A280 of MnSOD purified from supernatant and pellet.

| | **MnSOD (supernatant)** | **MnSOD (pellet)** |
|---|---|---|
| **Activity (1000 U/mg)** | 19 ± 2 | 12 ± 3 |
| **Activity (1000 U/metal site)** | 11 ± 1 | 9 ± 2 |
| **Mn/Dimer** | 1.8 ± 0.3 | 1.4 ± 0.3 |
| **A260/A280** | 0.63 ± 0.06 | 0.57 ± 0.05 |

The protein specific activity was determined by the standard xanthine/xanthine oxidase/cytochrome c assay at pH 7.4.[71] The concentration of Mn were quantified by ICP-OES. The protein dimer concentration was determined via Absorbance at 280 nm using the molar absorptivity 86600 $M^{-1}$ $cm^{-1}$ for dimer of manganese superoxide dismutase.[7] MnSOD protein from supernatant is purified following the method in 2.2.2, while MnSOD protein from pellet is purified following the method in 2.2.1.

Table 2-2: Comparison of catalytic activity, metal content, amount of MnSOD purified from pellet w/o Mn addition to the medium

| | MnSOD (mg) | Mn/dimer | Activity (1000 U/mg protein) | Activity (1000 U/metal site) |
|---|---|---|---|---|
| **Culture-A (without additional Mn & MnSOD from pellet)** | 7.9 ± 0.4 | 1.1 ± 0.1 | 13 ± 1 | 12 ± 1 |
| **Culture-B (with additional Mn & MnSOD from pellet)** | 7.2 ± 0.3 | 1.4 ± 0.3 | 12 ± 3 | 9 ± 2 |
| **Cultura-B (with additional Mn & MnSOD from supernantant)** | 7.8 ± 1.5 | 1.8 ± 0.3 | 19 ± 2 | 11 ± 1 |
| **Culture-C (without additional Mn & MnSOD from pellet)** | 5.0 ± 1.9 | 1.2 ± 0.1 | 11 ± 1 | 9 ± 1 |
| **Cultura-C (without additional Mn & MnSOD from supernantant)** | 6.0 ± 0.3 | 1.7 ± 0.2 | 16 ± 4 | 10 ± 3 |

Culture-B was supplemented with Mn-NTA solution at a final 10 µM after 3 hours IPTG induction, while Culture-A and C was not. The MnSOD protein of the cell pellet was purified from the culture cell pellet following the method 2.2.1. The MnSOD in the supernatant was purified from the clarified culture supernatant following the method 2.2.2. Both the 2 L cell cultures A, B and C in m9 medium experienced slowing down the growth rate and extending the time interval up to a total 55 hours for protein expression. The protein specific activity was determined by the standard xanthine/xanthine

oxidase/cytochrome c assay at pH 7.4.[71] The concentration of Mn were quantified by ICP-OES. The protein dimer concentration was determined via Absorbance at 280 nm using the molar absorptivity 86600 $M^{-1}$ $cm^{-1}$ for dimer of MnSOD. Data are analyzed from triplet samples.

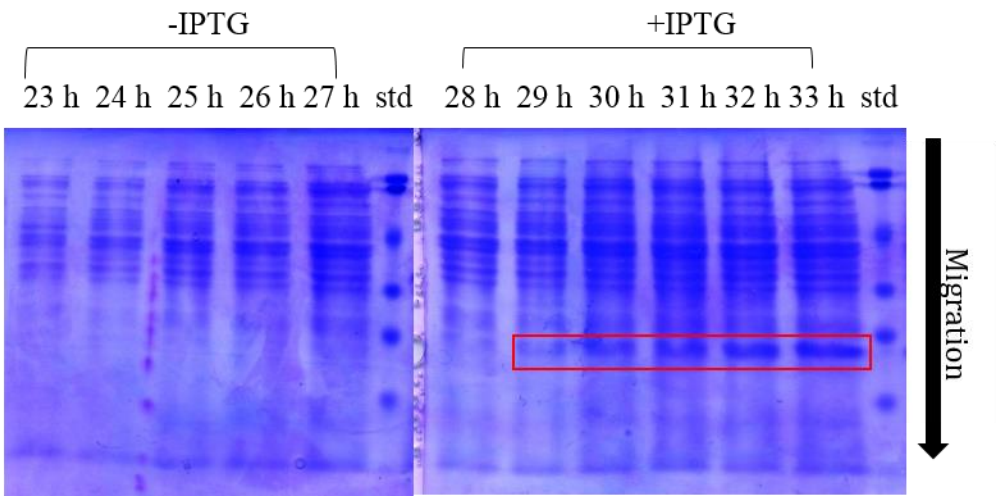


Figure 2-1: 12% SDS-PAGE (sodium dodecyl sulfate-polyacrylamide gel electrophoresis) profile of MnSOD overexpression.

The left gel including cell samples represents a control before IPTG induction. The right gel including cell samples represents the culture after IPTG was added. From left to right: cell samples at 23 h, 24 h, 25, 26 h, 27 h, protein plus protein molecular weight standards (Bio Rad Laboratories 4110027), cell samples at 28 h, 29 h, 30 h, 31 h, 32 h, 33 h, protein plus protein standards (Bio Rad Laboratories 4110027). The protein plus protein molecular weight standards from top to bottom the bands size are 104KD, 94KD, 51.5KD, 36.8KD, 28.5KD, 19.5KD. *E. coli* MnSOD was overexpressed by *Ox326-A* cells in 2 L m9 medium with respect to culture time since inoculation. IPTG was added at 27 h. 1 ml samples were collected from the cell culture at each indicated time. Samples were centrifuged at 12,000 xg for 2 min. After discarding the supernatant, 150 µl SDS-PAGE sample buffer and 50 µl 4x SDS loading buffer were added to the cell pellet. After suspended in the buffer by vortex mixing, cell samples were incubated at 90 - 95 ℃ for 10 min and cooled on ice bath for another 5 min before loading 20 ul of each sample on the SDS gel.

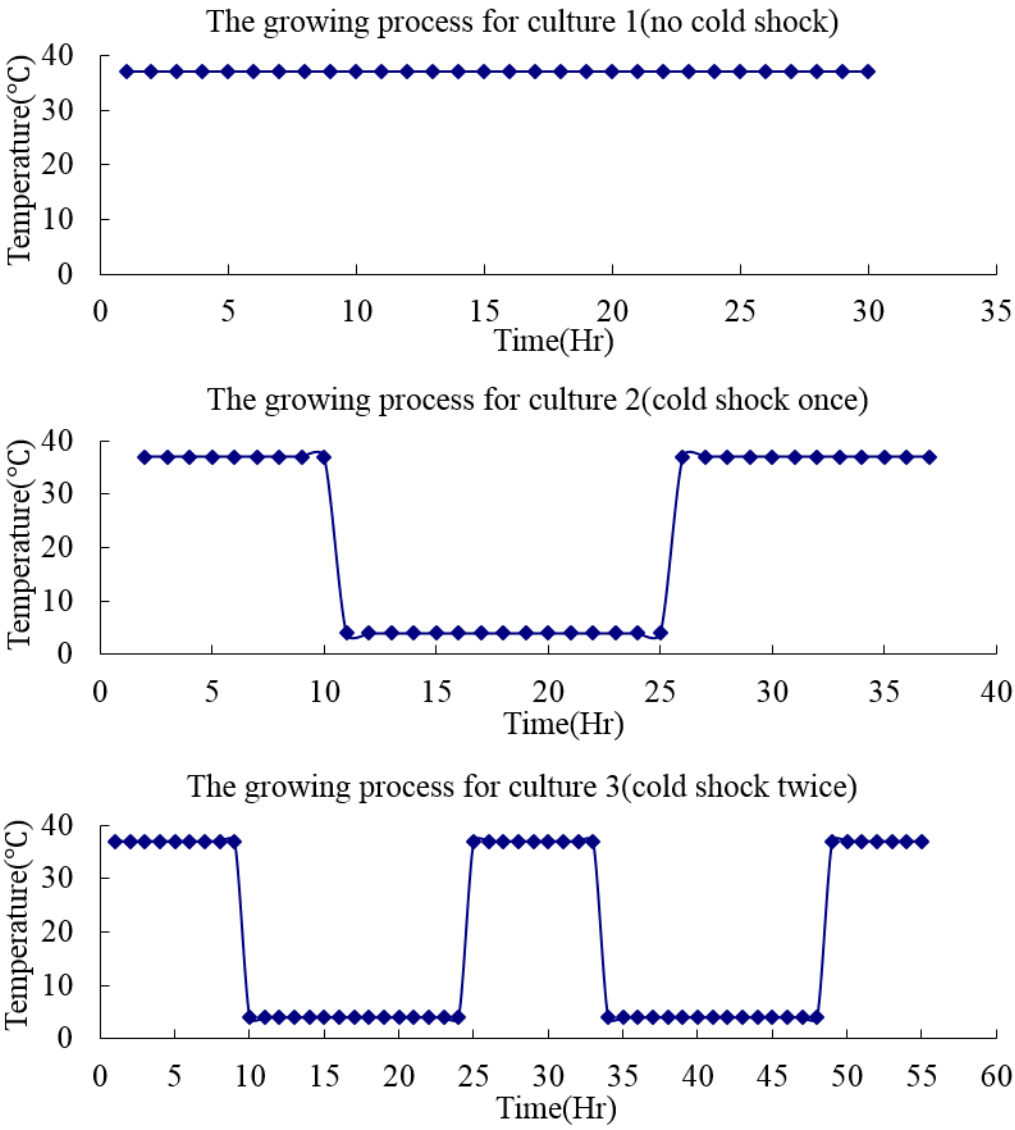


Figure 2-2: Temperature profiles for the cell culture growth.

This figures was showing different growth regimes experienced by bacterial cell cultures. In order to prolong the cell culture growth phase and provide more time for Mn incorporation, selected cultures were cooled to 4°C at 0 rpm in the refrigerator for approximately 12 hours before being returned to 37 °C at 220 rpm by the shaker incubator. The cultures experienced the different amount of time length of 30 hours, 37 hours and 55 hours. This cooling was repeated once or twice during the cell growth, as indicated.

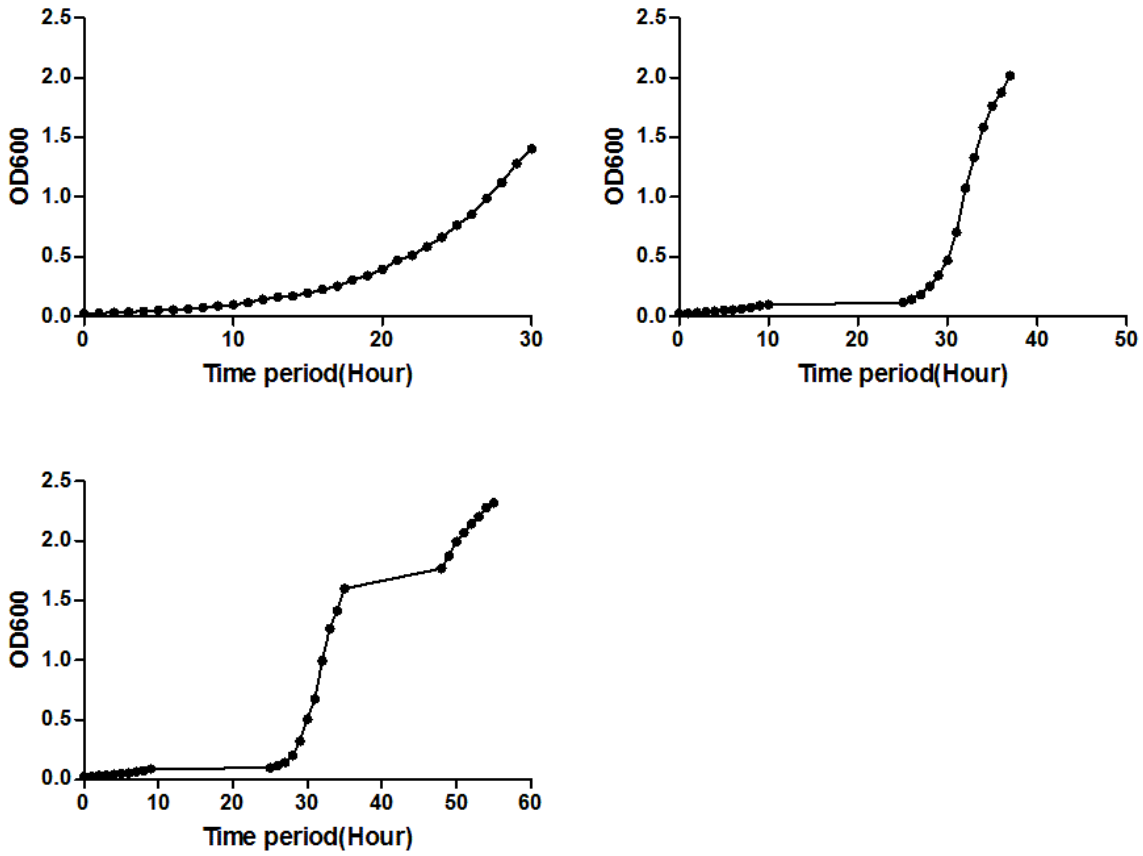


Figure 2-3: Growth curve of cell *Ox326-A* expressing wild-type MnSOD over 30, 37 or 50 hours.

MnSOD was overexpressed by *Ox326-A* cell ($sod^-$) in 2 L m9 medium. IPTG was added into the medium at OD600 ~ 0.5. 1 ml bacterial cell were sampled from the growth culture at each indicated time. The optical density of the culture OD600 was measured by a Hewlett Packard model 8453 diode array spectrophotometer. The content composition of some sample was analysis by SDS-PAGE and shown in Figure 2-6 and 2-7.

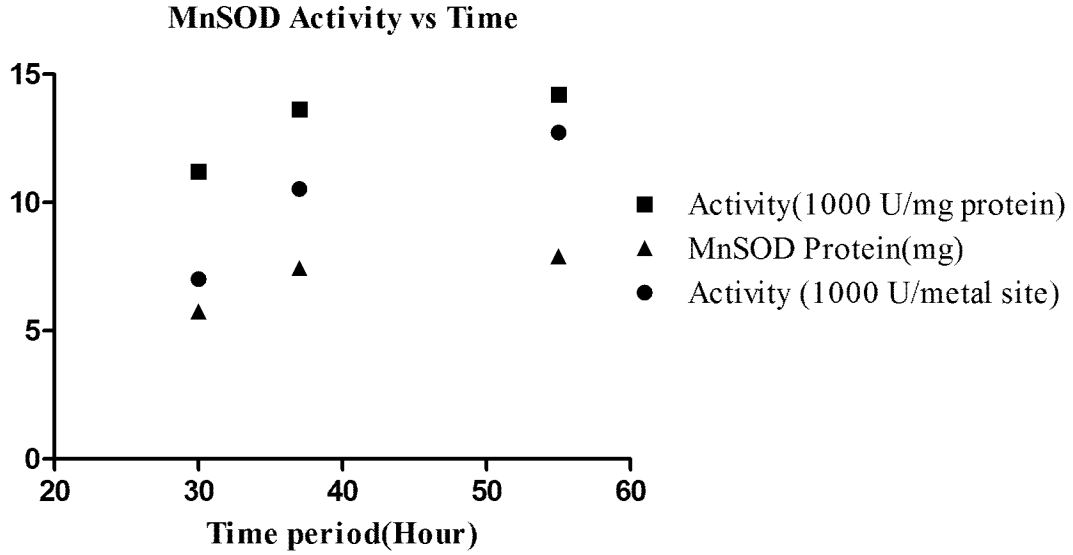


Figure 2-4: Specific activity of E. coli MnSOD with respect to the cultivation time for *Ox326-A* growing in m9 medium.

The cell cultures experienced the different period of time, 30 hour, 37 hour or 55 hours as described by Figure 2-2. The protein concentration was determined by measuring absorbance at 280 nm ($\varepsilon_{280}$ = 86600 $M^{-1}cm^{-1}$ for MnSOD dimers[10,58]) in 50mM potassium phosphate buffer at pH 7.4. The manganese concentration was determined via ICP-OES assay as described in the methods section.[72] The MnSOD enzymatic activity was measured via the xanthine/xanthine oxidase cytochrome c assay.[7] The amount of protein was the total mg MnSOD synthesized by 2 L of *Ox326-A* cells in m9 medium. Replicate cell cultures for each time period are prepared in parallel. The temperature condition profile for each culture was descried in Figure 2-2.

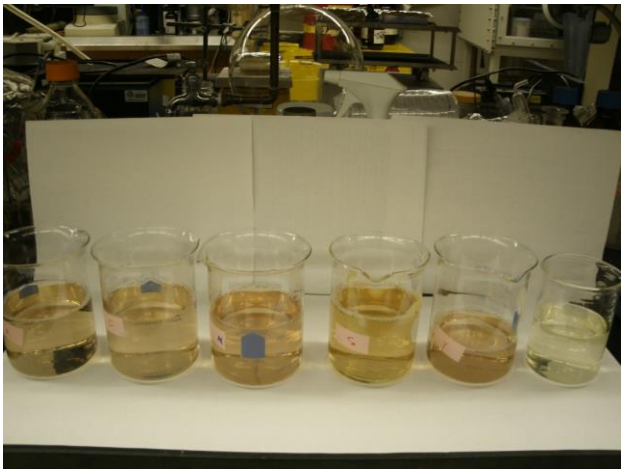

Figure 2-5: Clarified supernatant of Ox326-A cell cultures.

From left to right, the sample is the supernatant of wild-type MnSOD, and other mutants Q146A, Q146C, Q146N, Q146S, Q146Y cell culture. *Ox326-A* cells was inoculated in 500 ml m9 medium as described in the method. MnSOD protein and its variants was induced under IPTG. Mn-NTA solution was added to the medium about 3 hours after IPTG induction to a final concentration 10 μM.

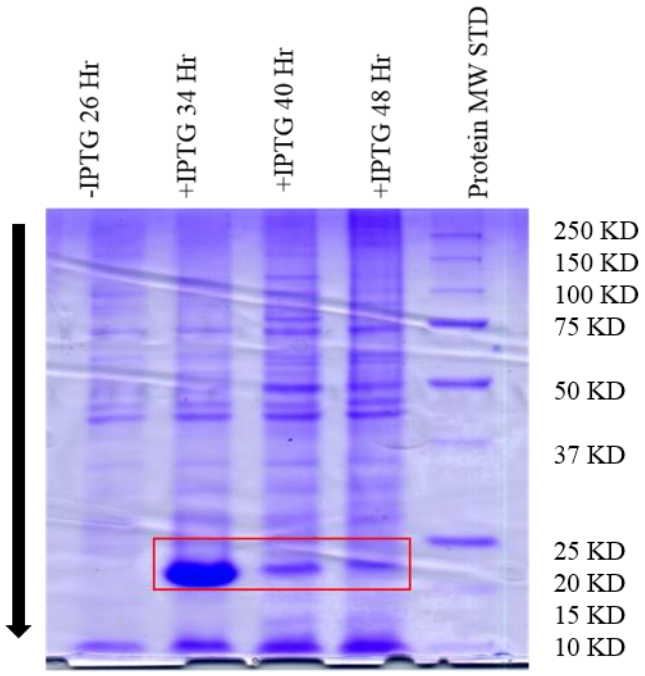


Figure 2-6: The protein composition of *Ox326-A* cell expressing wild-type MnSOD over 50 hours.

Bacterial cells growing in 2 L m9 medium are sampled at 26 h without IPTG (-IPTG) and 34 h, 40 h and 48 h with IPTG (+IPTG) respectively. The cell pellet are collected by centrifugation. The protein MW standard was provided by Bio Rad Laboratories (1610363). MnSOD protein is highlighted by the red rectangle.

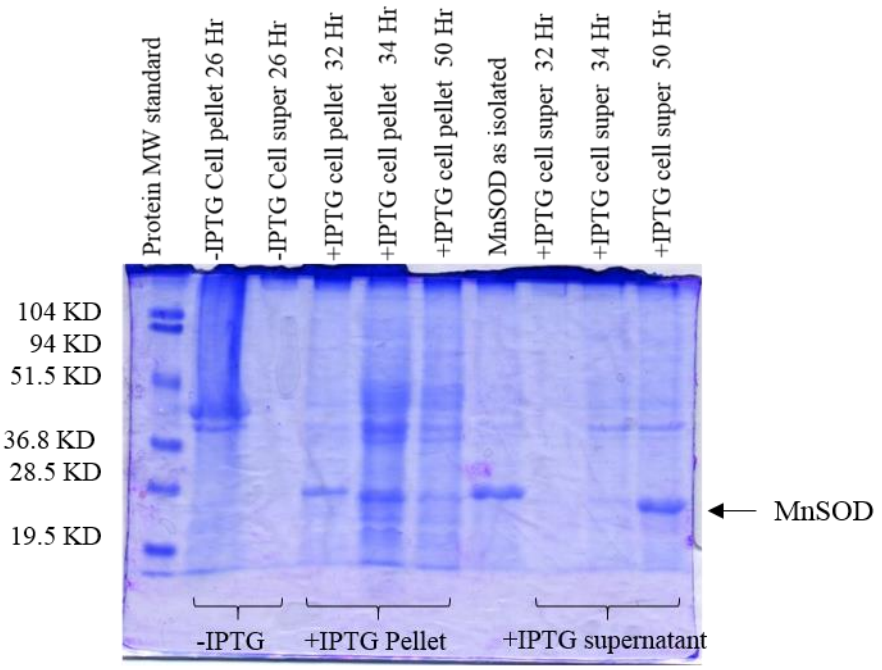


Figure 2-7: Gel electrophoresis of *Ox326-A* cell pellets and supernatant.

1 mL sample of 2 L bacterial cell culture in m9 medium was collected at each indicated time, representing cells and cell supernatant at 26 hour (-IPTG) or 32 hour, 34 hour, 50 hour (+IPTG) respectively. IPTG was added at 30 hr when OD600 reaches ~ 0.5. The cell pellet was separated from supernatant by centrifugation. The supernatant and pellet as loaded separately. The protein MW standard was provided by Bio Rad. MnSOD protein as isolated is loaded as a control.

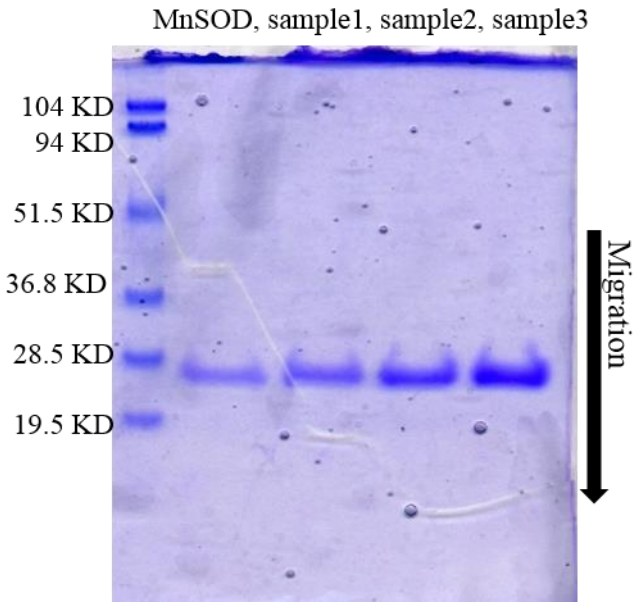


Figure 2-8: 12% SDS-PAGE (sodium dodecyl sulfate-polyacrylamide gel electrophoresis) profile of purified MnSOD from supernatant of cell culture.

From left to right is protein molecular weight standards, control MnSOD and triplicate protein sample 1, 2, and 3 purified through simplified method. Protein plus protein molecular weight standards (Bio Rad Laboratories 4110027). The overexpressed MnSOD is purified through simplified method as stated in the method 2.2.2. Samples of protein after purification were subjected to 12 % SDS-PAGE and stained with the Coomassie brilliant blue R250 afterwards.

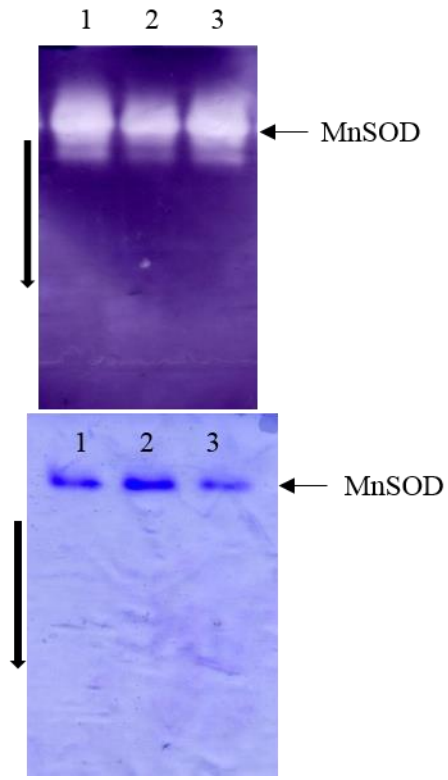


Figure 2-9: Non-denaturing gel electrophoresis of MnSOD.

Comparison of the simplified method to traditional method for activity of purified MnSOD by non-denaturing gel electrophoresis. Lane 1 – MnSOD purified by traditional method; Lane 2 – MnSOD purified by simplified method; Lane 3 – MnSOD purified by simplified method. Protein samples were separated using electrophoresis through 4-12 % acrylamide gels. About 5.5 µg protein was loaded to the bottom gel per lane and stained with Coomassie brilliant blue R-250. About 2.8 µg protein was loaded to the top gel per lane and stained using the nitroblue tetrazolium/riboflavin photochemical method.[7] Both gels were running under the same condition in parallel as described in the methods.

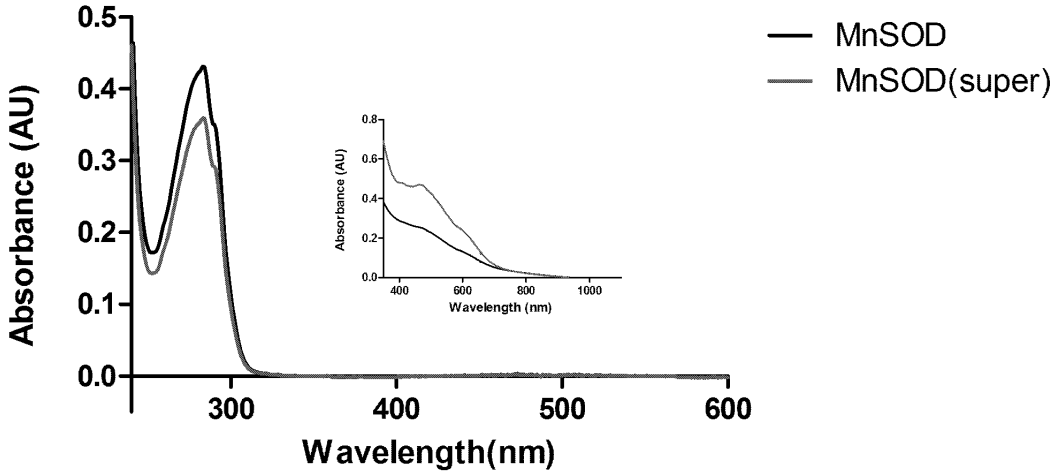


Figure 2-10: A comparison of absorbance spectrum of the clarified MnSOD from supernatant and cell pellet.

MnSOD indicates protein isolated following the traditional method 2.2.1. MnSOD (super) indicates protein sample is purified following the simplified method 2.2.2. The spectrum covers 220 nm through 600 nm to show the UV bands of nucleic acids and protein. Inset graph is to show a vertical expansion of the visible ranges of both protein samples reflecting the signature of $Mn^{3+}$ SOD at 478 nm. MnSOD and MnSOD (super) is measured under different concentration.

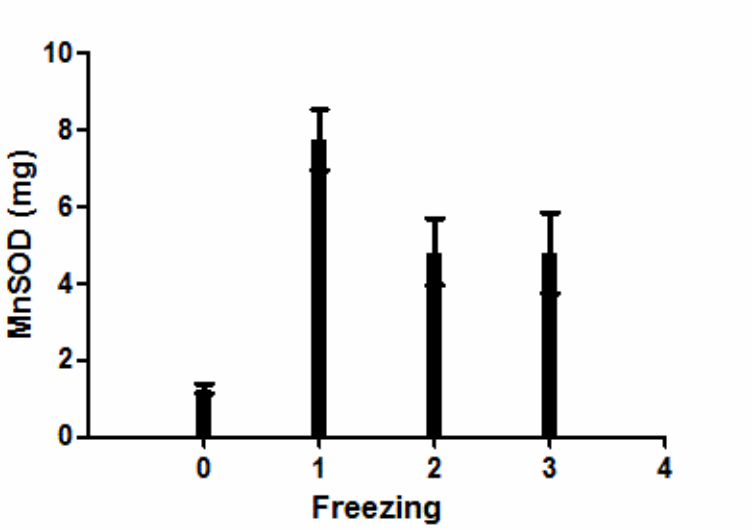


Figure 2-11: The amount of MnSOD protein released into the cell suspension buffer upon freeze/thaw.

The figure is to compare the amount of MnSOD protein released from *Ox326-A* cell paste without freezing (labeled as 0) or through successive freeze/thaw cycles (label as 1, 2, 3). Bar -0: the amount of MnSOD protein released into the cell suspension buffer from cell pellet that was not subjected to freeze/thaw. Bar -1, -2, -3: the amount of MnSOD protein released into cell suspension buffer from cell pellet at the first, second and third freeze/thaw cycle. The protein in the supernatants of successive freeze/thaw cycles were also compared by SDS-PAGE upon staining with Coomassie brilliant blue R250 (Figure 2-12).

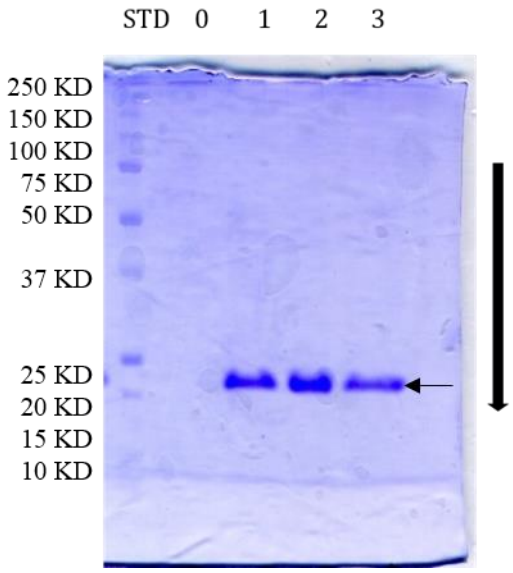


Figure 2-12: The MnSOD protein collected from cell supernatant through freeze/thaw.

Arrow indicates the band of MnSOD protein. Lane -0: supernatant from cell that didn't go through freeze/thaw cycle. Lane -1, -2, -3: supernatant from the cell pellet that went through freeze/thaw for the first, second, or third time. Protein sample were loaded onto SDS-PAGE and stained with Coomassie brilliant blue R250.

## Chapter 3 Characterization of MnSOD and its mutant Q146E

### 3.1 Introduction

Four different types of superoxide dismutase (SOD) were identified, based on the identity of their redox-active metal cofactor: the manganese-containing SODs(MnSODs), the iron-containing SODs(FeSODs), the copper and zinc-containing SODs(CuZnSODs) and the nickel-containing SODs (NiSODs).[73] Although encoded by different genes, FeSOD and MnSOD are believed to have evolved from a common ancestor because they display homologous structures and similar amino acid sequences. Their amino acid conservation are particularly strong near the active site with all four ligands to the metal ion being identically conserved in all FeSODs and MnSODs.[5, 74] Thus it is not surprising that MnSODs can be prepared with Fe bound instead of Mn ion[19c, 28, 45b, 75] and similarly some FeSODS have been prepared with Mn bound.[42a, 64, 75b] In each case native-like coordination geometry is still retained,[25a, 48, 54, 74, 76] with the major difference being the expected altered Lewis acidity which is manifested by a higher affinity for small anions including $OH^{-\cdot}$ on the part of $Fe^{3+}$.[10, 31, 33, 54] While a few so-called 'cambialistic' Fe/MnSODs have been identified that are display activity under physiological conditions regardless of which of Fe or Mn is bound,[77] the canonical Fe- and MnSODs each require that their cognate metal ion be bound in order to perform with optimal enzymatic activity[19c, 26, 64]. The bases for SOD's metal ion specificity provide insights into the crucial interface between protein and metal ion wherein the protein tunes the metal ion reactivity and the metal ion gives rise to the enzyme's signature activity.

MnSOD employs a ping-pong mechanism to convert two equivalents of superoxide to one each of peroxide and dioxygen.

$$E - Mn^{3+}(OH^-) + O_2^{\cdot-} + H^+ \rightarrow E - Mn^{2+}(H_2O) + O_2 \quad (3.1)$$

$$E - Mn^{2+}(H_2O) + O_2^{\cdot-} + H^+ \rightarrow E - Mn^{3+}(OH^-) + H_2O_2 \quad (3.2)$$

where E stands for the SOD protein and Mn indicates the active site Mn ion.[5] The capacity of the enzyme to both oxidizing and reducing substrate depends on its reduction midpoint potential, *E*°. The inactivity of metal ion substituted SODs has been explained on the basis of their too-high (Mn-substituted FeSOD) or too-low (Fe-substituted MnSOD) *E*°s.[31, 42a, 43] Indeed, mutation of the conserved Gln69 that distinguishes FeSODs from MnSODs resulted in large changes in *E*°, with the Q69H and Q69E mutant FeSODs displaying *E*°s elevated by 250 mV and >600 mV respectively.[45b]

The most highly conserved difference between FeSODs and MnSODs is the origin of a Gln or His residue present in both of their active sites.[22, 78] The two types of SOD employ the same coordination sphere: three histidine (His26, His81 and His171, *Escherichia coli* MnSOD numbering) and an aspartate (Asp167), plus a coordinated solvent molecule (interpreted as a water or hydroxide depending on whether the metal ion is $Mn^{2+}$ or $Mn^{3+}$, respectively).[50b, 54, 79] The coordinated solvent molecule is the terminus of an active site hydrogen bond network that connects it to bulk solvent via a second-sphere glutamine (Gln146 in *E. coli* MnSOD and Gln69 in *E. coli* FeSOD) which H-bonds with the hydroxyl group of conserved Tyr34 which in turn H-bonds with a solvent molecule in the channel connecting the active site to bulk solvent (Figure 1-2 and 1-3).[10, 42b, 79] The coordinated solvent contributes a proton essential to the reaction (equation 3.2) in which

superoxide becomes reduced to peroxide and the active site returns to its oxidized state containing $Mn^{3+}$ and coordinated $OH^-$.[51, 80] It acquires the needed proton in conjunction with $Mn^{3+}$ reduction to $Mn^{2+}$, and proton acquisition is coupled to Mn reduction over the full physiological range[80] as in FeSOD.[81] Hence the *E*° reflects the energy associated with protonation of coordinated solvent.[43] Indeed the Gln that H bonds to coordinated solvent has been shown to modulate the *E*° over many hundreds of mV.[42b, 43, 45b] This consistent with the fact that the H-bond with Gln connects the coordinated solvent to the SOD protein beyond the coordination sphere and thus enables the protein to modulate the coordinated solvent's $pK_a$s. It also makes chemical sense of the different placements of the Gln or the His that takes its place, in FeSODs vs. MnSODs. Indeed MnSODs contribute the conserved Gln from a position between a beta strands in the C-terminal domain (Figure 1-1 and Figure 1-2, residue 146 in *E. coli* MnSOD numbering) whereas FeSODs contribute the Gln from an alpha helix in the N-terminal domain.[22, 78]

Gln146 has been replaced by several different residues in human and *E. coli* MnSOD. Replacements with His and Leu retain only 5 – 10 % of the dismutase activity of the wild-type enzyme and produced changes in the metal ion spectral signatures, anion binding and the contribution of a dead-end complex to the catalytic cycle.[53,54,55,31] The observed changes were also compatible with altered midpoint reduction potential *E*°*s*, although this is a difficult parameter to measure.[42b] These effects parallel those observed when the corresponding Gln69 of FeSOD was mutated to His or Glu.[45] The Gln146 to Glu mutation has also been made for MnSOD, however for both the *E.coli* and the human enzyme, the Q146E mutant was isolated as inactive apo-protein.[35b, 42b, 49] Because SOD activity is absolutely dependent on the redox-active metal ion, these studies were not able

to proceed nor revealing the effect of the amino acid side chain alternation on activity. However, given that the reduction potential of the enzyme represents the difference between the stability of the protein complex with the 2+ ion *vs*. that of the complex with the 3+ ion, a proposed role in redox tuning for Gln146 is not inconsistent with destabilization of either or both Mn complexes. However failure of Q146E-MnSOD to assimilate Mn could also represent failure of co-translational Mn insertion steps.

To learn whether the predominance of the apo-Mn form of the Q146E variant, Q146E-apoMn-SOD, represents a kinetically trapped failure to acquire Mn during folding or the result of thermodynamic destabilization of the holoMn form, we have compared the thermal stabilities of both the apo proteins, Q146E-apoMn-SOD and WT-apoMn-SOD, as well as those of the metal containing forms WT-holoMn-SOD, using far-UV CD to quantify secondary structure as a function of temperature. Our data reveal that the Q146E substitution results in an apoMn protein that is much more thermally stable than the WT apoMn protein, and moreover confers greater stabilization than does Mn binding! We find that Mn or Fe binding greatly stabilizes the WT-SOD protein but not the Q146E mutant. Thus we propose that the conservation of Gln over Glu at position 146 represents selection for high-affinity acquisition of metal ions by SOD, at the cost of the stability of the protein folding. The natural conservation of the destabilizing amino acid, Gln, at position 146 is superficially counterintuitive but can be understood as part of a strategy favoring metal ion binding, as well as possible $E°$ tuning.

## 3.2 Materials and methods:

This chapter deals with MnSOD proteins that may or may not contain metal ion, and may be either WT or mutant with an amino acid substitution at position 146. Therefore we have developed the following nomenclature. Manganese superoxide dismutase, WT-Mn-SOD, is properly referred to as wild-type manganese containing superoxide dismutase protein. Manganese superoxide dismutase protein lacking Mn ion is referred to as apo-manganese superoxide dismutase, apoMn-SOD. FesubMn-SOD indicates Fe-containing Mn-SOD, *i.e.* iron substituted manganese superoxide dismutase. The Q146E variant of MnSOD incorporates a substitution of Glu for Gln at position 146 in the MnSOD protein. Q146E-apoMn-SOD was the apo protein of mutant Q146E normally produced by expression of the corresponding gene in bacteria growing in manganese supplemented medium ([Mn] = 35 μM). Q146E-FesubMn-SOD indicates the iron substituted version of this protein Q146E and was normally produced by overexpression of the mutated gene in bacteria grown in iron supplemented growth medium ([Fe] = 10 μM) to which Mn had not been added. Nevertheless both Q146E-apoMn-SOD and Q146E-FesubMn-SOD was found predominantly as apo-protein, lacking both Mn and Fe ion and possessing very limited catalytic activity regardless of whether Fe or Mn was supplemented to the growth medium. Thus in brief Q146E was generally used to referring the apo-protein Q146E, the mutant of wild-type MnSOD.

MnSOD protein was overexpressed in *Ox326-A Escherichia coli (E. coli)* which is a double deletion cell strain lacking the chromosomal genes for both FeSOD and MnSOD (ΔsodAsodB). *Ox326-A* was transformed with the sodA gene-bearing plasmid pET21 pAK0. Protein was purified following the simplified method as described in the section

2.2.2 of chapter 2. Protein concentrations were determined by molar absorptivity at 280 nm, with extinction coefficients of 86600 $M^{-1}$ $cm^{-1}$, 91900 $M^{-1}$ $cm^{-1}$, and 89500 $M^{-1}$ $cm^{-1}$ per dimer for Mn-SOD, FesubMn-SOD, and apoMn-SOD, respectively.[7]

### 3.2.1 Activity assay by nondenaturing PAGE

Specific activity was assessed qualitatively by resolving SOD using nondenaturing PAGE (polyacrylamide gel electrophoresis) and then staining using nitroblue tetrazolium (NBT) and riboflavin.[7] Nondenaturing PAGE was carried out with 4 – 12 % polyacrylamide gel in a Tris-HCl/glycine buffer at pH 8.3. Each gel was loaded with ~50 μg of protein and electrophoresed for ~ 2 hours at 100 volts. The activity assay was conducted by soaking the gel in 0.3 mM NBT solution for 30 min in dark and next in 28 μM riboflavin solution for 30 min in dark before irradiating with UV light for 20-30 min. In this assay, SOD activity manifests itself as an absence of the purple color which results from the reaction of photochemically-produced superoxide with NBT to form blue-purple formazan. As a control, to reveal the mobility of protein bands, a duplicate gel was run in parallel and stained by Coomassie brilliant blue R250 solution and de-stained by solution of 10 % acetic acid, 50 % methanol and 40 % $H_2O$.

### 3.2.2 Metal ion reconstitution

A solution of Q146E-apoMn-SOD was dialyzed against 3.5 M guanidinium hydrochloride (GdmCl), 20 mM Tris-HCl, and 10 mM EDTA at pH 3.1 overnight at 4 °C until the pH inside the dialysis bag was pH 3.1. A freshly prepared dialysis buffer solution containing 2.5 M GdmCl and 20 mM Tris-HCl at pH 8.0 was deoxygenated by sparging with nitrogen $N_2$ for an hour, and then used to dialyze the solution of SOD protein for

another 8 h to remove EDTA. $FeCl_2$ solution was directely added into the dialysis bag to produce a final concentration of 1 mM. To eliminate the contamination from EDTA, the dialysis bag containing unfolded Q146E-apoMn-SOD and $Fe^{2+}$ was transferred to EDTA-free dialysis buffer, 2.5 M GdmCl and 20 mM Tris-HCl at pH 8.0 and incubated at 45 °C for 30 min (a range of times were tried, 30 min proved best). SOD was allowed to refold by dialyzing against 25 mM $K_2HPO_4$, pH 7.4 for 8 – 12 h at 4 ℃, during which time the solution was kept anaerobic by continuous sparging with $N_2$ gas. To remove excess Fe, EDTA was added to a final concentration of 1 mM. After 20 - 30 min, the protein solution was cleaned by chromatography over DEAE-Sephadex G-25 (5 cm × 30 cm) pre-equilibrated and eluted with 5 mM phosphate pH 7.4.

### 3.2.3 Circular dichroism (CD)

Measurement of circular dichroism was performed on a Jasco J-810 circular dichroism spectropolarimeter (Jasco, Tokyo, Japan) equipped with a temperature controller and a Peltier multicell holder. Wavelength scans were performed between180 and 250 nm in 5 mM potassium phosphate buffer pH 7.4 with 6 µM protein sample in 1-mm quartz cuvettes at room temperature. The bandwidth was 1nm and at least 4 scans were accumulated per spectrum. A baseline was obtained by collecting the CD spectrum of the protein free buffer solution also. Secondary structure were analyzed using the program SELCON3 from the CDPro software package and the SP29 protein data base.[82]

To characterize protein stability, CD spectra were acquired as a function of temperature from 20 ℃ to 100 ℃. To mitigate protein aggregation and attendant irreversibility, the proteins samples were all in buffer comprised of 0.8 M GdmCl and 5

mM potassium phosphate pH 7.4. Because GdmCl solution absorbs light very strongly at wavelengths shorter than 205 nm, short path-length cuvettes (1 mm) were required to permit wavelength scans from 250 to 210 nm. All spectra were recorded at a scanning rate of 100 nm/min with a wavelength step of 0.2 nm in the far UV range from 210 to 250 nm. The temperature of the protein solution was controlled to an accuracy of 0.1 ℃ using a Peltier thermoelectric device coupled to the cell holder. The temperature was increased at a speed at 1 ℃/min and data points were recorded every 5 ℃ or 1 ℃ from 20 to 100 ℃. For thermal denaturation profile, the reduction of ellipticity at 222 nm was used to measure the loss of protein secondary structure.

The value of apparent denaturation midpoint ($T_m$) of the individual thermal unfolding curves were obtained from the program CD analysis program called "CDpro" following the least-squared minimization to a two-state model. Each curve is fitted into a two-state model with unconstrained linear baselines for the folded and unfolded state. The fitting each includes adjustable six parameters: $T_m$, $\Delta H_m$ (the enthalpy of unfolding at the *Tm*) and linear equation (y = ax+b) as the baselines for foleded and unfolded states.

Analysis of the CD ellipticity at 222 nm vs. temperature allows the melting curves to be interpreted in terms of thermodynamics parameters of protein unfolding by utilizing the van't Hoff equation:

$$\Delta G = -RTlnK_{eq} = \Delta H - T\Delta S \tag{3.3}$$

$$lnK_{eq} = \frac{-\Delta \mathrm{H}}{\mathrm{R}}\frac{1}{T} + \frac{\Delta S}{R} \text{ where } \quad _{eq} = \frac{[U]}{[N]} \tag{3.4}$$

A van't Hoff plot of the data, wherein ln($K_{eq}$) is plotted versus 1/T is expected to yield a straight line. If so, using of the van't Hoff equation (equation 3.4) permits determination of the enthalpy of unfolding, $\Delta H$, from the slope, $\Delta H/R$, where R is the ideal gas constant.

We describe protein denaturation as a transition from Native (N) to unfolded (U): $N \rightarrow U$. The temperature at which [U] equals [N] is called the melting temperature $T_m$, and at $T_m$ temperature $\Delta G = -RTlnK_{eq} = -RTln(1) = 0$ (equation 3.3), meanwhile $\Delta G = \Delta H - T\Delta S = 0$ (eqs 3.2), thus ΔS can be determined from $\Delta S = \Delta H/T_m$.

The free energy of protein denaturation determined by utilizing van't Hoff equations $\Delta G = -RTlnK_{eq} = \Delta H - T\Delta S$ (equation 3.3). According to classical thermodynamics, the values of $\Delta H$ and $\Delta S$ at two different temperatures $T_1$ and $T_2$ are related by the following equations (equations 3.5 and 3.6), respectively where $\Delta C_p$ is the specific heat capacity and the temperature dependence of $\Delta C_p$ is neglected over small temperature differences $T_2$-$T_1$.

$$\Delta H_{T_2} = \Delta H_{T_1} + \Delta C_p(T_2 - T_1) \quad (3.5)$$

$$\Delta S_{T_2} = \Delta S_{T_1} + \Delta C_p ln\frac{T_2}{T_1} \quad (3.6)$$

Hence, the free energy of unfolding $\Delta G = \Delta H - T\Delta S$ can be written as:

$$\Delta G_{T_2} = \Delta H_{T_1} + \Delta C_p(T_2 - T_1) - T_2(\Delta S_{T_1} + \Delta C_p ln\frac{T_2}{T_1}) \quad (3.7)$$

When an amino acid substitution or metal ion loss alters a protein's free energy of unfolding, this can cause a change in $T_m$, called $\Delta T_m$. By differentiating equation (equation

3.7) with respect to $T_m$, the change in the free energy of thermal denaturation caused by the substitution (or absence metal ion cofactor) can be determined as follows.[47]

$$\Delta\Delta G \approx \Delta T_m \Delta S \approx \Delta H_{T_m} \frac{\Delta T_m}{T_m} \quad (3.8)$$

### 3.2.4 Reversibility assay by Circular Dichroism

Temperature induced refolding and unfolding was accomplished using a Jasco J-810 circular dichroism spectropolarimeter (Jasco, Tokyo, Japan) equipped with a temperature controller and a Peltier multicell holder. Circular dichroism (CD) spectroscopy has been used to monitor protein secondary structure as a function of temperature, holoMn-SOD, apoMn-SOD and Q146E-apoMn-SOD, in the presence of 0.8 M GdmCl pH 7.4. Protein samples were warmed to a temperature at which its melting curve indicates substantial completion of the first stage of the melting but not the second (70 ℃ for holoMn-SOD, 60 ℃ for apoMn-SOD and 85 ℃ for Q146E-apoMn-SOD). Protein was incubated with or without 100 μM Mn for 30 min and then cooled down to 20 ℃ at a rate of 1 ℃ / minute while measuring the ellipticity [Θ] at 222 nm every 5 ℃.

To make sure the proteins have been fully folded after the temperature of sample cooling down to 20 ℃, all the SOD samples were allowed to save in refrigerator for 8 – 12 h at 4 ℃. Then the fully recovered protein samples experienced the temperature induced unfolding following the method described in 3.2.3.

### 3.2.5 Batch scale temperature-induced metal ion binding

Temperature induced metal ion reconstitution was accomplished using a temperature-controlled water bath. Because the results of fluorimetrically-detected metal ion uptake assays indicated that metal ion reconstitution occurs during thermally-induced protein melting,[32c] protein samples were incubated at elevated temperature in the presence of desired metal ions (70 ℃ for holoMn-SOD, 60 ℃ for apoMn-SOD and 85 ℃ for Q146E-apoMn-SOD). Temperature based on $T_m$ values observed by the CD-detected protein melting curves. Metal ions were added at a final concentrations of 100 μM and the concentration of protein was 100 μg/ml (= 4.35 μM with respect to monomers) in a buffer of 5 mM phosphate buffer and 0.8 M GdmCl at pH 7.4. After $MnCl_2$ was added to the protein solution, the protein solution was incubated for 30 min at each designated temperature. Q146E-apoMn-SOD solution was incubated at 85 °C and apoMn-SOD solution at 45 °C, temperatures chosen to be ~5°C lower than the respective $T_m$s. To allow the protein to refold to its native structure after incubation, the protein sample solution was stored at 4 °C overnight 8 – 12 hours before characterizing its enzymatic activity by xanthine/cytochrome c, nondenaturing PAGE and the NBT catalytic activity assay.

## 3.3 Results and discussion:

### 3.3.1 UV-Vis absorption spectrum of MnSOD and its mutant Q146E

The ultra-violet (UV) absorption spectrum of the *E. coli* WT-Mn-SOD is compared with that of its Q146E variant in Figure 3-1. The spectrum of WT-Mn-SOD is very similar to those of Q146E-FesubMn-SOD and Q146E-apoMn-SOD. The strong absorption at near UV reflects the enzyme's content of tryptophan, tyrosine and phenylalanine residues. The molar absorptivity at 280 nm is 86600 $M^{-1}$ $cm^{-1}$ for dimer of MnSOD.[83] Besides the peak

at 280 nm characteristic of Trp,[75a] shoulders at 290 nm were observed also. The salient features of the spectra are summarized in Table 3-1.

### 3.3.2 Protein catalytic activity and metal content

Q146E protein was found to be predominantly apo-protein as isolated (0.5 % Mn per site, Q146E-apoMn-SOD) and possessing very limited catalytic activity regardless of whether or not Mn was provided as a supplement to the medium (Table 3-3). Due to the lack of active site metal ion, it was not possible to investigate the effect of the Q146E mutation on activity, and efforts were made to bind Mn or Fe to the Q146E-apoMn-SOD protein.

The failure of Q146E-apoMn-SOD to accept Mn or Fe ion could reflect possible competition with another metal ion. Given the absence of a spectroscopic signature, and based on literature precedent,[84] we examined the possibility that Zn could have been entered into the active site during maturation in vitro, by assaying as-isolated proteins for Zn content. ICP-OES revealed a bound Zn ion stoichiometry of about ~ 0.03 per dimer, indicating that Zn did not take the active sites and thereby preclude binding of Mn or Fe.

To incorporate metal ion into mutant Q146E-apoMn-SOD, the method of Yamakura as modified by Vance and Miller was applied, using either Mn or Fe as described in 3.2.2.[31, 85] The metal ion contents after reconstitution are reported in Table 3-2 as "metal/dimer after reconstitution". The metal ion content could only be increased to 10 % when reconstituting with Mn ion, or 15 % when reconstituting with Fe ion. We attributed this weak yield of metal ion-replete sites to the Q146E mutation because application of the same method to WT-apoMn-SOD reconstituted Mn to 80-90 % of the active sites.

The low metal ion content of Q146E-Mn-SOD or Q146E-FesubMn-SOD does not suffice to explain the low specific activities measured. Relative to the WT Mn-supported specific activity of ~20,000 u/mg protein, we calculate that specific activity of 2,000 u/mg protein would constitute 100% activity on a per-Mn ion basis. However Mn-reconstituted Q146E-SOD displayed activity < 1 u/mg protein. Therefore it represents a per-Mn ion adjusted activity of only ~0.05 % WT activity and we conclude that under the standard assay conditions, Q146E-Mn-SOD and Q146E-Fe-SOD have negligible activity compared to the WT-holoMn-SOD, and therefore that the Q146E mutation impairs catalytic function even when metal ion is present, in addition to preventing its acquisition on metal ion.

### 3.3.3 Protein thermal-stability by circular dichroism

The reconstitution experiments indicate that Q146E-apoMn-SOD has a low affinity for metal ions. This could be because the metal-bound form is relatively unstable and/or the apo-form is relatively more stable. To test the stability of Q146E-apoMn-SOD and compare it with that of WT-apoMn-SOD and the WT-holoMn-SOD, far-UV circular dichroism (CD) was applied to monitor protein secondary structure as a function of temperature for these three protein samples, in the presence of 0.8 M GdmCl. This concentration of GdmCl has been used as a buffer additive in studies of MnSOD denaturation to prevent protein aggregation and thereby create conditions where the protein unfolding is more reversible and amenable to van't Hoft analysis.[86] Superimposable far-UV CD spectra were obtained for Q146E- and WT- apoMn-SOD as well as WT-holoMnSOD (Figure 3-2), with negative CD peaks at 208 nm and 222 nm consistent with SOD's strong alpha helix content about 25 – 35 % (Figure 3-3). The ellipticity at 222 nm

reflects contributions from both alpha helices and beta sheets and therefore provides a measurement of the amount of secondary structure retained by the protein.[82a]

For WT-holoMn-SOD, the ellipticity at 222 nm ($\theta_{222}$) changed only slightly between 20 °C and 60 °C (Figure 3-4). However above 65 ℃, $\theta_{222}$ decreased sharply with approximately 95 % of the ellipticity loss occurred within a 5 ℃ range centered at 67 °C indicating cooperative protein unfolding. A shoulder at lower temperature has been attributed to active site conformation change including Mn loss.[48]

Unlike the single dominant helix-coil transition evident for WT-holoMn-SOD, two melting phases can be discerned for the unfolding process for apoMn-SOD (Figure 3-4, 16 % Mn ion per dimer, in Table 3-3), one beginning as early as 45 °C and the second beginning at 70 ℃. The higher-temperature phase has a temperature profile very similar to that of WT-holoMn-SOD so we assign it to the same event. Its amplitude is consistent with the percentage of active sites occupied by metal ion (16 %), which is discussed further below.

Because Q146E-apoMn-SOD contains Mn in only 0.5 % of the active sites (Table3-3), it is most appropriately compared with WT-apoMn-SOD with a lower temperature induced unfolding (Figure 3-4). But unlike WT-apoMn-SOD, melting of Q146E-apoMn-SOD required heating over 80 °C, and a transition complete within the rage (80.1 - 93.1) ℃ = 13.02 ℃ accounts for ~77 % of the ellipticity loss. The melting temperature of $T_m$ = 87.9 ℃ $\pm$ 0.1 is significantly higher than that of either WT sample (Figure 3-4) and its sharp shape suggests a highly cooperative event associated with very stable structure. The melting

temperature of Q146E-apoMn-SOD is more than 35 ℃ higher than that of WT-apoMn-SOD indicating that replacement of Gln146 by Glu stabilizes the structure of this protein substantially. Thus, for the apo-proteins, the WT is *not* the most stable variant of this protein, contrary to common expectation. The form of this protein that is subject to selection is not the apoMn form but the holoMn form. However even that is less stable than Q146E-apoMn-SOD under these conditions. Thus mutation of Gln146 to Glu confers greater stabilization than does binding of Mn.

In addition to the major transition at high temperature, Figure 3-4, hints at a small amplitude (~ 3 %) loss of ellipticity for Q146E-apoMn-SOD in the temperature range of 45 °C to 60 °C. This could represent possible another event that has a subtle effect on secondary structure, or the signature of a minority form of the protein (sample heterogeneity).

In a fully metallated MnSOD, each monomer has an independent metal ion binding site buried in the interior of the protein, surrounded by hydrogen bonding from amino acid side chains arising from the second shell. Two of the ligands (His30 and His81) derived from the N-terminal domain whereas the other two (Asp167 and His171) derived from the C-terminal domain. Circular dichroism (CD) spectroscopy was used to monitor protein secondary structure as a function of temperature for these three proteins, holoMn-SOD, apoMn-SOD and Q146E-apoMn-SOD, in the presence of 0.8 M GdmCl. The hypothesis that the metal cofactor in the active site significantly stabilizes the protein structure and enhances its thermostability, is reflected by the ~25 °C shift in melting temperature distinguishing MnSOD (71 ℃) from apoMn-SOD (53 ℃) (Figure 3-4 and 3-5). The melting

temperature ($T_m$) of Q146E-apoMn-SOD of ~ 88 °C (Figure 3-4 and 3-6) is more than 35 ℃ higher than that of apoMn-SOD (53 ℃ ) and even 20 ℃ higher than that of holoMn-SOD (metal ion-replete) (67 ℃). For Q146E-apoMn-SOD, given that the active site hydrogen bond network that surrounds the metal ion cofactor is crucial for the protein thermalstability, it is plausible that center of the hydrogen network, a mutated Glu at position 146, can't 100 % be involved in the hydrogen bonding at the active site, unlike the native amino acid at position 146. When matching the metal content of protein with the changes of ellipiticity at melting temperature (Figure 3-6 and 3-8), the extreme low metal content of Q146E-apoMn-SOD is mostly in agreement with the amplitude change of ellipiticility appearing at 55 – 65 ℃ contrast to the results of wildtype apoMn-SOD (Figure 3-5 and 3-7). The structure of Q146E-Mn-SOD which may simply be less stable than Q146E-apoMn-SOD. Therefore when the mutant protein Q146E-apoMn-SOD were given the access to metal ion, very little Q146E-Mn-SOD is formed. The partially breaking of hydrogen bonding network of Q146E-apoMn-SOD for metallation or the losing of protein stability by metal uptake might be responsible for very small portion of the metalated protein Q146E-MnSOD.

### 3.3.4 Metal content *vs* melting temperature

Minor transitions were observed in the melting curves of both WT-apoMn-SOD and Q146E-apoMn-SOD, in addition to their respective major transitions. To learn whether the presence and relative amplitudes of the minor CD transitions could be explained by sample heterogeneity with respect to metal ion occupancy, we compared high-resolution CD melts of a series of WT-SOD samples with varying metal ion compositions (Figure 3-5), and a similar series of Q146E-SOD samples (Figure 3-6).

In figure 3-5, samples of WT-SOD with varying active site occupancy are compared. The percentage of total ellipiticity loss occurring at the high temperature transition (above 60 ℃) proves to be linearly proportional to the percentage of active sites containing metal ion, even when the identity of the metal ion was varied between Mn and Fe ion (Figure 3-7). Therefore we attribute the high-temperature transition to enzyme subunits containing metal ion and the remaining amplitude (the low-temperature transition) to the enzyme subunits lacking metal ion.

Figure 3-6, presents the analogous experiment for Q146E-apoMn-SOD, wherein the amplitude of the high temperature phase (above 60 ℃ ) accounted for ~ 91 %, ~ 90 %, and ~ 77 % of total ellipticity loss, while the percentage of active sites occupied by metal ions was only ~ 0.5 %, ~ 1 % and ~ 10 %, respectively. This result contrasts with the conclusion reached for WT-SOD. It is evident that the fraction of Q146E-SOD melting at high temperature (above 60 ℃) is not in proportion to metallated Q146E-holoMn-SOD. However the percentage of ellipticity lost in the minor transition near 50 °C is in better agreement with the percentage of active sites containing metal ion. A plot of % secondary structure loss associated with the lower-T transition vs. % metal ion occupancy (Figure 3-8) indicates that these values are indeed correlated, although the low metal occupancies attainable limit the amplitude of the plot and the accuracy of its slope (Figure 3-8). The data nonetheless argue that the low-temperature and high-temperature transitions are most reasonably attributed to the population metal ion-containing and metal ion-free subunits, respectively. This constitutes a reversal of the assignments reached for WT-SOD.

### 3.3.5 Protein refolding as a function of free metal ion presence

The reversibility of the CD transitions was tested for both WT- and Q146E- apo-SOD. After unfolding each at its appropriate melting temperature for ~ 30 min ( 60 ℃ for apoMn-SOD, 70 ℃ for holoMn-SOD and 85 ℃ for Q146E-apoMn-SOD), samples of WT-holoMn-SOD, WT-apoMn-SOD and Q146E-apoMn-SOD were cooled again gradually by 1 ℃/min and ellipticities were measured every 5 ℃ (Figure 3-9). All samples displayed at least partially reversibility with respect to secondary structure loss at the higher-temperature $T_m$ (Figure 3-9 left column). Because one aspect of unfolding of MnSOD is loss of bound metal ion, the recovery of ellipticity was compared in the presence vs. the absence of excess free $Mn^{2+}$ in the buffer. Figure 3-9 indicates that more ellipticity is recovered when refolding occurs in the presence of 100 μM Mn. Interestingly, this was true even for Q146E-apoMn-SOD although the above data suggested that the resulting species: Q146E-holoMn-SOD, is less stable than the apo form. In all cases, the value of the ellipticity recovered in the presence of 100 μM $Mn^{2+}$ after the cooling was some 80% of the ellipticity observed for sample protein prior to heating. In comparison only ~35 % of the initial ellipticity was recovered in the absence of $Mn^{2+}$. This suggests that Mn binds to a substantial fraction of active sites while cooling down. The amplitude of ellipticity recovered could be somewhat different for apo vs. holo-SOD, although the crystal structure of WT-apoMn-SOD has been solved and found to be superimposable on that of WT-holoMnSOD.[25a, 54] Finally, unlike the melting process, the recovery of ellipticity did not occur with well-defined temperature transitions but instead occurred over a broad span of temperature from the $T_m$ to the endpoint of ~ 30 ℃. Studies elucidating on this process will

need to include characterization of its rate, as well and the metal ion composition of the protein formed as a function of temperature, but are beyond the scope of the current effort.

Although only ~ 80 % of WT-SOD's ellipticity was recovered, this is still very significant and can be shown to reflect recovery of secondary structure by the fact that reheating of these samples while monitoring ellipticity at 222 nm reproduced the $T_m$ values observed of samples that had not been previously unfolded (Figure 3-9 right column). The lower prominence of the lower-temperature transition for WT-Mn-SOD refolded with added Mn further confirms its assignment to WT-apoMn-SOD. Moreover the lower-temperature transition is less striking for samples that had initially been WT-holoMn-SOD than for samples initially WT-apoMn-SOD, consistent with rebinding of the $Mn^{2+}$ carried into the samples by the starting holoMn protein.

Figure 3-9, also shows that the melting curve of WT-apoMn-SOD that had been cooled in 100 μM $Mn^{2+}$ no longer displayed the strong low-temperature transition of apoMn-SOD (Figure 3-5) but instead displayed a much stronger and sharper higher-temperature $T_m$, becoming more similar to the melting curve of holo-MnSOD (compare Figure 3-9 with Figure 3-5 and 3-4). These observations support the hypothesis that $Mn^{2+}$ binds during the incubation at 60 °C and stabilizes the secondary structure of the MnSOD protein.

The recovery of the high-temperature transition with the characteristic very high $T_m$ of Q146E-apoMn-SOD upon cooling suggests that the protein refolded and recovered the starting structure, as for WT-SOD (Figure 3-9). The melting curve of Q146E-apoMn-SOD after incubation and cooling with 100 μM $Mn^{2+}$ was similar to that of Q146E-apoMn-SOD

with respect to the large loss of ellipticity at approximately 95 ± 1 ℃ (compare Figure 3-9 and Figure 3-6), but displayed a low-temperature transition at 42.4 ± 0.4 ℃ of greater amplitude than that of the initial Q146E-apoMn-SOD, more similar to the melting curve of Q146E-recMn-MnSOD containing 0.1 Mn ion per site. The dependence of the low-temperature transition amplitude in the presence of $Mn^{2+}$ during refolding suggests that the protein was able to bind some $Mn^{2+}$ and that similar to WT-SOD, this is associated with greater ellipticity, which could reflect greater population of the native secondary structure or a greater extent of it. Unfortunately the concentrations of these samples are too low to permit analysis of their Mn content to quantify acquired $Mn^{2+}$ and the very low activity of Q146E-holoMn-SOD makes the enzyme activity relative insensitive as well.

### 3.3.6 Metal status of protein after reconstitution by nodenaturing PAGE

To learn whether SOD proteins bind Mn when incubated with $Mn^{+2}$ at their $T_m$, we exploited the capacity of non-denaturing electrophoresis to resolve apoMn-SOD from SOD with one Mn bound ($Mn_1$-SOD) and SOD with two Mn bound ($Mn_2$-SOD).[25a, 60, 87] Samples of WT-apoMn-SOD and Q146E-apoMn-SOD were incubated with 100 μM $Mn^{2+}$ at temperatures equal to their respective $T_m$s for 30 min (as in the above experiments, detailed procedure described in section 3.2.5) and then analyzed by non-denaturing PAGE in which the set of samples was loaded in each gel. One half of the gel was stained to reveal protein bands and the other to visualize SOD activity.[83]

Figure 3-10 shows the electrophoretic pattern before and after incubation with $Mn^{2+}$ for each of WT-apoMn-SOD and Q146E-apoMn-SOD. The WT-holoMn-SOD control in land 1 is isolated predominantly in di-manganese form shown as the predominance of the

upper band, consistent with the result of Mn ion analysis (Table 3-2). Before incubation, WT-apoMn-SOD is predominantly in the mono-manganese and apo-manganese forms forms (Figure 3-10 lane 2). However after incubation at $T_m$ for 30 min in the presence of 100 μM $Mn^{2+}$, the band attributed to the WT-apo-manganese form (lower band) disappears and the majority of the protein sample becomes the di-manganese form $Mn_2$-SOD (upper band) (Figure 3-10 lane 3). For WT-apoMn-SOD, Mn binding is expected to be accompanied by acquisition of catalytic activity. This is indeed observed (Figure 3-10, lane 7 and 8). The catalytic activity is concentrated in the upper band ($Mn_2$-SOD) with some visible in the band attributed to $Mn_1$-SOD as well, consistent with twice as much activity on a protein basis in the upper band. The recovery of catalytic activity upon incubation with $Mn^{2+}$ demonstrates that the $Mn^{2+}$ was incorporated into the active site appropriately.

The findings for Q146E-SOD were different. The comparison of lanes 4 and 5 of figure 3-10 indicates that the metallation state of Q146E-apoMnSOD stays the same after incubation in the presence of 100 μM $Mn^{2+}$ at its *Tm* (Figure 3-10), because the electrophoretic mobility of the protein bands was unchanged after incubation. Although it is possible that Q146E- does not undergo the change in charge/size upon metal ion binding that affects WT-SOD, this seems unlikely given that its overall mobility very similar to those of WT-SOD. Therefore we interpret the absence of an effect to indicate that Q146E-apoMn-SOD does not acquire $Mn^{2+}$ or very minor of Q146E-apoMnSOD protein binds $Mn^{2+}$ in the course of the incubation but the nodenaturing PAGE is not sensitive enough to detect.

### 3.3.7 Discussion

Although process of metal binding is poorly understood for the majority of metalloproteins, it is an essential step for maturation of metalloproteins.[15] In the SODs family of proteins the antioxidant function heavily relies on the metal ion at the active center region.[8] The temperature induced reconstitution treatment did increase the metal ion content, accomplishing metal incorporation to be 80-90 % of active sites in the WT protein, but when the same protocol was applied to Q146E-apoMn-SOD only 10 % of sites acquiring Mn ion and 15 % acquiring Fe ion.

The active site of Mn-SOD and Fe-SOD employs analogous amino acids to coordinate their Mn or Fe cofactor: three histidines (His26, His81 and His171 MnSOD numbering), an aspartate (Asp167), and a coordinated solvent molecule interpreted as a water or hydroxide depending on whether the metal ion is reduced or oxidized[45a, 85] (equation 3.1 and 3.2). The solvent molecule accepts a hydrogen bond from an outer-sphere residue (Gln146 in *E. coli* MnSOD and Gln69 in *E. coli* FeSOD). Gln146 also forms an important additional hydrogen bond with the hydroxyl group of highly-conserved Tyr34.[35b, 54] Substitutions of any of the highly conserved amino acid residues, Gln146, Tyr34, His30 or Asp167 in the hydrogen bond network substantially influence the metal ion reactivity and substrate binding affinity.[45b, 79a]

In a fully metallated holoMn-SOD, an independent metal ion binding site buried in the interior of each monomer, surrounded by hydrogen bonding from amino acid side chains arising from the second shell. Circular dichroism (CD) spectroscopy has been used to monitor protein secondary structure as a function of temperature, holoMn-SOD, apoMn-

SOD and Q146E-apoMn-SOD, in the presence of 0.8 M GdmCl pH 7.4. The hypothesis that the metal cofactor significantly stabilizes the protein structure and enhances its thermostability, is reflected by the ~25 °C increment in melting temperature distinguishing holoMn-SOD (71.3 ± 1.0 ℃) from apoMn-SOD (53.0 ± 0.5 ℃) (Figure 3-4). But the melting temperature ($T_m$) of Q146E-apoMn-SOD of ~ 87.9 ± 0.1 °C (Figure 3-4) is more than 35 ℃ higher than that of apoMn-SOD (53.0 ± 0.5 ℃ ) and even 20 ℃ higher than that of holoMn-SOD (metal ion-replete) (67.4 ± 0.2 ℃). For Q146E-apoMn-SOD, given that the active site hydrogen bond network that surrounds the metal ion cofactor is crucial for the protein stability, it is plausible that at center of the hydrogen network, a mutated Glu at position 146, can't 100 % be involved in the hydrogen bonding at the active site, unlike the native amino acid at position 146. When observing the metal content of protein with the changes of ellipiticity at melting temperature (Figure 3-5, 3-6), the extreme low metal content of Q146E-apoMn-SOD is mostly in agreement with the amplitude change of ellipiticility appearing at 55 – 65 ℃ (Figure 3-8) contrast to the results of WT-apoMn-SOD (Figure 3-7). The structure of Q146E-holoMn-SOD which may simply be less stable than Q146E-apoMn-SOD. Therefore when the mutant protein Q146E-apoMn-SOD were given the access to metal ion, very little Q146E-holoMn-SOD is formed. The partially breaking of hydrogen bonding network of Q146E-apoMn-SOD or the losing of protein stability by metal uptake might be responsible for very small portion of metallated Q146E-Mn-SOD.

Mn ion binding is not a determinant factor to the nature of SOD structure, because the X-ray crystal structure of apoMn-SOD is essentially superimposable to that of holoMn-SOD at 1.9 Å resolution.[25a]The crystal structure of apoMn-SOD indicates that these

domains are pre-positioned by the dimer structure. But acquisition of the metal ion clearly renders their arrangement much more stable since the metal ion is between of the two domains. ApoMn-SOD and Q146E-apoMn-SOD was incubated to its melting temperature indicating substantial completion of the first stage of the melting but not the second as seen in Figure 3-4. After the protein samples were cooling down at rate of 1 ℃ per min and returned to 20 °C, significant amounts of ellipticity were recovered. Figure 3-9 shows that the presence of 100 μM $Mn^{2+}$ at incubation would render apoMn-SOD and Q146E-apoMn-SOD in acquisition of more intense ellipicility than if the incubation is conducted without $Mn^{2+}$. This suggests to the optimist that $Mn^{2+}$ becomes bound to partially unfolded apoMn-SOD and Q146E-apoMn-SOD.

To determine metal status of protein after temperature induced unfolding and refolding, we deployed non-denaturing PAGE. The different mobility of the different Mn ion states of MnSOD in non-denaturing PAGE have been explained on the basis of different charges, as these species have different isoelectric points.[26, 60] This is very useful for assessing protein metal uptaking independent of resulting activity. For sample apoMn-SOD (Figure 3-10 lane 2 and lane 3), the mono-manganese $Mn_1$-SOD (blue arrow) and apo-manganese apoMn-SOD (orange arrow) (Figure 3-10 lane 2) was eliminated significantly after protein incubation with $Mn^{2+}$ and the population of di-manganese $Mn_2$-SOD (black arrow) was increased accordingly (Figure 3-10 lane 3). Combining the results of refolding and melting by CD (Figure 3-9) and nondenaturing PAGE (Figure 3-10) reflected that partially unfolded apoMn-SOD could interact with $Mn^{2+}$ to produce a more structured form $Mn_2$-SOD and $Mn_1$-SOD (Figure 3-9 and Figure 3-10). But those changes of Q146E-apoMn-SOD is not as drastic as that of Mn-apoMn-SOD. A mild transition

emerged at lower temperature 40-60 ℃ at melting curve of recovered Q146E-apoMn-SOD sample (Figure 3-9). The protein band patterns of nondenaturing PAGE indicates $Mn^{2+}$ did not bind substantially, because no alternation on its structure or metallation state has been observed. Either $Mn^{2+}$ binding does not produce any structural alternation in addition to that already extremely well stabilized in the Q146E mutant, or the metallated Q146E-Mn-SOD didn't stable enough to survive the heat generated by nondenaturing PAGE.

This dramatic stabilization of the protein structure by the mutation Q146E goes against our normal preconceptions that WT proteins have been always evolved towards the most stable variants consistent with the folding. To our further surprise, the metal bound mutant protein Q146E-Mn-SOD exhibited a disturbed thermal-stability. In the specific case of apoMn-SOD we believe that residue Gln146 is the one that destabilized the apo-Mn form of the SOD protein which contributes to metal binding. On the other hand mutation Q146E prevents Q146E-apoMn-SOD from taking Mn ion, particularly if the amino acid substitution affects the same interactions at active site that Mn binding does or Mn binding by mutant introduces the same unstable interactions as metal binding site is vacant in wild type. Given that the residue at position 146 is central to the active site hydrogen bond network that surrounds the metal ion cofactor, it is plausible that with a Glu at position 146, Mn ion binding confers negligible additional advantages over the apo protein.

Regardless, our studies succeed in explaining why the Q146E variant is isolated in Q146E-apoMn-SOD form. The high affinity found for SOD enables it to acquire metal ions without known chaperone assistance, despite the presumed low availability of Fe and

Mn under the conditions when SOD activity became critical to survival. The large magnitude of the shift in $T_m$ upon mutation of Gln146 to Glu reveals the large sacrifice in protein stability that was worth making for the sake of high metal ion affinity, and also reflects the high intrinsic stability of the SOD structure, consistent with its role as a first line of defense. Also, note that in FeSOD, the Q to E mutation also stabilizes the protein, but in this case metal ion binding is preserved.[42a, 45b, 88]

### 3.3.8 Conclusion

For industrial applications like agriculture, medical treatments, cosmetics et al, improving protein resistance to heat and stress becomes a major standard for the quality of commercial proteins because thermal denaturation is a common cause of protein inactivation. Factors contributing towards the thermal stability of proteins are complicated and numerous, other than certain types of amino acids,[89] increasing hydrophobicity,[90] extensive ion pair interactions[91] and amino acid replacement.[92] Although increasing protein stability is one of major goals of protein engineering, our current results demonstrate that the naturally evolved amino acid composition of a protein is not always the one that gives the optimal protein stability. Because Gln146 is a strongly conserved amino acid of MnSODs, our results are not restricted to a peculiarity of the MnSOD from *E.coli*. The purpose for the conservation of Gln146 is clearly not to maximize protein stability. We now know Q146E-apoMn-SOD displayed a thermal stability much stronger than WT-apoMn-SOD even beyond that of WT-holoMn-SOD based on the thermal quantities determined from CD melting curve. However for metal binding, maximal stabilization of the apo-protein may not constitute optimal stability. An understabilized apo protein may provide the critical benefit of favoring formation of the holo protein instead.

Thermally assisted reconstitution of metal ions on recombinant apo-SODs has been conducted on a batch scale for several SODs.[93] Reorganization of the domain interface are required for the metal ion binding by apoMn-SOD and Q146E-apoMn-SOD,[37] and has been proved to be the rate limited step. The requirement for elevated temperatures has been attributed to weaken contacts in the domain interface that also control metal access to the active site.[87] Our results are consistent with the published conclusions that protein motion and flexibility are required for incorporation of the metal cofactor as part of maturation of MnSOD.[35, 86, 94] Moreover we find that Q146E-apoMn-SOD fails to generate the mono-manganese and di-manganese forms even when temperatures at its elevated $T_m$ are used. The stability of this variant Q146E-apoMn-SOD has the additional effect of shifting the equilibrium between apo- and holo- protein in favor of the former since it has been proved that Q146E-apoMn-SOD is much more thermally stable than Q146E-holoMn-SOD. This sheds new light on the role of Gln146 which has previously been considered primarily as an agent of proton delivery to the active site as a key participant in the active site hydrogen bond network.[42b, 49] While the Q146E variant had been reported not binding Mn ion, we have now demonstrated that this can be understood in terms of a dramatic thermal stabilization of the apo-metal ion form of this protein and a dramatic thermal destabilization of the holo-metal ion form of this protein.

Future work in determining the crystal structure of the protein Q146E could be very significant in revealing the improved thermal stability conferred by substituting Glu for Gln146. Preparing a fully metal bound protein and applying neutron diffraction on the structure of mutant Q146E–MnSOD would allow a direct measure of contributions to the conformational entropy changes arising from metal binding or mutations. More

investigation on the role of Gln 146 will be conducted by introducing other kinds of mutations at this position in chapter 4.

Table 3-1: Salient Features of Ultraviolent Absorption Spectra of *E. coli* MnSOD

| **Neutral pH** | **$\lambda_{max}$(nm)** | **$\lambda_{min}$(nm)** | **Inflexious λ(nm)** |
|---|---|---|---|
| MnSOD from Mn-medium | 283 | 252 | 298 |
| Q146E-apoMn-SOD from Mn-medium | 279 | 250 | 298 |
| FesubMn from Fe-medium | 283 | 251 | 298 |
| Q146E-FesubMn-SOD from Fe-medium | 278 | 251 | 298 |

An inflexious point is a point on an absorbance curve at which the slope of the curvature changes where the shape of the curve changes from being concave to convex or vice versa. It depends on the transmittance of the substance in solution.[95]

Table 3-2: Comparison of metal content and catalytic activity of Q146E-FesubMn-SOD, Q146E-apoMn-SOD and apoMn-SOD after Fe or Mn ion reconstitution

| | **Metal ions /Dimer** | **Metal content** | **Activity(Unit/mg)** |
|---|---|---|---|
| Mn-SOD | 1.9 ± 0.2 (Mn/Dimer) | 95 % | 14400 ± 120 |
| rec-FesubMn-SOD | 1.5 ± 0.2 (Fe/Dimer) | 75 % | 80 ± 10 |
| rec-Q146E-MnSOD | 0.2 ± 0.0 (Mn/Dimer) | 10 % | 0 ± 15 |
| rec-Q146E-FesubMn-SOD | 0.3 ± 0.0 (Fe/Dimer) | 15 % | 0 ± 13 |

apoMn-SOD accommodate a lot of Mn or Fe at the active site after reconstitution. While the metal content of Q146E-apoMn-SOD only was increased by 10 – 15 %. The concentration of Mn and Fe were quantified by ICP-OES. The protein specific activity was determined by the standard xanthine/xanthine oxidase/cytochrome c assay at pH 7.4. Protein concentrations were determined using molar absorptivity at 280 nm, with extinction coefficients of 86600 $M^{-1}$ $cm^{-1}$, 91900 $M^{-1}$ $cm^{-1}$, 89500 $M^{-1}$ $cm^{-1}$ and 83200 $M^{-1}$ $cm^{-1}$ per dimer for Mn-SOD, FesubMn-SOD, apoMn-SOD, and apoMn-SOD respectively. During metal reconstitution, Fe was added to protein samples Q146E-apoMn-SOD and apoMn-SOD to prepare iron incorporated protein. Mn was added to protein samples Q146E-apoMn-SOD and apoMn-SOD to prepared manganese incorporated protein. The mutant Q146E-Mn-SOD is mostly purified as apo protein lacking the metal ion presenting at the active site, with very limited activity no matter if Fe or Mn was added as a supplement in the medium.

Table 3-3: Comparison of metal content and catalytic activity of protein apoMn-SOD, holoMn-SOD and Q146E-apoMn-SOD as-isolated

| | **Ratio (Mn/Dimer)** | **Metal content** | **Activity (Unit/mg)** |
|---|---|---|---|
| apoMn-SOD | 0.3 ± 0.1 | 16% | 2840 ± 80 |
| holoMn-SOD | 2.0 ± 0.2 | 100% | 24710 ± 260 |
| Q146E-apoMn-SOD | 0.01 ± 0.00 | 0.5% | 0 ± 10 |

The concentration of Mn and Fe were quantified by ICP-OES. The protein specific activity was determined by the standard xanthine/xanthine oxidase/cytochrome c assay at pH 7.4. Protein concentrations were determined using molar absorptivity at 280 nm, with extinction coefficients of 86600 $M^{-1}$ $cm^{-1}$, 89500 $M^{-1}$ $cm^{-1}$ and 83200 $M^{-1}$ $cm^{-1}$ per dimer for holoMn-SOD, apoMn-SOD and Q146E-apoMn-SOD respectively.

Table 3-4: Thermodynamic parameters of denaturation of holoMn-SOD, apoMn-SOD and Q146E upon heating in 0.8 M guanidinium HCl under 60 ℃

| | **ΔH (kJ/mol)** | **ΔS ( J/(mol*K))** | **$T_m$ (℃)** |
|---|---|---|---|
| **holoMn-SOD** | NA | NA | NA |
| **apoMn-SOD** | 270 ± 30 | 820 ± 100 | 53.0 ± 0.5 |
| **FesubMn-SOD** | 250 ± 30 | 760 ± 110 | 50.9 ± 0.6 |
| **Q146E-Mn-SOD** | 1300 ± 200 | 3900 ± 700 | 51.3 ± 0.2 |

The thermodynamic parameters upon protein thermal denaturation $N \rightarrow U$ under 60 ℃ was analyzed by following the van't Hoff analysis in the method part based on the refined melting curve in Figure 3-5, 3-6, 3-7and 3-8 using CDpro analysis provided by Jasco Co. Under 60 ℃, the protein went through unfolding is apo protein for apoMn-SOD and FesubMn-SOD and holo protein Q146E-Mn-SOD based on the linear relationship between the metal content and the amplitude change of ellipiticity at high temperature (Figure 3-9).

Table 3-5: Thermodynamic parameters of denaturation of holoMn-SOD, apoMn-SOD and Q146E upon heating in 0.8 M guanidinium HCl above 60 ℃

| | **ΔH (kJ/mol)** | **ΔS ( J/(mol*K))** | **$T_m$ (℃)** |
|---|---|---|---|
| **holoMn-SOD** | 240 ± 10 | 700 ± 40 | 67.4 ± 0.2 |
| **apoMn-SOD** | 600 ± 200 | 1700 ± 700 | 71.3 ± 1.0 |
| **FesubMn-SOD** | 190 ± 100 | 500 ± 300 | 80.0 ± 1.6 |
| **Q146E-apoMn-SOD** | 670 ± 50 | 1900 ± 100 | 87.9 ± 0.1 |

The thermodynamic parameters upon protein thermal denaturation $N \rightarrow U$ above 60 ℃ was analyzed by following the van't Hoff analysis in the method part based on the refined melting curve in Figure 3-5 and 3-6, using CDpro analysis provided by Jasco Co. Above 60 ℃, the protein went through unfolding is holo protein fraction of apoMn-SOD and FesubMn-SOD and apo protein Q146E-apoMn-SOD based on the linear relationship between the metal content and the amplitude change of ellipiticity at high temperature (Figure 3-9).

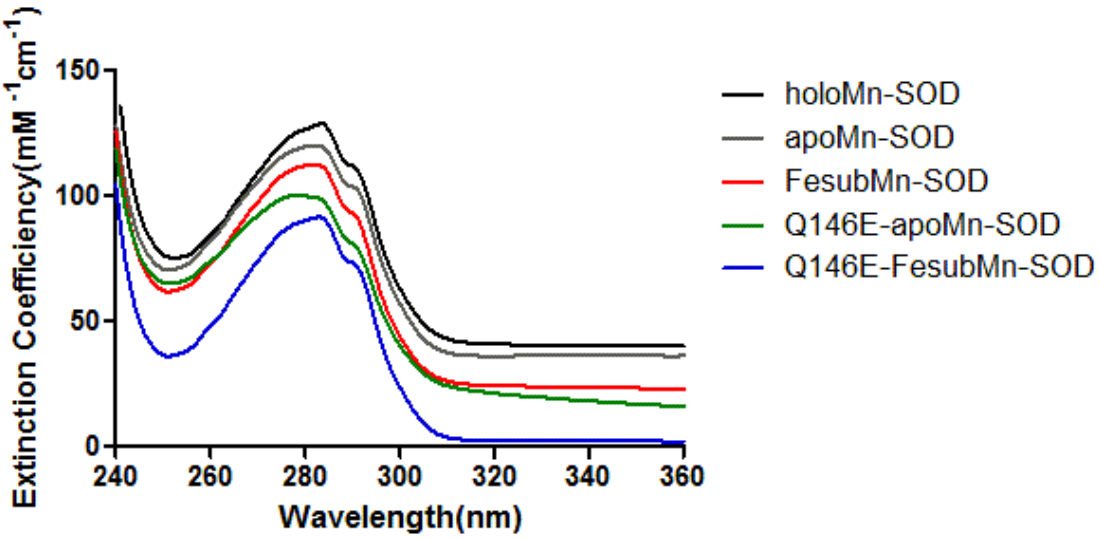


Figure 3-1: Ultraviolet absorption spectra of *E. coli* superoxide dismutase as isolated.

The sample spectra were recorded in buffer 5 mM phosphate buffer pH 7.4. Offset vertically as needed to relieve overlap. HoloMn-SOD, apoMn-SOD, FesubMn-SOD and Q146E-apoMnSOD were offset vertically by 40, 30, 20 and 10 $mM^{-1}cm^{-1}$ respectively to improve visibility.

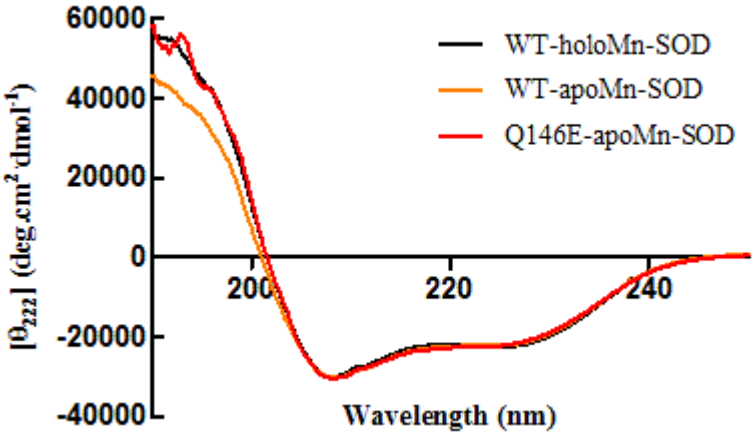


Figure 3-2: Scanning CD spectra for holoMn-SOD, apoMn-SOD and Q146E from 210nm to 250 nm.

The CD spectra for each samples was recorded in the far UV range from 180 to 250 nm at room temperature. 6 uM of protein sample was added to the buffer 5 mM $KH_2PO_4$, 0.8 M GdmCl pH 7.4. The scanning rate is 100 nm/min with a wavelength step of 0.2 nm and four accumulations for each curve. A baseline was obtained by collecting the CD spectra of the buffer solution of 5 mM Phosphate $KH_2PO_4$ and 0.8 M GdmCl at pH 7.4.

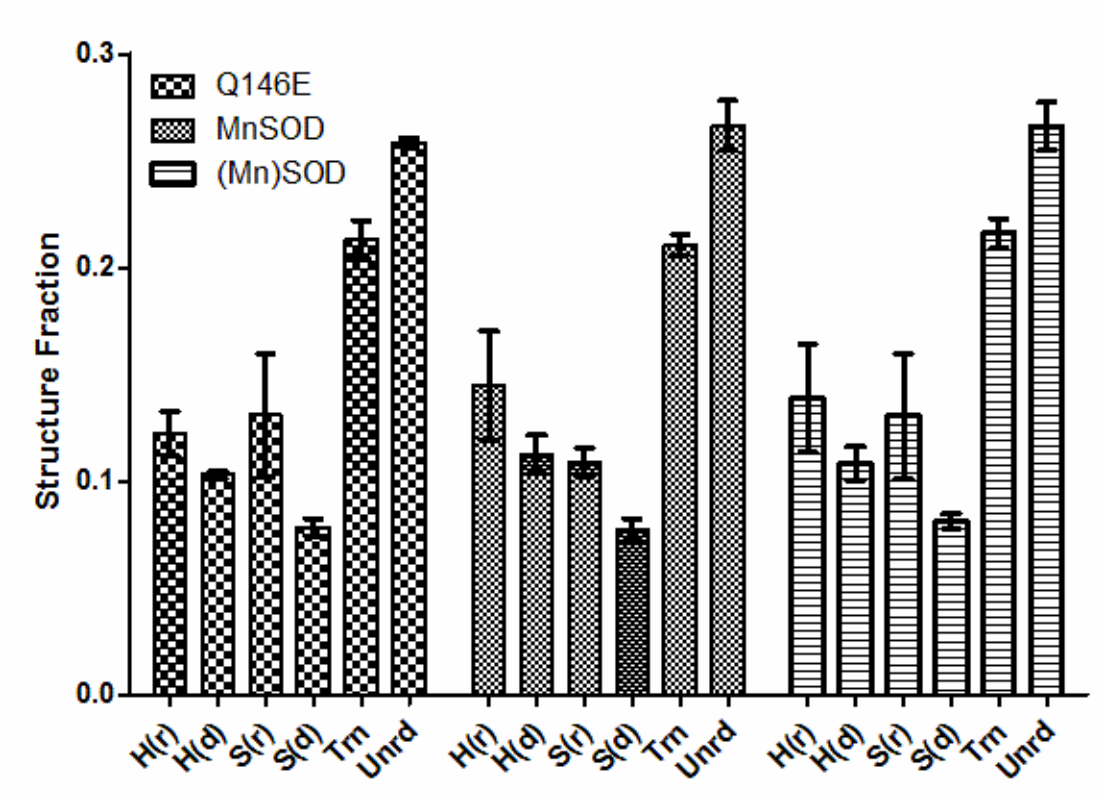


Figure 3-3: Secondary structure of MnSOD, Q146E and apoMn-SOD proteins in 5 mM sodium phosphate buffer pH 7.4.

Far UV CD spectra of MnSOD and Q146E in solution were estimated into secondary structure fractions using the CD Pro$^{82a}$ software package. Hr represents ordered helix content; Hd, distorted helix; Sr, regular β-strand; Sd, distorted β-strand; Trn, turns; and Unrd, unordered. Error bars represent the standard deviation of three repetitions. ApoMn-SOD is abbreviated as (Mn)SOD in the notation.

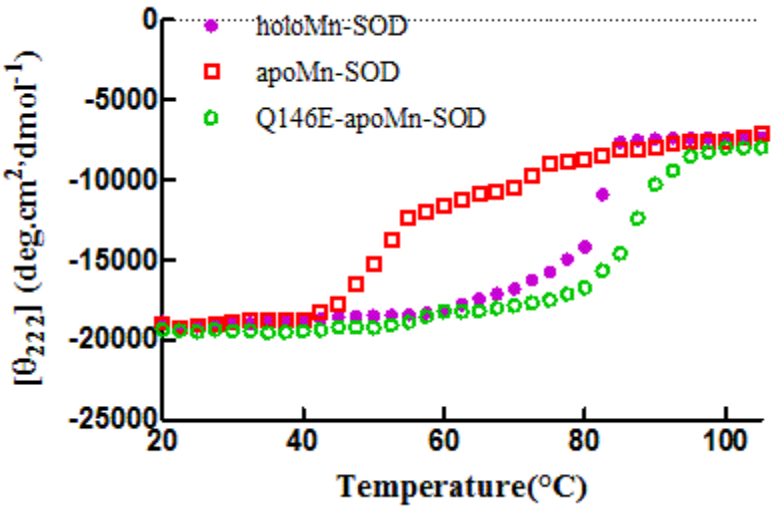


Figure 3-4: Temperature-induced unfolding of holoMn-SOD, apoMn-SOD and Q146E-apoMn_SOD.

The temperature-dependence of the ellipticity at 222 nm reveals a drop in α-helix content as the temperature increasing in the presence of 0.8 M GdmCl at pH 7.4. Data was monitored via the ellipticity [θ] at 222nm every 2.5 ℃. For the temperature-dependent unfolding experiment, 15 uM of protein sample was incubated in the buffer 5 mM $KH_2PO_4$, 0.8 M GdmCl pH 7.4 and the temperature was scanned from 20 to 100 ℃ at 1 ℃/min. At each temperature four accumulations of spectra were collected and the average value was recorded.

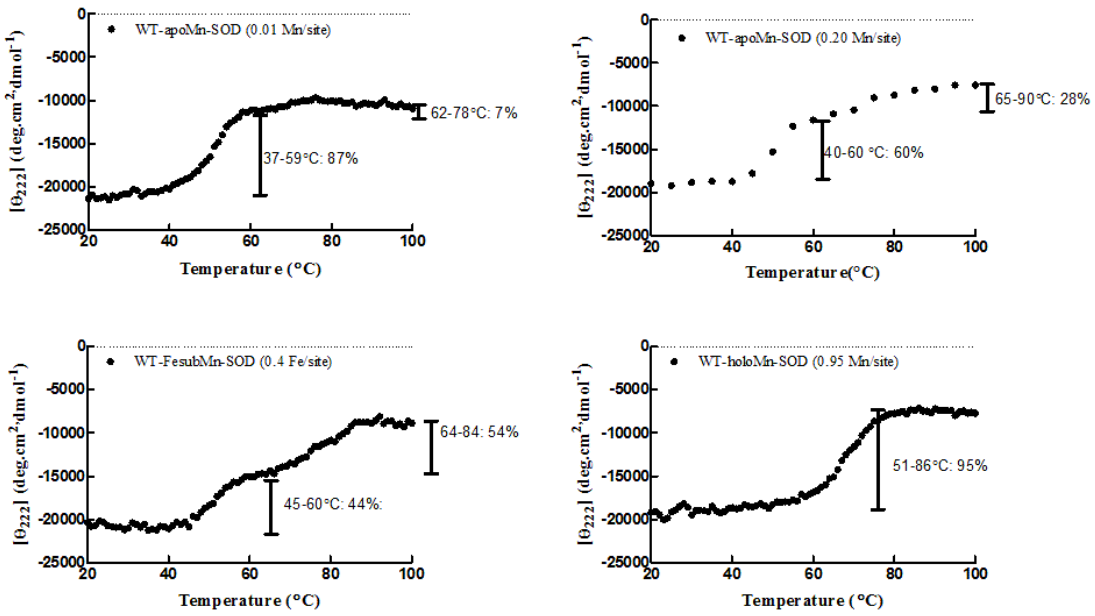


Figure 3-5: Temperature-induced unfolding of WT-Mn-SOD protein.

From top to bottom, the samples includes WT-apoMn-SOD (0.01 ± 0.00 Mn/site), WT-apoMn-SOD (0.20 ± 0.01 Mn/site), WT-Fe(Mn)-SOD (0.4 ± 0.01 Fe/site) and WT-holoMn-SOD (0.95 ± 0.03 Mn/site) upon heating in 0.8 M Gdm HCl. Data was monitored via the ellipticity [θ] at 222nm every 1 or 5 ºC. For the temperature-dependent unfolding experiment, 15 uM of protein sample was incubated in the buffer 5 mM $KH_2PO_4$, 0.8 M GdmCl pH 7.4 and the temperature was scanned from 20 to 100 ℃ at 1 ℃/min. The thermodynamic parameters upon protein thermal denaturation $N \rightarrow U$ was analyzed following the van't Hoff analysis in the method part based on the refined melting curve using CDpro analysis provided by Jasco Co. Mn content was measured by ICP-OES. Fe ion content was measured by Ferrozine assay.[101]

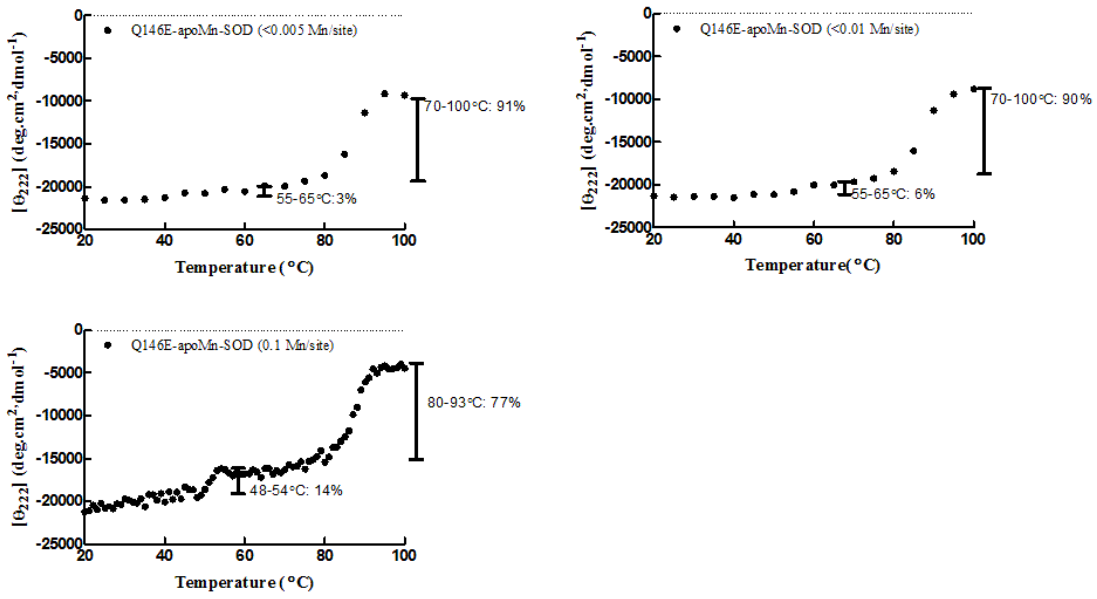


Figure 3-6: Temperature-induced unfolding of Q146E-apoMn-SOD.

From top to bottom, metal content of protein sample is < 0.05 Mn/site, < 0.01 Mn/site, 0.10 Mn/site. Data was monitored via the ellipticity [θ] at 222nm every 1 ℃ or 5 ℃. Data was monitored via the ellipticity [θ] at 222nm every 1 or 5 ℃. For the temperature-dependent unfolding experiment, 15 uM of protein sample was incubated in the buffer 5 mM $KH_2PO_4$, 0.8 M GdmCl pH 7.4 and the temperature was scanned from 20 to 100 ℃ at 1 ℃/min. At each temperature four accumulations of spectra were collected and the average value was recorded. The thermodynamic parameters upon protein thermal denaturation $N \rightarrow U$ was analyzed following the van't Hoff analysis in the method part based on the refined melting curve using CDpro analysis provided by Jasco Co.

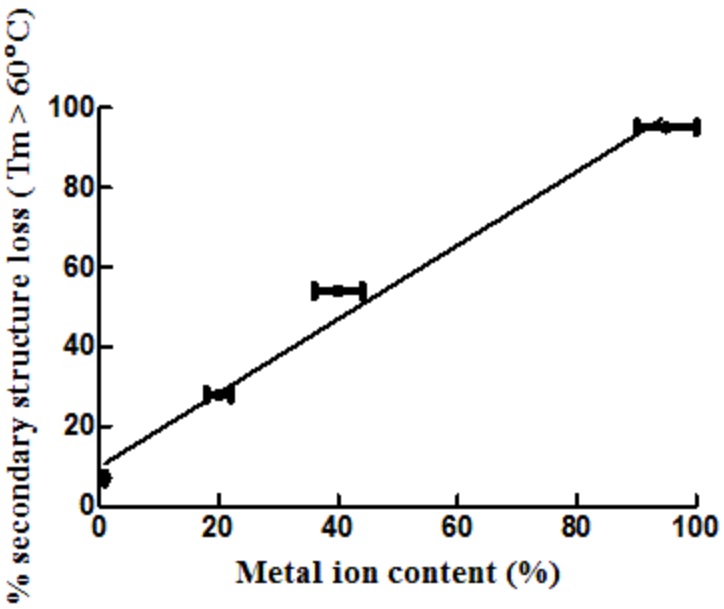


Figure 3-7: linear regression fitting of secondary structure loss *vs* metal ion content.

The plot is in an effort to relate the metal content regarding the protein stability to the secondary structure loss during protein melting occurring above 60 ℃. Linear regression fitting is in an effort to relate the metal ion content of apoMn-SOD (0.01 Mn/site = 1%, 0.20 Mn/site = 20%), FesubMn-SOD (0.4 Fe/site = 40 %) and holoMn-SOD (0.95 Mn/site = 95 %) regarding the protein stability in Figure 3-5 to the ellipticity loss during protein melting occurring above 60 ℃.

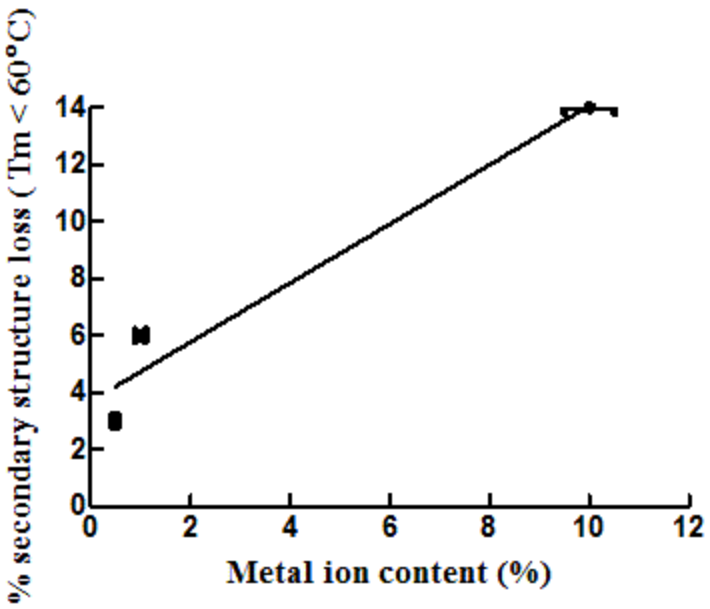


Figure 3-8: linear regression fitting of secondary structure loss *vs* metal ion content.

The plot is in an effort to relate the metal content regarding the protein stability to the secondary structure loss during protein melting occurring below 60 ℃. Linear regression fitting is in an effort to relate the metal content of Q146E-apoMn-SOD (0.005 Mn/site = 5 %, 0.01 Mn/site = 1 %, 0.10 Mn/site = 10 %) regarding the protein stability in Figure 3-6 to the ellipiticity loss during protein melting occurring below 60 ℃

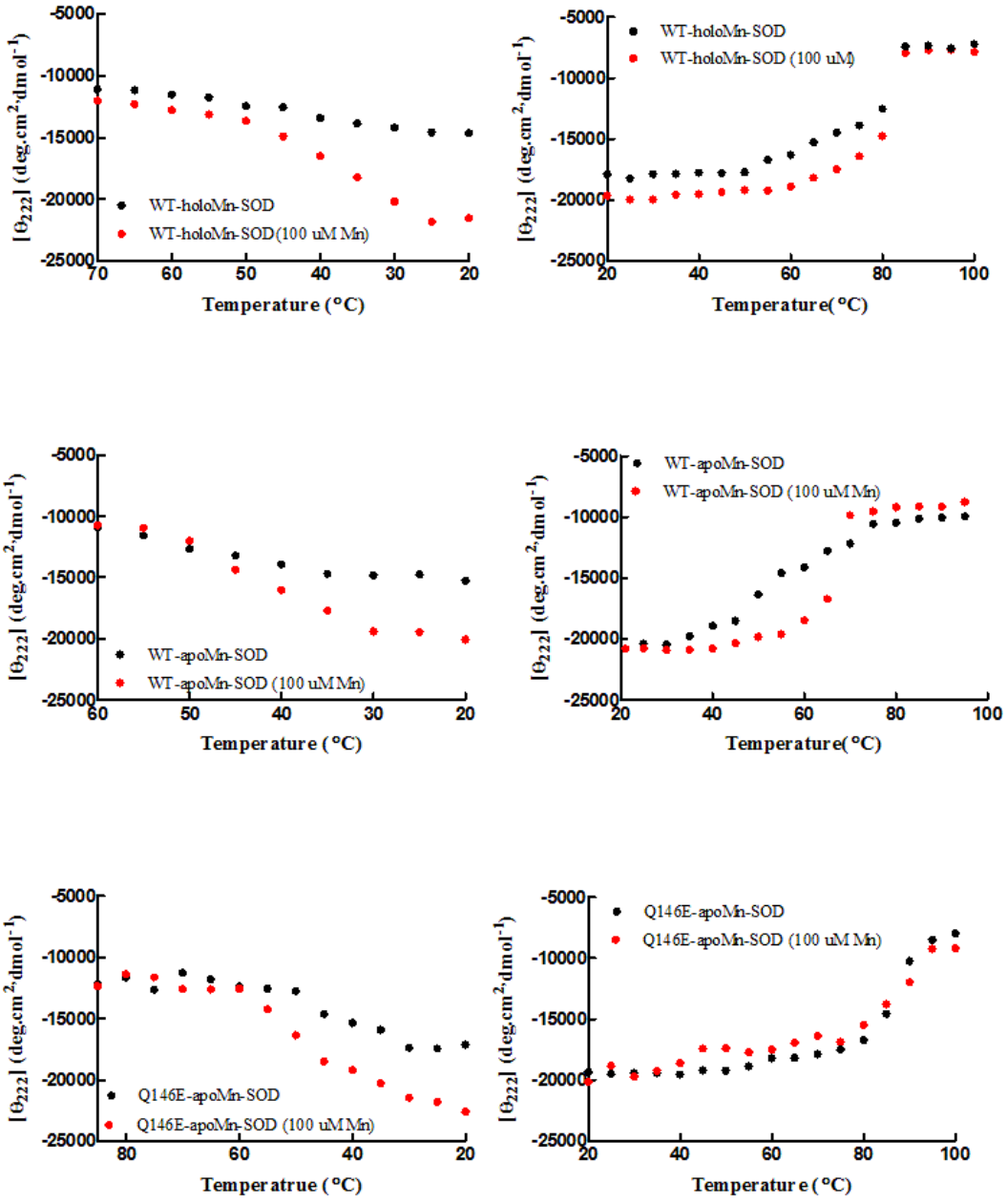


Figure 3-9: Temperature-induced recovery and re-melting of secondary structure of SOD proteins.

Refolding of holoMn-SOD, apoMn-SOD and Q146E-apoMn-SOD (left hand side from top to bottom) are monitored via the ellipticity [θ] at 222 nm every 5 ℃ from their melting temperature to 20 ℃. Temperature-induced unfolding of recovered holoMn-SOD, apoMn-SOD and Q146E-apoMnSOD is presented at right hand side from top to bottom, which have experienced refolding with (red dot) or without (black dot) 100 µM $Mn^{2+}$. The proteins were in buffer comprised of 0.8 M GdmCl and 5 mM potassium phosphate (pH 7.4) with100 µM $Mn^{2+}$ (red dot) or 0 µM $Mn^{2+}$ (black dot).

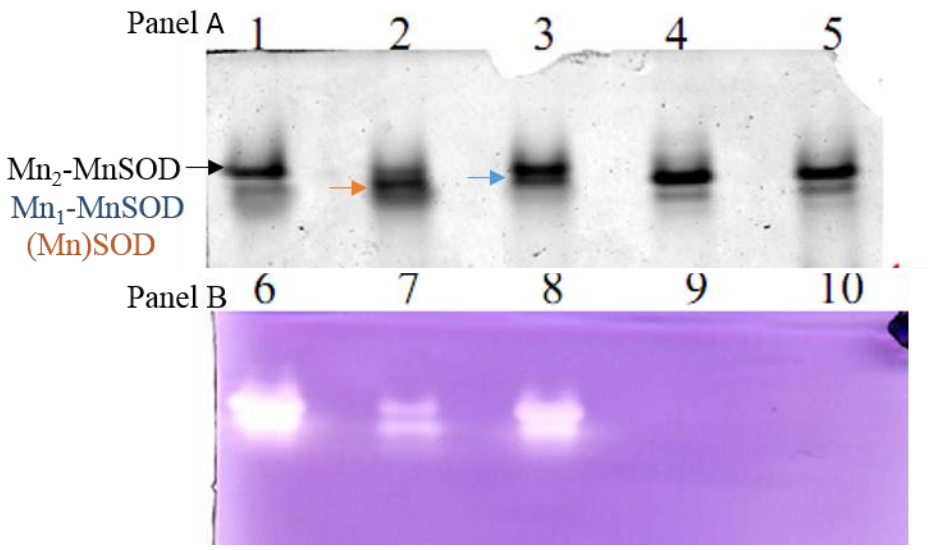


Figure 3-10: Non-denaturing gel electrophoresis of WT-apoMn-SOD and Q146E-apoMn-SOD samples.

The protein samples were WT-holoMn-SOD as isolated (lane1, 6), WT-apoMn-SOD (lane 2, 7), WT-apoMn-SOD after incubation with 100 µM $Mn^{2+}$ at $T_m$ (lane 3, 8), Q146E-apoMn-SOD as isolated (lane 4, 9), Q146E-apoMn-SOD after incubation with 100 µM $Mn^{2+}$ at $T_m$(lane 5, 10). This gel (panel A) was stained using Coomassie brilliant blue R-250 to visualize protein bands. The gel (panel B) subjected to the NBT assay shows SOD activity in the form of colorless zones.[7] Protein after incubation was prepared as described in the methods 3.2.5. Protein samples were separated using electrophoresis through 4-12 % acrylamide gels. The two gels were run in parallel as described in the methods 3.2.1. About 5.5 µg protein were loaded to the upper gel per lane whereas approximately 2.8 µg protein were loaded in each lane of the lower gel. The arrows show which band corresponds to $Mn_2$SOD(→), $Mn_1$SOD (→) and apoMn-SOD (→).[64]

## Chapter 4 Role of Gln146 to the stability and activity of MnSOD

### 4.1 Introduction:

Manganese-containing superoxide dismutase (MnSOD) catalyzes the following ping pong reactions:

$$E - M^{3+}(OH^-) + O_2^{\cdot -} + H^+ \rightarrow E - M^{2+}(H_2O) + O_2 \quad (4.1)$$

$$E - M^{2+}(H_2O) + O_2^{\cdot -} + H^+ \rightarrow E - M^{3+}(OH^-) + H_2O_2 \quad (4.2)$$

where E stands for the SOD protein and M strands for Mn ion at the active site.

Due to the structural homology of MnSOD and FeSOD, metal ion misincorporation sometimes occurs *in vivo*.[64] Thus *E. coli* MnSOD protein as-isolated is often a mixture of metallation isomers including holoMn-SOD, Fe-substituted MnSOD (FesubMn-SOD) and sometimes apoMn-SOD,[64] in addition to some partially metallated forms. The MnSOD does bind metal ion based on environment availability, but the optimal catalytic activity requires Mn ion bound at active site, rather than Fe. In chapter 3 we found that the replacement of Gln 146 of MnSOD with Glu substantially improves the thermal stability of Q146E-apoMn-SOD but rupturing that of metallated Q146-holoMn-SOD. Thus to clarify the role of Gln146 in metal binding in this chapter we decide to introduce other kinds of mutations at this position. [42b, 96]

Substitution of Gln143 in human MnSOD (equivalent to Gln146 in *E.coli* MnSOD) by Ala introduced further water molecules at active region without modifying the characteristic protein folding.[42b] In *E. coli* MnSOD, replacement of Glu146 by Leu or His

reduced enzymatic activity to less than 10 % with little structural changes.[79a] Further kinetics studies using spectrophotometer, pulse radiolysis and stop-flow in conjunction with site-directed mutagenesis by Silverman and his coworkers found that His30, Tyr34, Trp161, particularly Gln143 alleviated manganese superoxide dismutase product inhibition.[49, 97] Certain variants of human MnSOD at position Gln143 (with Ala, Val, Asn, Glu, and His) dramatically reduced product inhibition and the catalytic activity ($k_{cat}$) by 2-3 orders of magnitude approximately.[42b, 79b, 97c] Even the most conservative replacement of Gln143 with Asn reduced the length of side chain, exposed the active site of the enzyme to one solvent molecule and exhibited a drastically reduced enzymatic activity.[42b] The substitution of Gln69 of FeSOD (analogous residue of Gln146 in MnSOD) with Glu has been shown to produce a > 660 mV increment in the $E^{o}$ of bound Fe ion.[45a,45b]

Here we proposed to deepen our understanding of Gln146 of MnSOD by introducing a series of amino acid substitutions at position Gln146 designed to confer activity on FesubMn-SOD protein. In chapter 3, we already described some properties of the mutant Q146E. Compared to the wild-type apoMn-SOD protein, Q146E-apoMn-SOD displayed dramatically enhanced structural stability, diminished metal binding ability and non-catalytic activity. In this chapter we described the properties of five other variants of *E. coli* MnSOD, Ala, Cys, Asn, Ser and Tyr at Gln146. These variants were chosen to learn how the size or charge of the side chain of amino acid at position Gln146 affects metal binding affinity and structure stability.

Optical and EPR spectra indicated that all the five foregoing SOD variants incorporate some Mn and/or Fe ion.[49, 98] Among all these mutants Q146A displays the highest catalytic activity.[49] Due to the bulk side chain, Q146Y displays perturbed secondary structure and thermal stability.[42b] Although exhibiting different properties, all five mutations of the well-conserved residue Gln146 still retained at least some enzymatic activity.[97] A series of variants would extend our understanding on the special role of Gln146 in supporting active site structure and catalytic activity.

## 4.2 Materials and methods:

### 4.2.1 Materials

Xanthine Oxidase, bovine heart cytochrome c, and nitroblue tetrazolium are products of Sigma chemical Co. Resin G-25 was a product of Whatman. Protein molecular weight standards are products of Bio-Rad Laboratories. All other chemicals are of the highest available quality and all operations utilized doubly-deionized water from a Millipore plus QPAK® purification system.

### 4.2.2 Determine the molar extinction coefficients of mutants

In 8 M Guanidine hydrochloride (GdmCl), a denaturing medium, the extinction coefficient of the protein at 280 nm can be approximated as the sum of the contributions of the Trps and the Tyrs by the equation:

$$\text{molar extinction coefficient of protein} = n\text{Trp} \bullet \varepsilon\text{Trp} + n\text{Tyr} \bullet \varepsilon\text{Tyr} \qquad (4.3)$$

where at 280 nm $\varepsilon$Trp = 5690 $M^{-1}cm^{-1}$ and $\varepsilon$Tyr = 1280 $M^{-1}cm^{-1}$.

For a better accuracy on reading by Hewlett Packard model 8453 diode array spectrophotometer, dilute the protein solution carefully into denaturing conditions 8 M GdmCl to adjust the absorbance at 280 nm at 0.5 - 0.8. Record the absorbance at 280 nm as the absorbance of denatured protein. Apply Beer's law ($A = \varepsilon lc$) using the calculated molar extinction coefficient (by equation 4.3) of denatured protein ($\varepsilon$) and the recorded absorbance at 280nm ($A$) to determine the concentration of protein sample after dilution.

Dilute the protein solution by 5 mM potassium phosphate buffer pH 7.4 at the same order as that under the denaturing condition 8 M GdmCl. Record the value of absorbance at 280 nm of the native protein. Apply Beer's law using the absorbance and the concentration of protein sample determined under denaturing conditions to calculate the molar extinction coefficient of native protein. The corrected extinctions for protein samples Q146X (X = A, C, N, S, Y) are summarized in Table 4-2.

### 4.2.3 Protein analysis

The concentration of purified protein MnSOD was determined using optical absorption at 280 nm, by the published molar extinction coefficient ($\varepsilon_{MnSOD,\ 280nm}$ = 86600 $M^{-1}$ $cm^{-1}$)[75a]. The concentration of mutants are determined by the corrected extinction coefficient (Table 4-2). Optical absorption spectra were obtained using a Hewlett Packard model 8453 diode array spectrophotometer.

Protein homogeneity was decided by SDS-PAGE wherein purified protein was loaded onto 4-12 % precast Tris-HCl SDS-PAGE gels (Bio-Rad Laboratories) running at

100- 80 Volts for approximately 2 hours. For denaturing SDS PAGE, ~ 5 % 2-mercaptoethanol (2-ME) was included in the sample buffer to reduce the S-S bond.

Specific activity of superoxide dismutase was measured using the xanthine oxidase/cytochrome c inhibition assay by McCord and Fridovich.[7] And the polyacrylamide electrophoretic gels is also utilized to visualize catalytic activity,[71] as described in the previous chapters 3.2.1.

### 4.2.4 Determine metal content by ICP-OES

Metal concentrations were determined by ICP-OES (Inductively Coupled Plasma – Optical Emission Spectrometry)[72] at the Environmental Research and Testing Lab located in room 316 of the Raymond Building of the College of Engineering College of University of Kentucky. In order to account for any possible contamination from water and human error, triplicates of each protein sample, a water blank and a series of duplicate standardized Mn solutions at different concentrations were prepared in parallel. Add 1 ml 0.1 M Nitric acid ($HNO_3$) slowly to each 1 ml sample. Incubate all samples on ice for 10 - 15 min to allow the release of all metal ions into solution. Denatured protein and cell debris were removed by centrifugation at 13,000 rpm for 2 min. Transfer the supernatant to a clean tube. Discard the precipitate. Add 8 ml of distilled water to each 2 ml sample getting a total volume of 10 ml before fed into the plasma (dilution ensures that there is enough sample for loading). The light emitted by Mn atoms was detected at the characteristic wavelength of 257.61 nm, 259.37 nm and 260.568 nm, by the optical spectrometer. The light emitted by Fe atoms was detected at the characteristic wavelength of 238.204 nm, 259.94 nm and 261.187 nm. Calibrated curve was made by plotting reading obtained for

the standard samples vs. the Mn ion concentration, which was used to determine the concentration of Mn ion of the protein samples.

### 4.2.5 Assay on Mn content by EPR

Electron paramagnetic resonance (EPR) was also used to quantify the Mn content of MnSOD. Protein was hydrolyzed to release all Mn as $Mn^{2+}(H_2O)_6$ in solution by addition of 1 ml of 1 M hydrochloric acid (HCl) to 1 ml protein solution. Incubate protein samples on ice for 10 -15 min to let the denaturing reaction complete. Centrifuge protein solution at 13,000 rpm for 2 min to remove protein precipitates. Transfer the supernatant to another clean tube to which glycerol was added to produce a 50 % v/v solution. In order to account for possible contamination from the water as well as human error, a replicate protein sample solution, a water blank and a series of duplicate standardized Mn solutions at different concentrations were prepared in parallel.

To detect single-digit μM concentrations of $Mn^{2+}$ ion, all the operations were implemented at 110 K. Samples were frozen by liquid nitrogen and maintained at low temperature in the evaporated liquid $N_2$ flow of an Oxford cryostat when measuring EPR spectra. EPR spectra were collected at X-band (9.49 GHz) using a Bruker 300 EMX spectrometer over a sweep of 0 - 6000 G at a nominal microwave power of 160 mW. The other parameters are 10 G modulation amplitude, 2048 points at time constant of 40.96 msec and sweep time of 335.50 sec. Signal amplitudes of the EPR spectra were determined as the peak-to-trough height of the lowest-field line of the $Mn^{2+}(H_2O)_6$ signal. The standard curve was plotted as signal amplitudes *vs*. Mn ion concentration in the standard samples. A straight line was obtained with $R \sim 0.968$ at the range of 40 to 1500 $\mu$M $Mn^{2+}$ (Figure 4-

3), which confirmed a linear relationship between the magnitude of the peak and the concentration the $Mn^{2+}$. From the standard curve, the $Mn^{2+}$ concentration of acid-denatured MnSOD could thus be determined.

$Mn^{3+}$/Mn ratio can be calculated by signal of EPR. The $Mn^{2+}$ content of MnSOD is in proportion to the signal amplitude of EPR spectra new g'=4.5. The amplitude is quantified by measuring the peak-to-trough heights of the third and fourth hyperfine lines. The signal amplitude before treatment of dithionite reflects the initial $Mn^{2+}$ content as isolated. After treatment with dithionite, scan sample solution and calculate the signal amplitude again. Because treatment with dithionite reduces any $Mn^{3+}$ to $Mn^{2+}$, the signal amplitude after treatment indicates the total Mn ion content (both $Mn^{3+}$ and $Mn^{2+}$). The content of initial $Mn^{3+}$ thus can be calculated as total $Mn^{2+}$ after reduction minus Mn present as $Mn^{2+}$ beforehand.

### 4.2.6 Site-Directed Mutagenesis of MnSOD

Variants of *E. coli* WT-Mn-SOD were prepared by site-directed mutagenesis of the WT-Mn-SOD gene from *E. coli* using the plasmid pET2 pAK0 as a template. Follow the method coming with the Quik-Change Site-Directed Mutagenesis kits (Agilent). Design the appropriate oligonucleotide mutagenic primers (Table 4-1) (synthesized by IDT, Integrated DNA Technologies, Inc). After PCR amplification, template DNA was degraded using Dpn I restriction enzyme at 37 °C for about 2 hours. Dpn I was inactivated by incubating the DNA mixture at 65 °C for about 10 min. Take 0.2 μL of the PCR product, mutated DNA, and transform to 100 μL freshly-made competent *Ox326-A* cells, which lack the ability to produce WT-Mn-SOD or Fe-SOD (ΔsodAsodB). Transformants cell colonies

were recovered in 500 ml SOC medium for 30-60 min 180 rpm at 37 ºC before spreading on LB plates with Kanamycin and Ampicillin. After growing on LB plates at 37 ºC overnight, the positive clones were screened by DNA sequencing using T7 primers to specify the *sodA* coding region on the pET21 plasmid (Eurofins Genomics Company).

Recombinant protein expression and purification were performed following the simplified method described in chapter 2 section 2.2.2. The cell-free supernatant from the cell growth was collected, concentrated and treated with 1 mM EDTA. Size exclusion chromatography (sephadex G-25 column, 5cm × 30 cm) was used to transfer SOD protein to fresh made buffer 5 mM phosphate buffer pH 7.4 and clean it from DNA fragments and other small molecules. The flow through containing SOD were collected, pooled and concentrated to ~ 1 mM for storage at 4 ºC.

### 4.2.7 Electronic structure characterization by EPR

EPR spectroscopy could also be used to characterize the electronic structure of $Mn^{2+}$SOD because the unpaired electrons of $Mn^{2+}$ yields the signal. EPR spectra were collected for reduced WT-$Mn^{2+}$-SOD and its variants: Q146A, Q146C, Q146N, Q146S, Q146Y- $Mn^{2+}$-SOD. Protein samples were prepared in 4 mm quartz EPR tubes with 50 % glycerol as the cryoprotectant. The samples were frozen by liquid nitrogen and then maintained at low temperature in evaporated liquid $N_2$ flow of an Oxford cryostat when measuring EPR spectra. EPR spectra were collected at 9.32 GHz at 110 - 120 K, with 160 mW nominal microwave power. The other parameters included 10 G modulation amplitude, 2048 points at time constant 40.96 msec per point and a spectral range from 0 to 6000 G. EPR spectra were calibrated at $g' = 2.0023$ using DPPH in 100 mM phosphate buffer.

### 4.2.8 Azide titration

The azide binding affinities for wild-type $Mn^{3+}$SOD and its Gln146 variants were determined by titrating the protein solutions with aliquots of $NaN_3$ solution. All visible absorption spectra of WT-$Mn^{3+}$-SOD and its variants were recorded by a Hewlett-Packard 8453 diode array spectrophotometer at ~ 25 °C, room temperature. The optical spectra were collected after each addition. The $N_3^-$ titration was carried out in a 400 µl quartz cuvette. Initially 0.1 mM MnSOD dimers in 5 mM potassium phosphate buffer pH 7.4 was used to ensure a sufficiently high concentration of protein at the conclusion of the titration. To minimize dilution influence on protein concentration while covering a large span of azide concentrations, four different concentration of stock solutions of $NaN_3$ were used: 0.1 mM, 1 mM, 10 mM and 100 mM, each in 50 mM $KH_2PO_4$, pH 7.4. For each 250 µl protein sample, a total of 10 – 50 ul of $NaN_3$ solution was added by 1-2 µl per aliquot. As the titration in progress, a shoulder at 390 nm[10] could be observed. The recorded absorbance at 390 nm was corrected counting for protein dilution using the cumulative volume of additions before applied to analysis.

The dissociation constant ($K_d$) of azide of each MnSOD sample was obtained by fitting the corrected $A_{390}$ to the equation for tight binding (equation 4.4),

$$y = A_0 + (A_{max} - A_0)\frac{(K_d + E + x) - \sqrt{((K_d + E + x)^2 - 4 \times E \times x)}}{2 \times E} \qquad (4.4)$$

where y is the absorbance at 390 nm, $A_{max}$ is the absorbance at 390 nm when SOD protein is saturated with azide, $A_0$ is the absorbance at 390 nm when [azide] = 0 mM, x is

the concentration of azide, $K_d$ is in the same unit as x, E is the concentration of enzyme dimer.

### 4.2.9 Circular dichroism (CD).

Circular dichroism was measured on a Jasco J-810 spectraporalimeter (Japan) equipped with a Peltier multicell temperature controller. The method and the instrumental settings were described in Chapter 3 section 3.2.3. Protein samples were at a concentration of 4 μM in a buffer solution of 0.8 M guanidium HCl (GdmCl) 5 mM phosphate buffer at pH 7.4. The temperature of the protein solution was controlled to an accuracy of ± 0.1 ℃. The temperature was increased at a speed at 1 ℃ per min and data were recorded every 1 ℃ from 20 to 105 °C.

## 4.3 Results and discussion

Substitutions of any of the highly conserved amino acid residues, Tyr34, His30 or Asp167 that are highly involved in the hydrogen bond network would substantially influence the metal ion reactivity and substrate binding affinity.[46, 99 45b, 50c] Gln146 in combination with Tyr34, Asp167 and nearby solvent molecules forms an extensive hydrogen bond network that links the active site of MnSOD to bulk solvent from the environment (Figure 1-2 in chapter 1).To aid our understanding on the role of Gln146 in the ping-pong mechanism by SOD (equation 4.1 and 4.2), a series of different amino acids Q146X (X = A, C, N, S, or Y) were introduced at the 146 position by mutation (Figure 4-1).

### 4.3.1 Optical spectrum of Mutants Q146X-MnSOD

The UV/Vis spectra of all the variant SODs in phosphate buffer pH 7.4 at room temperature are shown in Figure 4-2 bottom right. The absorbance at 478 nm caused by the d-d transition of $Mn^{3+}$ is characteristically observed in the spectra of the WT-MnSOD only. The expected absorption for $Mn^{3+}$ at 478 nm was absent from the spectra of all the Q146X-MnSOD variants. This could reflect absence of manganese ion at the active site if the variants all failed to bind Mn, as discovered for the Q146E variant (Chapter 3), or it could indicate that Mn is bound but in its $Mn^{2+}$ oxidation state.

Instead of the $Mn^{3+}$ signature absorption at 478 nm, a strong peak at 420 nm was observed in the visible spectrum of mutants (Figure 4-2 bottom right). The peak at 420 nm could possibly due to a metal complex formation at active site (Figure 4-2 top) or due to the iron content at the active site. Because a transient product-inhibited complex of SOD or FesubMn-SOD exhibits the same absorption property at 420 nm[81] of SOD spectra based on the published literature.[50d,99,100] But the lifetime for inhibitor complex at 420 nm decaying is ~ 10 sec observed by stopped-flow spectrophotometry.[97b] And the binding affinity of the inhibitor complex might be altered by mutation as the we demonstrated by Q146A in Figure 4-2 (bottom left). Fridovich has determined that the molar absorptivity of WT-FesubMn-SOD is 1860 $M^{-1}$ $cm^{-1}$ at 420 nm much stronger than that of WT-$Mn^{3+}$SOD, 850 $M^{-1}$ $cm^{-1}$ at 478 nm.[75a] Taking into account that Fe ion is ubiquitous in solutions and environment, thus it is not a surprise to find that Fe ion inserted at the active site of proteins and FesubMn-SOD of protein samples displayed a absorbance at 420 nm, which is stronger than that of Mn-SOD at 478nm even if its concentration is lower.

### 4.3.2 Metal content of Q146X-MnSOD

To clarify the optical spectra observed in the last section we decided to measure the metal content of each mutants. EPR was used to determine the total Mn content of acid-hydrolyzed samples of Q146X-SODs. All the Q146X-MnSOD variants displayed considerably lower Mn content than WT-MnSOD (Table 4-3). Less than 10 % of the active sites coordinated with Mn ions for most of Q146X (X = A, C, S, Y) variants. Even for the most conservative mutant Q146N, only 16 % of its active site contains Mn ion. The low Mn ion content of each protein samples explains the lacking of optical signature absorbance at 478 nm at the spectra of protein samples in section 4.3.1 (Figure 4-2 bottom right).

The total Fe concentration of Q146X-MnSOD in our research is measured by Ferrozine assay.[101] All the Q146X-MnSOD has about 0.2 – 7 % iron bound protein (Table 4-3). Noted that Q146A and Q146S displayed an iron content higher than their manganese content while Q146N and Q146Y exhibited a much lower iron content. Especially for Q146N, whose Mn content is highest among the mutants, had a Fe content as low as 0.2 %, which is even lower than that of WT-Mn-SOD. Fe is a ubiquitous metal ion in our water solution which is very difficult to eliminate.[15] As we know the metal cofactor at active site of MnSOD depends on the environment metal availability,[75a] it is not a surprising to find Fe ion at active site especially after introducing mutation. Leveque et al also found that mutations at position 143 increases iron content of the mutants, for example Q143A-Mn-SOD has as much as 10 % iron.[42b]

### 4.3.3 Catalytic activity on Q146X-MnSOD

All of the five variants of MnSOD at position Gln146 exhibited significantly lower catalytic activity (U/mg protein) than the wild-type (Table 4-3) from the perspective of protein quantity. Even taking into account their Mn ion stoichiometry, the catalytic activity most of the variants (1-20 U/umol Mn ion) was approximately two orders of magnitude lower than that of WT-MnSOD (460 U/umol Mn ion). The only exception was Q146A-Mn-SOD for which the catalytic activity per Mn ion was comparable to that of WT-Mn-SOD or even higher. It is possible that part of the activity is attributable to iron cofactor because Q146A displayed an iron content higher than its manganese content. But we found that its activity per Fe (50 U/Fe) (Table 4-6) was much lower than the activity per Mn (7600 U/Mn). These results agree with those of Silverman's group, who found that mutation of human MnSOD Gln143 to Ala, Val, Asn, Glu, His displayed a smaller value of the $k_{cat}/K_m$ and $k_{cat}$ by 2- 3 orders of magnitude by stop-flow. [42b, 49]

### 4.3.4 Reduction potentials

One possible reason behind the low catalytic activities on a per-Mn basis could be reduction midpoint potentials, $E°$. Prior work on FeSOD demonstrated that substitution of the analogous Gln69 produces changes of 200 mV or more effects on the $E°$ of the active site metal ion.[43, 45b] The $E°$ sets a thermodynamic limit on the metal site's ability to accept electrons from reductants and to donate them to oxidants.

The signal amplitude of EPR spectrum is quantized to estimate $Mn^{2+}$ concentration in solution (Figure 4-3). The amplitude used in calculation was the sum of the peak-to-trough heights of the third and fourth hyperfine lines because the peak-to-trough height of

signal is in proportion to $Mn^{2+}$ concentration. The signal reveals the $Mn^{2+}$ content of the active site as-isolated because $Mn^{3+}$ at active sites can't be not observed by our parallel-mode EPR spectrometer. After applying dithionite to protein sample, all the $Mn^{3+}$ ion in protein sample were presumed reduced and the EPR signal would represent the total Mn ion of protein sample. The fraction of $Mn^{3+}$ could therefore be estimated by the difference of the signal amplitude before and after the dithionite reduction. The changes of amplitude upon dithionite reduction is expected to agree with the visible absorption at 478 nm in the UV/Vis spectrum (Figure 4-1 bottom right).

It is interesting to note that reduction of $Mn^{3+}$ by dithionite increased the amplitudes of all the MnSOD signals but did not significantly alter their shapes (Figure 4-4, 4-5 and 4-6). Thus these samples do appear to contain two populations of sites where one population is readily reduced and therefore in the $Mn^{2+}$ state as-isolated but the other population is isolated as $Mn^{3+}$ and only rendered EPR-observable by chemical reduction.

The calculated fraction of the $Mn^{3+}$ state at active site is reported "$Mn^{3+}$/Mn" in Table 4-3. Whereas the oxidation state of Mn ion at active site of WT-Mn-SOD was mainly $Mn^{3+}$, accounting for approximately 90 % of total Mn, the percentage of $Mn^{3+}$ was decreased for all the Q146X variants, in consistence with finding by other groups.[42b] Data summarized in Table 4-3 suggests that only 40 % - 70 % of the total Mn ion at active site is in the oxidized state $Mn^{3+}$ in the Q146X. The decrease of $Mn^{3+}$ percentage in the Q146X suggests the increase of their reduction potential *E°*s. The lower percentage of $Mn^{3+}$ ion also explained the absence of shoulder at 478 nm in the spectrum of Q146X which is considered as the characteristic absorption of $Mn^{3+}$SOD (Figure 4-2).

The $E^o$ of the SODs' $Mn^{3+}/Mn^{2+}$ couples can be estimated following the simplest form of the Nernst equation, which relates the standard reduction midpoint potential to the ratio of the species participating in the redox reaction ($[Mn^{3+}]/[Mn^{2+}]$) (equatoin 4.6),

$$E = E^0 + \frac{RT}{nF} ln \frac{[Mn^{3+}]}{[Mn^{2+}]} \quad (4.6)$$

where $E^o$ is the redox potential measured under standard conditions, called standard reduction midpoint potential, n is the number of electrons transferred in the reaction, *F* is Faraday's constant, *R* is the universal gas constant and T stands for the absolute temperature.

Based on EPR signal, estimated ratios of $Mn^{3+}/Mn^{2+}$ at the active site of WT-MnSOD and its variants are summarized in Table 4-3. We infer that the *E*°s of the variants increased in the following order, WT-MnSOD < Q146N-MnSOD ≈ Q146S-MnSOD < Q146A-MnSOD < Q146C-MnSOD ≈ Q146Y-MnSOD.

The Nernst equation permits calculation of *E*° values if the ambient reduction potential, *E*, is known. Unfortunately MnSOD equilibrates excruciatingly slowly with mediators that could be used to determine E,[88] and this experiment was not done. Here we adopt the assumption that the use of the same buffer in all the protein preparations, and extensive equilibration with air for all samples, produces the same ambient potential in all cases, then we can infer the midpoint potential $E°_X$ for a mutant Q146X using equation 4.7 and 4.8.

$$E°x + \frac{RT}{F}\ln\frac{[Mn^{3+}]x}{[Mn^{2+}]x} = E°_{WT} + \frac{RT}{F}\ln\frac{[Mn^{3+}]_{WT}}{[Mn^{2+}]_{WT}} \quad (4.7)$$

$$E°x - E°_{WT} = \frac{RT}{F}\left(-\ln\frac{[Mn^{3+}]x}{[Mn^{2+}]x} + \ln\frac{[Mn^{3+}]_{WT}}{[Mn^{2+}]_{WT}}\right) \quad (4.8)$$

The difference of the $E°$ values ($\Delta E°$) caused by mutation at position 146 of MnSOD could be estimated approximately using equation 4.8. The substitutions of Gln146 with Ala, Cys, Asn, Ser, Tyr produced a ~80 - 150 mV increment on the $E°$ (Table 4-4), which is still an acceptable value to donate and accept electrons for the ping-pong reactions (equatoin 4.1 and 4.2). Considering $E°$ of mutants are close to that of WT-Mn-SOD, our results suggest that the decreased catalytic activity of the mutants Q146X are not attributable to the increased $E°$s.

### 4.3.5 Thermal-stability on Q146X-MnSOD

Chapter 3 raised the possibility that Q146E-apoMn-SOD failing to bind Mn is due to the hyper-stability of apo-Mn form protein. To see if the other variants at position Gln146 also alters thermal stability as Q146E and confirm the role of Gln146 in the protein metal binding, the melting curve of each was monitored by far-UV CD detected as temperature induced unfolding of secondary structure.

In Figure 4-7, ellipticity at 222 nm reveals the change in α-helix content as the temperature ascending from 20 ℃ to 100 ℃ in the presence of 0.8 M GdmCl pH 7.4, where GdmCl is used to prevent formation of protein from aggregating during the heating process. The ellipicity at 222 nm decreased substantially over a narrow temperature range indicating cooperative protein unfolding as a two-state helix-coil transition in all cases (Figure 4-7).

As summarized in Table 4-5, except that the $T_m$ of Q146Y is considerably lower than that of WT-Mn-SOD, all the other four variants Q146A, Q146C, Q146N, Q146S displayed a melting temperature $T_m$ higher than that of WT-Mn-SOD. Because all the Q146X variants have relatively little Mn ion or Fe ion at active site, most of the variants' melting behavior is most appropriately to compare to that of apoMn-SOD. From this perspective, it is interesting to note that the Q146Y variant is most WT-like, with its $T_m$ of 55 ℃ being close to the 52 ℃ for WT-apoMn-SOD. The Q146A, -S and -C all displayed higher $T_m$*s* (in that order) and lower Mn contents. However their Mn contents do not decrease in in the same order as their $T_m$*s* increase (instead the content varies as -N > (-C & S & Y) > -A). Thus our comparison of the different Q146X variants indicates that the degree to which Mn is assimilated depends on factors additional to those that determine the $T_m$. It appears that factors other than metal ion binding stabilizes the structure of this protein even more than Mn binding stabilizes WT-apoMn-SOD.

The five different residues introduced at position 146 has profound effects on the thermal stability of the enzyme (Table 4-5). Compared with that of apoMn-SOD, the high melting temperature of Q146X appears mostly due to a large value of $\Delta H$, suggesting that the Q146X has been stabilized thermally by higher enthalpy than the WT-Mn-SOD and apo Mn-SOD protein. On the other side, the relatively large $\Delta S$ of Q146X-Mn-SOD reflects that the unfolding process of mutant protein mainly driven by increasing the entropic energy at elevated temperature.

Figure 4-7 also displays overlaid CD spectra of Q146X at pH 7.4 in 5 mM potassium phosphate buffer over the UV range at room temperature. For background

baseline correction the spectrum of the buffer was subtracted from the sample spectrum. At the UV range, the CD spectrum mostly are contributed by absorption of peptide carbonyl groups which gives information on the secondary structure of the protein.[102] The spectrum of Q146X from the CD scanning closely resembles each other, indicating their similarity on secondary structure component.

### 4.3.6 Electronic configuration of metal cofactor of Q146X-MnSOD

For direct characterization of the electronic configuration of transition metal ion cofactors with unpaired electrons, electron paramagnetic resonance (EPR) is a very useful and sensitive technique via absorption of microwave radiation by electron spin transitions in an applied magnetic field. The microwave frequency used in this experiment is denoted as X-band ($\nu \approx 9.25$ GHz) and is held constant. The resonance condition is met by varying the external magnetic field $H_0$ and signals are observed when $g'\beta H_0 = h\nu$. EPR spectra of transition metal ions are generally recorded on frozen samples so as to slow electron spin relaxation and sharpen the lines for ease of detection. Because the samples are frozen solid, the spectrum represents the summation of all possible orientations of the active sites in the magnetic field. Therefore, all the data were acquired at 114–120 K. $Mn^{2+}$ has five unpaired electrons and occurs in the high-spin state (S=5/2) at the active site of resting $Mn^{2+}$SOD,[25a, 42a, 103] thus signals are expected near g' = 6, 4 and 2. Moreover the $^{55}$Mn nucleus has a nuclear spin of I = 5/2 so the hyperfine interaction would split the EPR signal and give rise to a characteristic six-line pattern. The ≈ 90 G magnitude of the splitting (the separation between the hyperfine lines) is diagnostic for mononuclear $Mn^{2+}$ sites.

The presence of $Mn^{2+}$ in Mn-SOD and its position-146 variants was confirmed by the EPR data in Figure 4-4, 4-5 and 4-6. But the EPR spectra of Q146Y-MnSOD do not show a clear hyperfine structure characteristic of $Mn^{2+}$, even after reducing $Mn^{3+}$ with dithionite (Figure 4-6). $Mn^{2+}$-SOD probably has experienced a strongly altered coordination geometry and electronic structure of active site Mn ion. Or it is not reducible by dithionite because the strong signal near 1570 G ($g' \approx 4.3$) is typical of rhombic $Fe^{3+}$ sites.[46] Indeed its intensity diminishes to almost zero upon reduction with dithionite and 7.3 % iron content of the Q146Y is much higher than its Mn content (3.9 %) and Fe content of other mutants (0.2 – 5 % ) (Table 4-3).

The shapes of the EPR signals are not identical. In particular the signal of the WT site displays a total of 9 lines in the region of $g' \approx 4.5$ and the three central lines are stronger, which indicates that two sextets of $Mn^{2+}$ six-line overlap. At X-band it is not easy to distinguish between effects of g-anisotropy vs. zero-field splitting. However adopting for simplicity the assumption that the different sextets stem from g-anisotropy ($g_x \neq g_y$), the situation in WT-$Mn^{2+}$-SOD is that the amplitude of the up-field three lines of the $g_x$ transition reinforce the three low-field lines of the $g_y$ transition. When the separation between $g_x$ and $g_y$ is not an integer multiple of the hyperfine splitting, or the hyperfine splittings of the two transitions are not the same, the two patterns may interfere destructively instead and produce apparent smoothing of the hyperfine structure. Second-order hyperfine effects can also produce broadening of the higher-field hyperfine lines and thus their apparent attenuation. Thus, the differing numbers of strong central hyperfine lines can be explained in terms of variations in the hyperfine constants, g-anisotropy of the different sites, and hence altered coordination geometries and electronic structures. EPR

spectra are very sensitive to even subtle electronic and geometric effects, However even these could be factors in the low per-Mn catalytic activities of the position-146 variants.

### 4.3.7 Q146A-Mn-SOD

The mutant Q146A exhibited the highest per-Mn activity (Figure 4-3). This is despite the fact that Q146N is considered as the most conservative mutation from a chemical perspective. Previous studies have demonstrated that Gln146 forms a hydrogen bond with Tyr34 which is thought to forms half of a gateway through which substrate accesses to the active site.[35b, 79a] The mutation of Gln146 to Ala of human Mn-SOD, removes the hydrogen bond between the carboxamide group and Tyr34 as well as the coordinated solvent molecule. However the small side chain of Ala leaves a lot of space and the crystal structure shows two solvent molecules which can sit in and serve as proton donors or acceptors.[42b] Studies by Silverman's and Tainer's teams showed that Q143A-MnSOD from human (equivalent to Q146A of *E. coli*) has higher degree of metal ion on its activity.[50c] Since our Q146A-MnSOD also displayed significantly higher per-Mn catalytic activity than the other position-146 variants, it is worthwhile to investigate its detail.

Azide is commonly used as a substrate analogue of superoxide for SOD since it has the same charge and is similar in size to superoxide.[104] Azide binding to WT-$Mn^{3+}$-SOD produces a shift in the optical band to shorter wavelength with a maximum absorption near 420 nm that has explained on the basis of conversion of the $Mn^{3+}$ site from five- to six-coordinate (Figure 4-8).[34] The azide titration showed that $Mn^{3+}$-SOD has a Kd of 7.7 ± 1.0

mM under the condition of 5 mM phosphate buffer pH 7.4 in Figure 4-8 from the absorbance at 400 nm. This agrees with published values of 7.2 mM by Whittaker.[30]

Figure 4-9 shows the spectra and data analysis of azide binding to Q146A-$Mn^{3+}$-SOD. The estimated Kd in 5 mM phosphate buffer pH 7.4 for Q146A-MnSOD azide binding is ~3 mM by monitoring the change of the absorbance at 400 nm. Unlike WT-Mn-SOD displaying a shift of the maximum absorbance towards 420 nm, the Q146A didn't exhibit such feature up to 260 mM azide titration and the amplitude for changes of absorbance at 420 nm are relatively small. The Kd of WT-$Mn^{3+}$SOD for azide is 7 mM.[30] Considering that azide binds 20 times less tightly to the Mn complex of SOD in WT-MnSOD than Fe complex (Table 4-6),[30] it is not a surprise to find weaker azide binding to the Mn forms of Q146A-SODs.

Consistent with the optical spectrum from azide titration, the EPR spectrum of Q146A-$Mn^{2+}$SOD shows no perturbation binding related to 260 mM azide (Figure 4-15) indicating conversion of the $Mn^{3+}$ site from five- to six-coordinate did not happen upon azide titration. The EPR spectra of the Q146A-$Mn^{2+}$SOD sample before and after azide titration closely resemble each other, indicating that there is not a significant change in the $Mn^{2+}$ coordination-sphere for azide addition up to 260 mM. Similarly, it is found that the azide inhibition is metal dependent in *psherm-camb*-Fe/MnSOD. The *psherm-camb*-FeSOD is more readily inhibited by azide than is *psherm-camb*-MnSOD.[77] The missing of 420 nm shoulder could also due to the low Mn content of Q146A-$Mn^{3+}$-SOD, given that the manganese ion per dimer is only 1.7 % and $Mn^{3+}$ only accounts for ~ 60 % of the total manganese binding at active site of Q146A.

Next we decide to try azide titration on Q146A-FesubMn-SOD. Q146A-FesubMn-SOD was produced by overexpressing the Q146A-MnSOD gene in bacteria growing in Mn-deprived Fe-enriched growth medium. The Fe content per active site was determined to be ~ 50 % based on the ferrozine assay and the Mn content was found to be < 0.5 % (based on acid hydrolysis limitation). The analogous WT-FesubMn-SOD was found to have ~ 75 % Fe and < 0.5 % Mn. Whereas WT-FesubMn-SOD had a specific activity of 53 Unit on a per-Fe basis, the Q146A-FesubMn-SOD had a specific activity of 51 U on a per-Fe basis (Table 4-6).

The optical spectrum of Q146A-FesubMn-SOD resembles that of WT-FesubMn-SOD at 420 nm (Figure 4-10). Titration with azide was used to assess Q146A-$Fe^{3+}$subMn-SOD's anion-binding affinity. The specra of azide titrations of Q146A-$Fe^{3+}$SOD and WT-$Fe^{3+}$subMn-SOD are shown in Figure 4-11 and Figure 4-12. The new feature that grows in near 420 nm has been assigned to a ligand-to-metal ion band[45a, 74] in FeSOD and WT-FesubMn-SOD. The similarities of spectra between WT-FesubMn-SOD and Q146A-$Fe^{3+}$subMn-SOD upon azide titration indicate that the oxidized states of the two systems react similarly with $N_3^-$ (and therefore likely superoxide). The azide Kd of WT-FesubMn-SOD and Q146A- FesubMn-SOD was found to be 0.33 ± 0.04 mM and 0.29 ± 0.02 mM. Both are in agreement with the published literature value of 0.3 mM at pH 7.0.[50a]

The coordination environment of the active site $Fe^{3+}$ was characterized by EPR. In agreement with the new optical signature formed at 420 nm upon azide binding (Figure 4-11 and Figure 4-12), the EPR spectra shown in the Figure 4-13 and 4-14 provided evidence of an expansion of the $Fe^{3+}$ coordination sphere in the two FesubMn-SOD proteins upon

azide binding. The binding of azide showed no prominently different behavior between mutants Q146A-FesubMn-SOD and wild type FesubMn-SOD. The EPR spectra of Q146A-FesubMn-SOD in Figure 4-13 showed that upon $N_3^-$ binding there was a decrease in axial signal intensity near 800 G, a strong increase in intensity near 1450 G (g' = 4.51) and also an increase in signal intensity near g'=3.51. For FesubMn-SOD (Figure 4-14), there was a much smaller reduction in axial signal intensity near 800 G compared with Q146A-FesubMn-SOD. Both FesubMn-SOD and Q146A-FesubMn-SOD represents the transition from a five-coordinate to a six-coordinate system as it exhibits a strong rhombic symmetry. When azide was added, disappearance of the anisotropy signals (g = 3.51, 3.85, 4.87) reflected a low rhombic $Fe^{3+}$ and exhibited a strong rhombic absorption at g = 4.31 (Figure 4-13). Increasing rhombicity is associated with lower symmetry for the site, which indicateds an octahedral $Fe^{3+}$ site,[31] suggesting that azide binding to the $Fe^{3+}$ center gives rise to a six-coordination state. (It should be noted that in Figure 4-13 and Figure 4-14 our FesubMn-SOD and Q146A-FesubMn-SOD sample contained a small but common amount of non-active site iron (NAS Fe)[31, 71] between 1500 G – 1600 G where g = 4.3.)

In summary, the thermal stability of the protein was improved by the mutation Q146A (Figure 4-7). The maximum absorbance at 420 nm might be due to the absorption of Fe-complex at the active center since FesubMn-SOD and Q146A-FesubMn-SOD both exhibit the same shoulder at 420 nm on their visible spectra (Figure 4-10). Although results in Table 4-4 show that the midpoint potential for Q146A-Mn-SOD is increased by 110 mv compared with wild type, but still appropriate for function. Elucidation of the structure of the Q146A-MnSOD should help to explain the chemical nature of the physical effects observed.

### 4.3.8 Q146C, Q146N and Q146S -MnSOD

Replacing Gln146 with Cys, whose side chain thiol has a much lower pK than the Gln side chain (pKa 8.4,  vs 17 for the free side chains),[105] is expected to facilitate proton transfer from the hydrogen-bond network to coordinated solvent. Cys has only one labile side chain H whereas Gln has two. The side chain of Cys is also a very active nucleophile after deprotonation, compared with the nitrogen and oxygen of the carboxamide group of Gln146. These differences are expected to alter the proton distribution in the hydrogen bond network.

The replacement of Gln146 with Ser, which carry a polar primary alcohol side chain with a pKa 13.5, are expected to also preserve the hydrogen bonding, but with consequences for the network. Because Ser with a single labile H, should be able to act as both a hydrogen donor and acceptor while keeping the hydrogen bonding with solvent molecules or other amino acids. Thus Q146S and Q146C substitutions could inform us as to the function of the nitrogen of the carboxamide group of Gln.

Asn is one of the 20 natural amino acids which is mostly structurally and functionally similar to the Gln. The crystal structure of Q143N human MnSOD shows that Asn has a carboxamide group only a shorter tether to the backbone, 1.7 Å more distance from the manganese ion than the wild type protein.[79a] At the active site of the equivalent mutant Q143N of human MnSOD, it is found that an extra water molecule fills the space vacated by mutation[49] and involves in the protonation relay by altering the its pKa by 7 unites.[106]

Q146C, Q146N and Q146S displayed diminished the catalytic activity in both protein (U/mg) and metal stoichiometry (U/ mM) by an order of 2- 3 magnitude (Table 4-3) compared to that of WT-Mn-SOD. All of these three mutants also displayed an improved thermal stability upon temperature induced unfolding (Figure 4-7). Both the EPR spectrum of MnQ146C, MnQ146S and MnQ146N (Figure 4-5 and Figure 4-6) are dominated by intense absorption near g = 6 (~ 1100 G) very similar to the WT-Mn-SOD. These similarities reflect that the metal coordination-sphere composition are not altered significantly by replacing Gln146 side chain by Cys, Ser or Asn near the active site of MnSOD.

Normally mutations at position 146 increased the iron content of the mutants,[25a, 42b, 49] but the most conservative mutation, replacing Gln146 with Asn exhibited Mn content(16 %) much higher than its Fe content(0.2 %) at its active site different from other mutants (Table 4-3). The Q146N-MnSOD has a Mn content which is 80 times than its Fe content, indicating the carboxamide group might have some selectivity on in metal binding.

### 4.3.9 Q146Y-MnSOD

Similar to other mutants of MnSOD at position Gln146, the MnQ146Y exhibited a reduced superoxide dismutase activity (Table 4-3). The thermal stability of Q146Y is also ruptured probably due to the bulk side chain (Figure 4-7). Q146Y preserved hydrogen bonding ability, with a pKa intermediate between those of Ser and Cys. The bulk side chain of the Tyr side was deployed in an effort to position the hydroxyl group close enough to the metal ion to displace coordinated solvent and possibly even coordinated the metal ion, as is observed in some catechol dioxygenases.[107] However our EPR data and ferrozine

assay suggest that Q146Y coordinates so little metal ion that it is difficult to assess the substitution's effect on metal ion coordination (Table 4-3).

### 4.3.10 Discussion

To clarify the role Gln146 in the putative proton relay and hydrogen bond network, we have combined structural, spectroscopic and biochemical methods together to characterize a series of *E. coli* WT-Mn-SOD variants Q146X (X= A, C, N, S, Y).

The SOD enzymes are known to be among the fastest metalloproteins with $k_{cat}/K_m$ values on the order of $10^8$ to $10^9$ $M^{-1}$ $s^{-1}$.[108, 109] The substrate is superoxide radicals, $O_2^{\cdot-}$ , a relatively small anion with a high solubility in water at pH = 7.[110] The superoxide and hydroxyl radical are strong and active oxidants, being able to oxidize lots of organic substances, including proteins, nuclei acids, lipids, and carbohydrates, at a rates, $k$ ( $M^{-1}$ $s^{-1}$) values in the order of $10^6$ to $10^9$.[111] At pH = 4.8, the non-catalyzed disproportionation reaction (equation 4.9) exhibits a fastest rate k = $9.7 \times 10^7$ $M^{-1}$ $s^{-1}$.[111] However at neutral pHs similar to physiological condition, the rate of spontaneous disproportionation decreases substantially, k = $10^4$ $M^{-1}$ $S^{-1}$.[112]

$$HO_2 + O_2^{\cdot-} \xrightarrow{H^+} H_2O_2 + O_2 \qquad (4.9)$$

Given the rates of the disproportionation of superoxide with SOD, k = $10^8$ to $10^9$ $M^{-1}$ $s^{-1}$,[108, 109] almost every molecule of superoxide $O_2^{\cdot-}$ that interacts with SOD is transformed.[112] The rate at which SOD catalyzes superoxide is comparable to the diffusion limit for the substrate.[113] Thus SOD is considered to be a “catalytically perfect” enzyme.

To maintain "catalytic perfection" SOD must be able to maximize the optimal rates of all the chemical catalytic events. MnSOD's active center is 15 Å away from the bulk solvent.[19c] The $Mn^{3+}/Mn^{2+}$ ion at the active site is coordinated by three histidine and one aspartate residue and one solvent molecule forming a trigonal bipyramidal shape. The amino acid residues are found involved in adjusting the net charge of the active site, steering the negatively charged superoxide ions and positively charged protons towards the active site, and enabling the uncharged dioxygen and hydrogen peroxide products to release from the active site.[45b, 50d] For example, the channel ~ 4.9 Å across, between the side chains of Tyr34 (hydroxyl oxygen) and the imidazole ring of His30, is on control of the possible approach of substrates and release of products.[94]

The optical spectra at pH 7.4 of Q146A-, Q146C-, Q146N-, Q146S-, and Q146Y-Mn-SOD resembled each other but lacking an absorbance shoulder at 478 nm which is observed in that of WT-$Mn^{3+}$-SOD (Figure 4-2). The low Mn content and low ratio of $Mn^{3+}/Mn^{2+}$ of the mutants could explain this. The maximum absorbance at 420 nm is probably due to the Fe complex of the mutant by comparing the visible spectrum of Mn-SOD, mutants and FesubMn-SOD (Figure 4-2).

The most conservative mutant Q146N with a shorter side chain, showed a preference for Mn ion over Fe ion. But the $Mn^{3+}$ percentage of the total Mn at active center was decreased to 40 – 70 % by mutation while that of WT-Mn-SOD is 90 %. Based on the ratio of $Mn^{3+}$ to the $Mn^{2+}$ at the active site of Q146N, the estimated $E°$*s* should still all be able to dismutase superoxide (Table 4-4).

## 4.4 Conclusion

Replacement of Gln with Ala, Cys, Asn, Ser significantly increased stability of the protein (Table 4-5 and Figure 4-7), although their metal content is low, presumably because the hydrogen bonding introduced by the side chains improved the hydrogen bond network around 146. In our studies, the protein stability was disrupted by mutation Q146Y, displaying the lowest $T_m$ of all the mutants. The bulk side chain of the Tyr is employed in an effort to displace coordinated solvent and possible the coordinated metal ion by placing the hydroxyl group close enough to the active site, as is observed in some catechol dioxygenases.[114] Overall this results confirmed our finding in chapter 3 that Gln146 is the one that destabilized the apo-Mn form of the SOD protein which contributes to metal binding.

The best per-Mn activity among the mutant is found in Q146A (its per-Fe activity is also comparable to the FesubMn-SOD). Replacing Gln146 with the small side chain of Ala leaves a lot of space. The crystal structure shows two solvent molecules would occupy that space and serve as proton donors or acceptor.[79a] The substrate analogue azide titration, showed that azide weakly binds to the metal ion of Q146A-MnSOD indicating a significantly less sensitivity to substrate. Based on the estimated Kd value of azide and EPR spectrum of the metal coordination, the accessibility of the active site to the substrate could be ordered from low to high, Q146A-MnSOD < MnSOD < Q146A-FesubMn-SOD < FesubMn-SOD (Table 4-6). The orientation of azide bound in active site is different between FeSOD and MnSOD.[23] Also the electrostatic interaction could influence Azide binding.[42b] Thus even if Q146A increases the space adjacent to the substrate access channel

by placing Ala instead of Gln, the extra solvent molecules in that space still might disfavor the new incoming substrate.

By applying amino acid substitutions that perturb but not break the hydrogen bond network, we conclude that the subtle alternations at position 146 nonetheless alters its ability in incorporating Mn ion, and Gln146 are responsible for maintaining the optimal metal coordination geometry and enzymatic chemistry. Our findings are important because numerous studies have shown that in many cases of cancers a minor alternation in MnSOD structure caused a significant loss of activity.[115] [113]

In the structures of MnSOD Gln146 forms a hydrogen bond with Tyr34 which is thought to be a major player in the substrate gateway (along with Trp 128 and His30). As such, the Tyr34, with a certain degree of conformational motion, lines the substrate access to and release from the active site,[94] is proposed to restrict the substrate's access to the active site.[35b, 79a] Collectively the Gln at position 146 also plays roles in maintaining the hydrogen bond networking, facilitating the substrate access and proton uptake, determining the rate limiting step for the overall reaction.

To completely clarify the role of Gln146, next we should prepare mutants with fully coordinated Mn (or Fe) ion at the active site, and investigate their proton transfer of the chemical reactions of MnSOD. For example we could begin with determination of the active site pKs and perform the azide titration of the protein samples at different pHs, since hydrogen bond network around the active-site is very sensitive to the environmental pH. We could also determine the crystal structure of Q146A-Mn-SOD and Q146A-FesubMn-SOD. We could find out their structure difference and whether there is additional solvent

molecules in the position that was occupied in the WT by the carboxamide of Gln. For the other Q146X variants, such structures would be valuable in revealing how side chains with only one labile H 'choose' between the different hydrogen bonding partners that must compete for it, via the orientation of the substituent side chains at position 146. Finally, it would be very informative to monitor the formation and decomposition of side-on peroxo complexes of $Mn^{3+}$-SOD and superoxide using pulse radiolysis or stopped-flow spectrophotometry.

Table 4-1: Oligonucleotides Primer Used in Site Directed Mutagenesis of MnSOD

| Name | sequence |
|---|---|
| **Q146A** | 5'- TG GTT TCT ACT GCT AAC GCC GAT TCT CC -3'<br>5'- T CAG CGG AGA ATC GGC GTT AGC AG T -3' |
| **Q146C** | 5'- G GTT TCT ACT GCT AAC TGC GAT TCT CC -3'<br>5'- T CAG CGG AGA ATC GCA GTT AGC AGT -3' |
| **Q146N** | 5'- G GTG GTT TCT ACT GCT AAC AAC GAT TC -3'<br>5'- CAG CGG AGA ATC GTT GTT AGC AGT A -3' |
| **Q146S** | 5'- CT ACT GCT AAC TCA GAT TCT CCG CT -3'<br>5'- CAT CAG CGG AGA ATC TGA GTT AGC A -3' |
| **Q146Y** | 5'- G GTT TCT ACT GCT AAC TAC GAT TCT CC -3'<br>5'- AT CAG CGG AGA ATC GTA GTT AGC AG -3' |

Table 4-2: Corrected Molar Extinction Coefficient at 280 nm for Mutant Q146X

| Protein | $\varepsilon_{280\ nm}$ ($M^{-1}cm^{-1}$) |
|---|---|
| **Q146A-Mn-SOD** | $8.43 \times 10^4$ |
| **Q146C-Mn-SOD** | $7.17 \times 10^4$ |
| **Q146N-Mn-SOD** | $8.25 \times 10^4$ |
| **Q146S-Mn-SOD** | $8.10 \times 10^4$ |
| **Q146Y-Mn-SOD** | $8.16 \times 10^4$ |

$\varepsilon_{MnSOD}$ is the molar extinction coefficient for *E. coli* MnSOD at 280 nm ($\varepsilon_{MnSOD\ 280\ nm}$ =$8.66 \times 10^4$ $M^{-1}cm^{-1}$).[75a] The calculated molar extinction coefficient of denatured protein (equation 4.3) is 86200 $M^{-1}cm^{-1}$ for Q146A, Q146C, Q146N, and Q146S, 88760 $M^{-1}cm^{-1}$ for Q146Y.

Table 4-3: Metal Content, Catalytic Activity and Melting Temperature of Wild-Type MnSOD and its Mutants Q146X

| | Q146A | Q146C | Q146N | Q146S | Q146Y | MnSOD |
|---|---|---|---|---|---|---|
| **Mn content** | 1.7 % ± 0.1 | 4.6 % ± 0.3 | 16 % ± 0.9 | 5.2 % ± 0.5 | 3.9 % ± 0.4 | 98 % ± 8 |
| **$Mn^{3+}/Mn$**[b] | ~60% | ~40% | ~70% | ~70% | ~40% | ~ 90% |
| **Fe content** | 2.9 % ± 0.2 | 2.9 % ± 0.2 | 0.2 % ± 0.0 | 5.0 % ± 0.3 | 7.3 % ± 0.5 | ~ 1 % ± 0.0 |
| **Activity (U/mg protein)**[C] | 260 ±20 | 2 ± 0 | 30 ± 5 | 10 ± 2 | 30 ± 3 | 20000 ± 180 |
| **Activity/Mn stoichiometry** | 7600 | 20 | 90 | 130 | 400 | 10000 |
| **Activity/Mn (U/µmol metal)**[d] | 620 | 1 | 4 | 6 | 20 | 460 |

[a] Mn content was expressed on a per dimer basis and measured by EPR after acid hydrolysis, as described in the methods section 4.2.5.The Mn standard curve was plotted as least squares linear fitting $R^2$-value > 0.97 by GraphPad Prism (Figure 4-3). The detection limit was as low as 40 µM $Mn^{2+}$ or 0.001 per dimer. [b] $Mn^{3+}/Mn$ ratio is measured by EPR. The $Mn^{2+}$ content in sample solution is proportional to the signal amplitude of EPR spectra new g'=4.5. The amplitude is quantified by measuring the peak-to-trough heights of the third and fourth hyperfine lines. [c] Catalytic activity was measured by the xanthine oxidase/cytochrome c assay at pH 7.8,[71] as described in the method. [d] Catalytic activity (U/mg) of SOD by the xanthine oxidase/cytochrome c assay was converted into the catalytic activity per µmole of metal site ( U/µmol) based on the Mn occupancy per Dimer (Mn/Dimer). [e] Melting temperature was estimated from the temperature-induced unfolding mutant of MnSOD, Q146A, Q146C, Q146N, Q146S, Q146Y (Figure 4-7). The melting temperature determined by software CDpro as described in the section 3.2.3.

Table 4-4: Estimated *Δ E°s* of Mutants Q146X-MnSOD

| **Protein** | **Q146A** | **Q146C** | **Q146N** | **Q146S** | **Q146Y** |
|---|---|---|---|---|---|
| **$Mn^{3+}/Mn^{2+}$** | 1.5 | 0.7 | 2.3 | 2.3 | 0.7 |
| ***ΔE°s* (mV)** | 110 | 150 | 80 | 80 | 150 |

Protein samples are in 5 mM phosphate buffer at pH 7.4. The $Mn^{3+}/Mn^{2+}$ ratio is estimated by Mn content expressed on a per dimer basis and measured by EPR after acid hydrolysis of protein samples, as described in the methods section 4.2.5. The changes of redox potential *E°s* of mutants Q146X-Mn-SOD (*ΔE°s*) was calculated following equation 4.8. *Δ E°s* was estimated as $\Delta E° = E°x - E°_{WT}$.

Table 4-5: Thermodynamic parameters of denaturation of holoMn-SOD, apoMn-SOD, and mutants Q146X upon heating in 0.8 M guanidinium HCl

| | **ΔH (kJ/mol)** | **ΔS ( J/(mol*K))** | **$T_m$ (℃)** | **$T_m$ [a](℃)** |
|---|---|---|---|---|
| **holoMn-SOD** | 240 ± 10 | 700 ± 40 | 67.4 ± 0.2 | 88.9 |
| **apoMn-SOD** | 270 ± 30 | 820 ± 100 | 53.0 ± 0.5 | NA |
| **Q146E-Mn-SOD** | 1300 ± 200 | 3900 ± 700 | 51.3 ± 0.2 | NA |
| **Q146E-apoMn-SOD** | 670 ± 50 | 1900 ± 100 | 87.9 ± 0.1 | 103.0 |
| **Q146A** | 390 ±30 | 1120 ± 90 | 80.1 ± 0.2 | 79.8 |
| **Q146C** | 490 ± 30 | 1400 ± 90 | 80.0 ± 0.1 | NA |
| **Q146N** | 320 ± 20 | 910 ± 60 | 74.6 ± 0.2 | 90.7 |
| **Q146S** | 280 ± 20 | 770 ± 50 | 87.9 ± 0.5 | 94.9 |
| **Q146Y** | 600 ± 50 | 1800 ± 200 | 56.2 ± 0.1 | NA |

The thermodynamic properties upon protein thermal denaturation $N \rightarrow U$ from 20 to 100 ℃ was analyzed by following the van't Hoff analysis in the method part of chapter 3 based on the refined melting curve in Figure 4-7 using CDpro analysis provided by Jasco Co. [a] From Leveque et al,[42b] transition temperatures was measured by scanning calorimetry for the unfolding of wild type human MnSOD and mutants at position 143.

Table 4-6: Azide Affinities and Specific Activities for MnSOD Complexes

| | MnSOD | Q146A-Mn-SOD | FesubMn-SOD | Q146A-FesubMn-SOD |
|---|---|---|---|---|
| **Kd(mM)** | 7.7 ± 1.0 | 3 ± 1 | 0.29 ± 0.02 | 0.33 ± 0.04 |
| **Mn content** | 98 % ± 8 | 1.7 % ± 0.1 | < 0.5 % | < 0.5 % |
| **Fe content** | 1% | 2.9 % | 76 % | 51 % |
| **Activity(U/mg)** | 20000 ± 180 | 260 ± 20 | 80 ± 10 | 60 ± 10 |
| **Activity/Metal stoichiometry** | 10000 | 7600 | 50 | 50 |

The published Kd for azide affinity of WT-Mn-SOD and FesubMn-SOD is 7.2 mM and 0.3 mM under pH 7.0 respectively.[30] The average error in these values is about 10 % based on multiple measurements. The Kd of FesubMn-SOD was measured under the same steps as described in the method 4.2.8. Unlike other protein samples, the Kd for azide affinity of Q146A-Mn-SOD was measured by the changes of absorbance at 400 nm upon azide titration by subtracting the zero-azide spectrum from absorption spectrum after each addition.

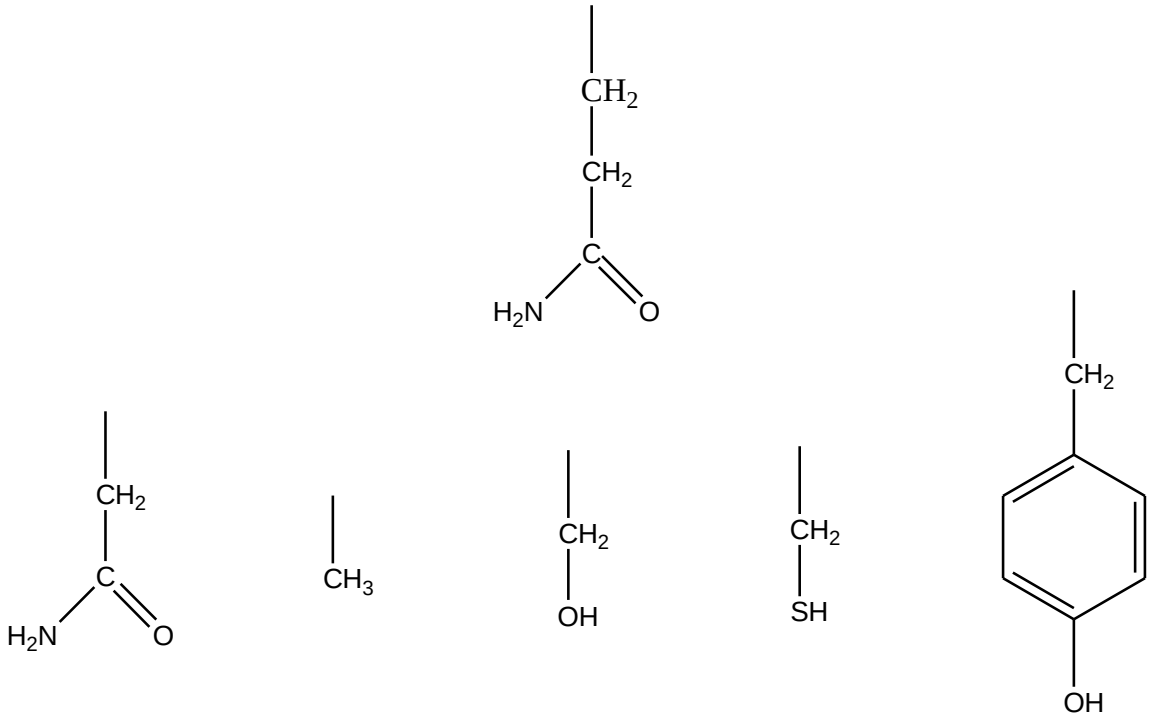


Figure 4-1: Mutations introduced at Gln146 of the *E. coli* MnSOD.

To study the role of glutamine 146 in the stability, catalysis and redox potential, mutation is introduced at Gln 146 of MnSOD. Top: side chain of Glutamine ( Gln, Q, MW: 128.14, pKa ~ 14). Bottom (from left to right): Asparagine ( Asn, N, MW: 114.11, pKa ~ 14), Alanine ( Ala, A, MW: 71.09, pKa >20), Serine ( Ser, S, MW: 87.08, pKa ~ 13), Cysteine (Cys, C, MW: 103.15, pKa = 8.35), Tyrosin ( Try, Y, MW: 163.18, pKa = 10.07)

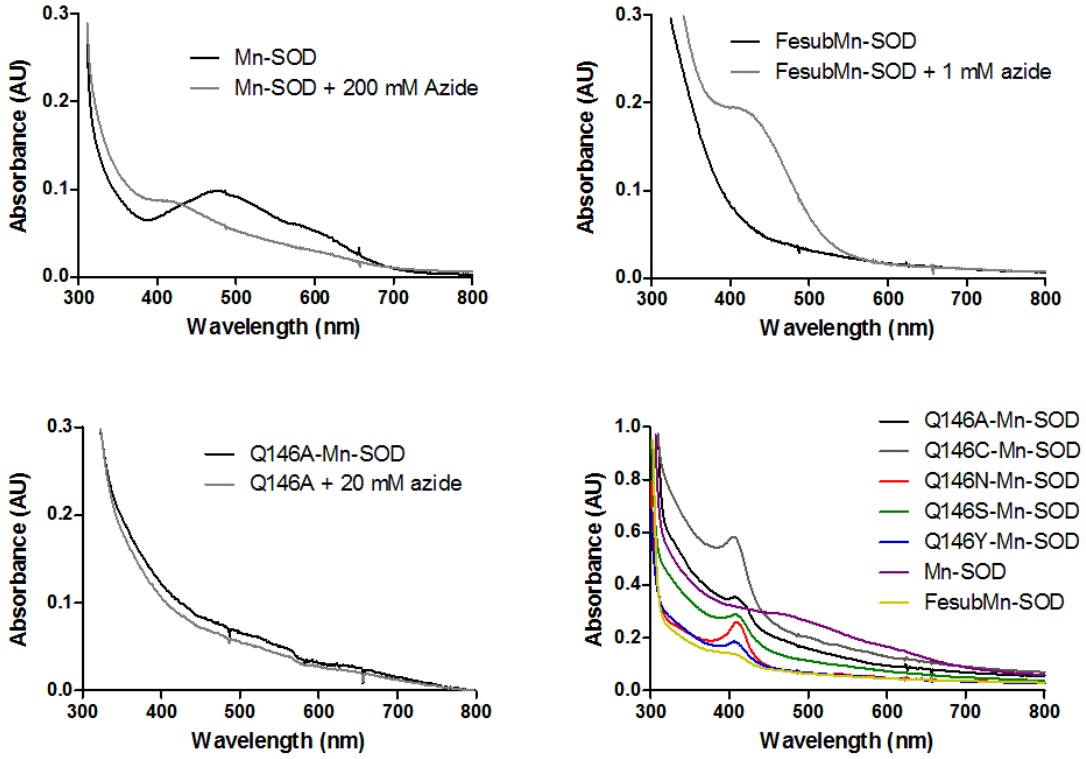


Figure 4-2: UV/Vis spectra of Mn-SOD, FesubMn-SOD and its mutants.

The bottom right is the UV/Vis spectrum of Mn-SOD and its mutants as purified measured at room temperature in 5 mM potassium phosphate buffer pH 7.4. A sharp absorption showed up at 420 nm for the signal of mutants. It was considered as the signature signal for Fe-complex.[50d, 99] The concentration of protein sample is approximate 77 µM for Mn-SOD, 95 µM for Q146A-Mn-SOD, 115 µM for Q146C-Mn-SOD, 70 µM for Q146N-Mn-SOD, 75 µM for Q146S-Mn-SOD, 64 µM for Q146Y-Mn-SOD, 70 µM for FesubMn-SOD by absorbance at 280 nm. All the spectrum were background corrected by absorption from 800 nm to 1000 nm as baseline. Top left, top right and bottom left is the visible absorption spectra of Mn-SOD, FesubMn-SOD, and Q146E with or without the azide bound.

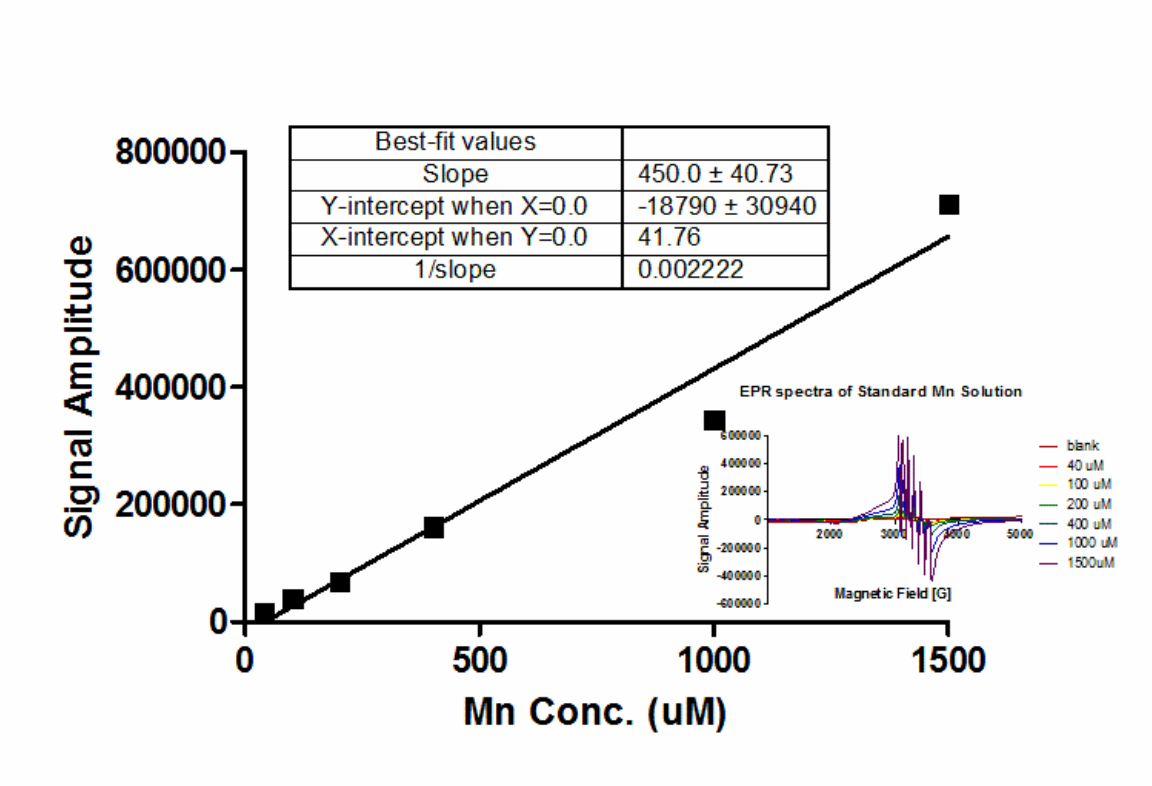


Figure 4-3: Standard curve for EPR spectrum of Mn content assay.

Standard curve of EPR assay on peak-to-trough height vs $Mn^{2+}$ concentration (µM) was linear with $R^2 = 0.968$. The points are the average of signal amplitude calculated from the peak-to trough height of the low-field third and fourth hyperfine line of $Mn^{2+}$. The inset plot is the EPR spectra for series of standard $Mn^{2+}$ solution at different concentration over the scanning magnetic field at ~110K.

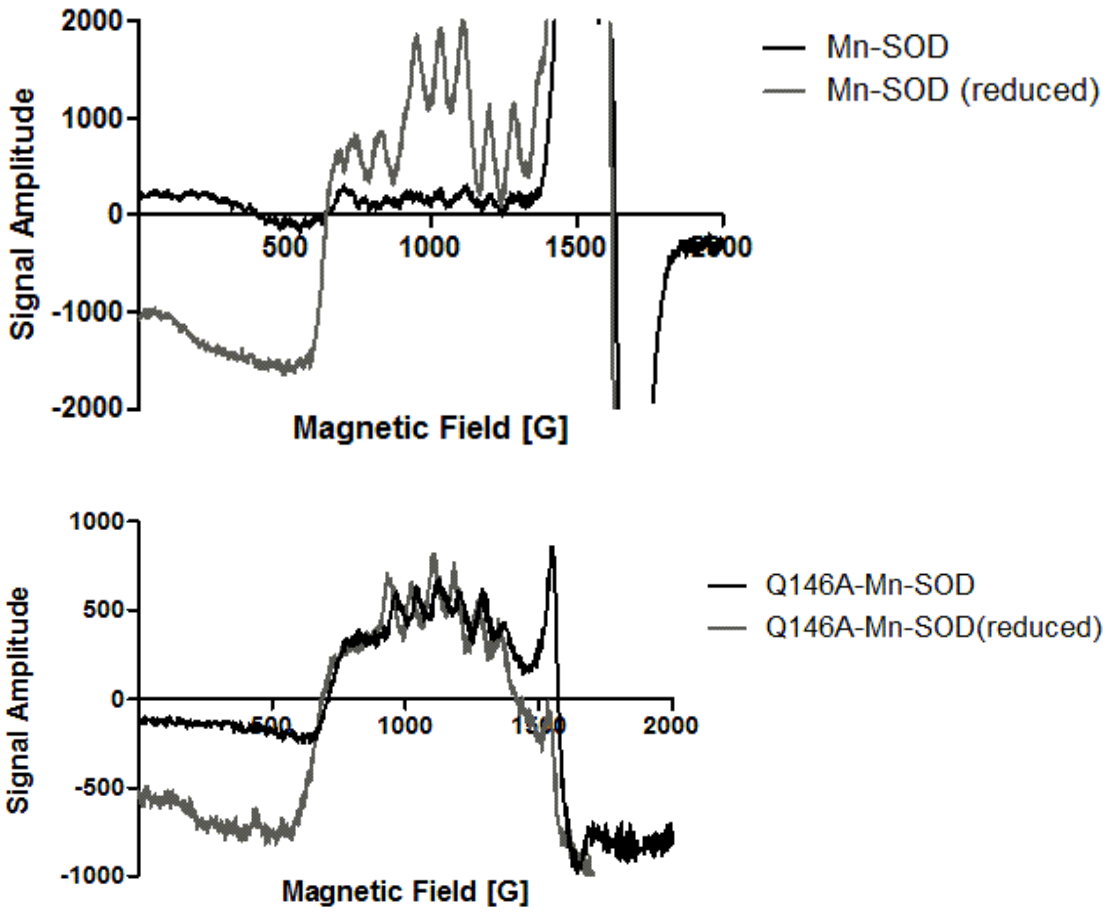


Figure 4-4: Effect of dithionite on the EPR spectra of $Mn^{2+}$-SOD (top) and its mutant Q146A-$Mn^{2+}$-SOD (bottom).

The EPR spectra of $Mn^{2+}$-SOD (top) and its mutant Q146A-$Mn^{2+}$-SOD (bottom) before (black line) and after (grey line) reduction by sodium dithionite is displayed. The amplitude of spectrum is in proportional to the $Mn^{2+}$ concentration. The spectrum upon reduction by sodium dithionite reflects the total of Mn ion concentration. EPR spectra were collected on a Bruker 300MX at 114K with a cytostat and liquid nitrogen flow as the coolant. Spectrum peak with the largest amplitude in the region of 1500G – 1600 G are due to those common amount of non-activesite iron (NAS Fe)[31, 71] where g = 4.3.

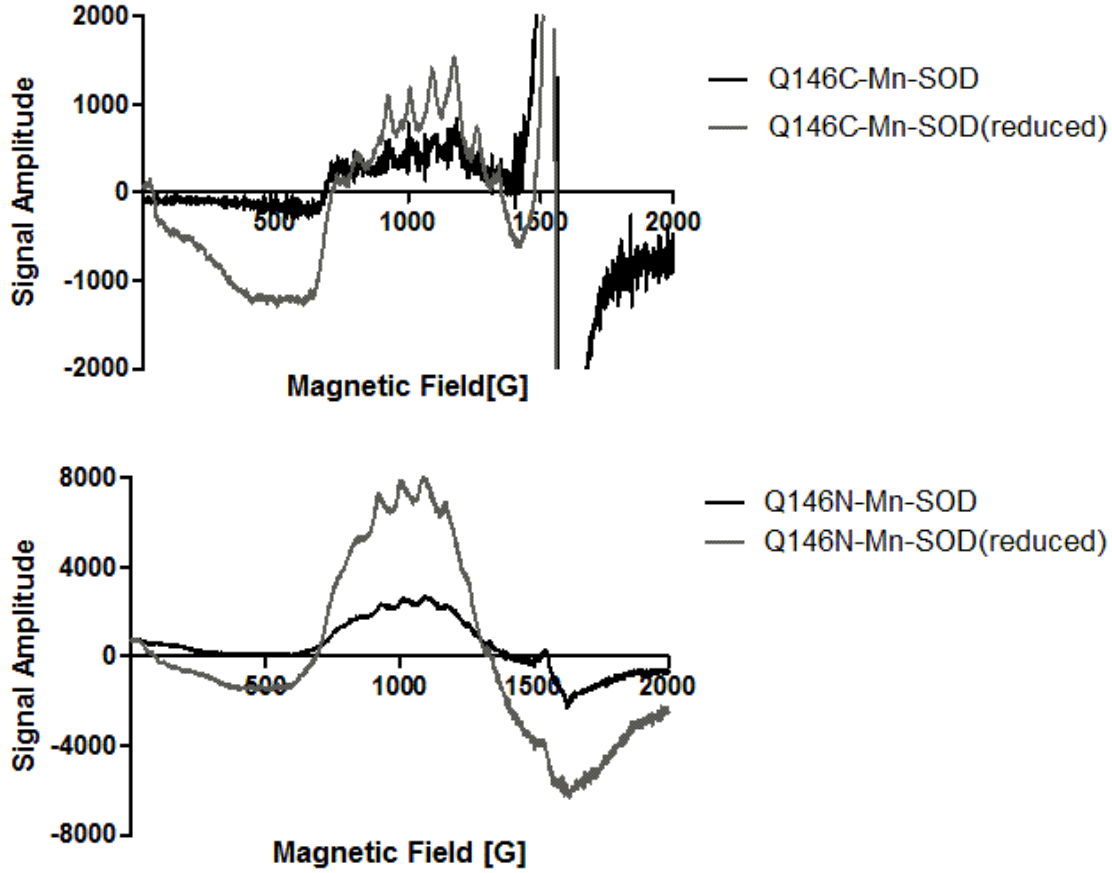


Figure 4-5: Effect of dithionite on the EPR spectra of mutants of MnSOD, Q146C-$Mn^{2+}$-SOD (top) and Q146N-$Mn^{2+}$-SOD (bottom).

The EPR spectra of mutants of MnSOD, Q146C-$Mn^{2+}$-SOD (top) and Q146N-$Mn^{2+}$-SOD (bottom) before (black line) and after (grey line) reduction by sodium dithionite is displayed. The amplitude of spectrum is in proportional to the $Mn^{2+}$ concentration. The spectrum upon reduction by sodium dithionite reflects the total of Mn ion concentration. EPR spectra were collected on a Bruker 300MX at 114K with a cytostat and liquid nitrogen flow as the coolant. Spectrum peak with the largest amplitude in the region of 1500G – 1600 G are due to those common amount of non-activesite iron (NAS Fe)[31, 71] where g = 4.3.

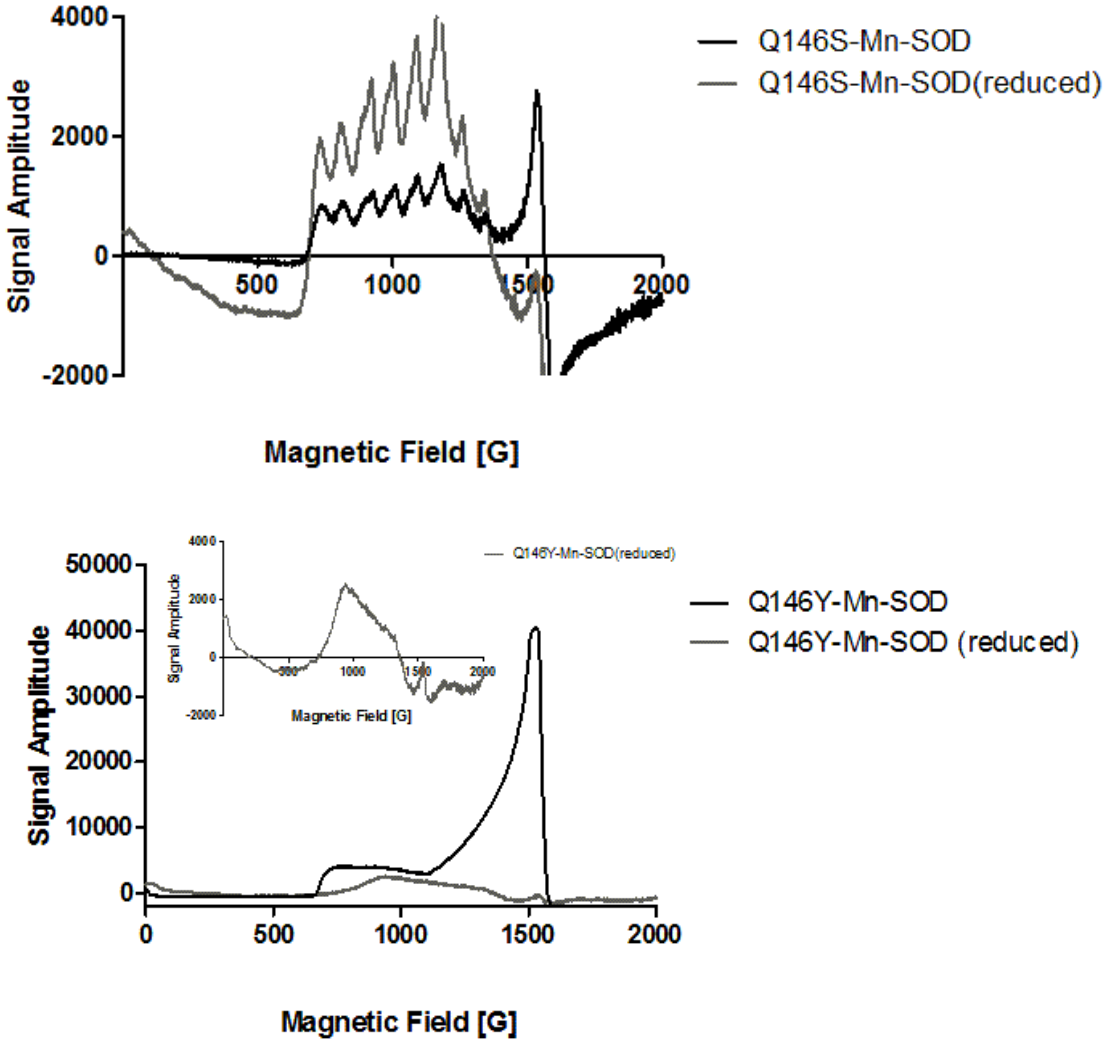


Figure 4-6: Effect of dithionite on the EPR spectra of mutants of MnSOD, Q146S-$Mn^{2+}$-SOD (top) and Q146Y-$Mn^{2+}$-SOD (bottom).

The EPR spectra of mutants of MnSOD, Q146S-$Mn^{2+}$-SOD (top) and Q146Y-$Mn^{2+}$-SOD (bottom) before (black line) and after (grey line) reduction by sodium dithionite is displayed. The amplitude of spectrum is in proportional to the $Mn^{2+}$ concentration. The spectrum upon reduction by sodium dithionite reflects the total of Mn ion concentration. EPR spectra were collected on a Bruker 300MX at 114K with a cytostat and liquid nitrogen flow as the coolant. Spectrum peak with the largest amplitude in the region of 1500G – 1600 G are due to those common amount of non-activesite iron (NAS Fe)[31, 71] where g = 4.3. The inset is the EPR spectrum of reduced MnQ146Y under a different y-axil scale.

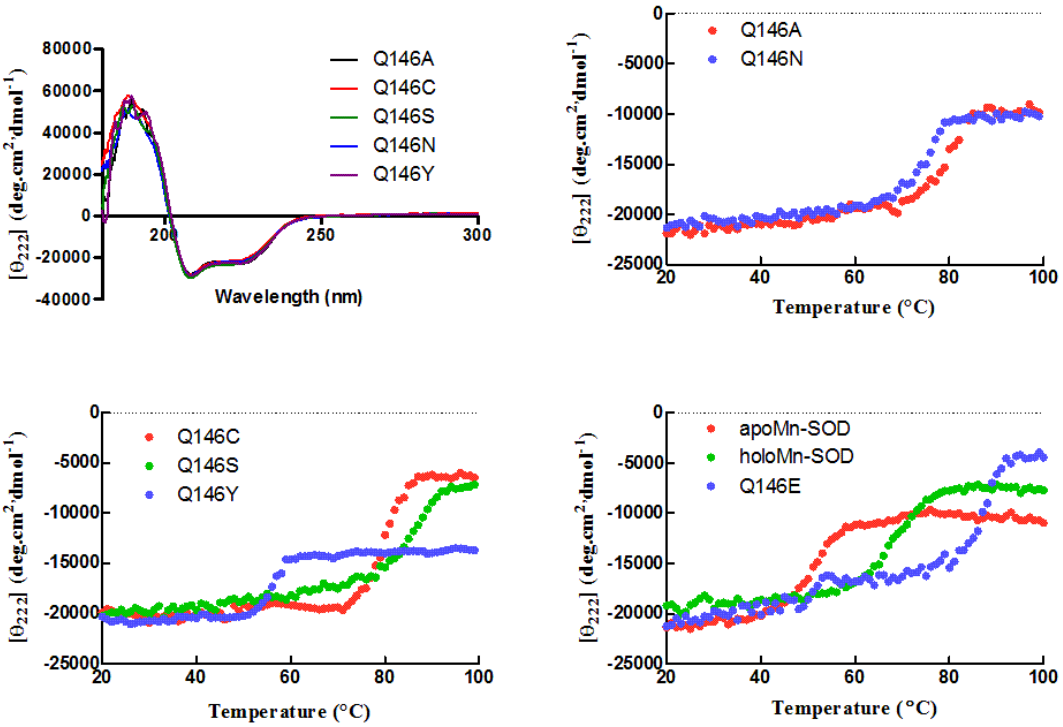


Figure 4-7: Temperature-induced unfolding of WT-holoMn-SOD, mutants Q146X-Mn-SOD and WT-apoMn-SOD.

Data was monitored via the ellipticity [θ] at 222nm. Top left is the CD spectra for each samples mutant Q146A, Q146C, Q146N, Q146S, Q146Y-Mn-SOD scanned in the far UV range from 180 to 300 nm at room temperature. The scanning rate is 100 nm/min with a wavelength step of 0.2 nm and four accumulations. A baseline was obtained by collecting the CD spectra of the buffer solution 5 mM Phosphate $KH_2PO_4$ at pH 7.4. For the temperature-dependent unfolding experiment of mutants (graph at top right and bottom left), 4-6 uM of protein sample of mutant was incubated in the buffer 5 mM $KH_2PO_4$, 0.8 M GdmCl pH 7. The graph at bottom right is obtained from chapter 3, 5 uM protein sample in the same buffer.

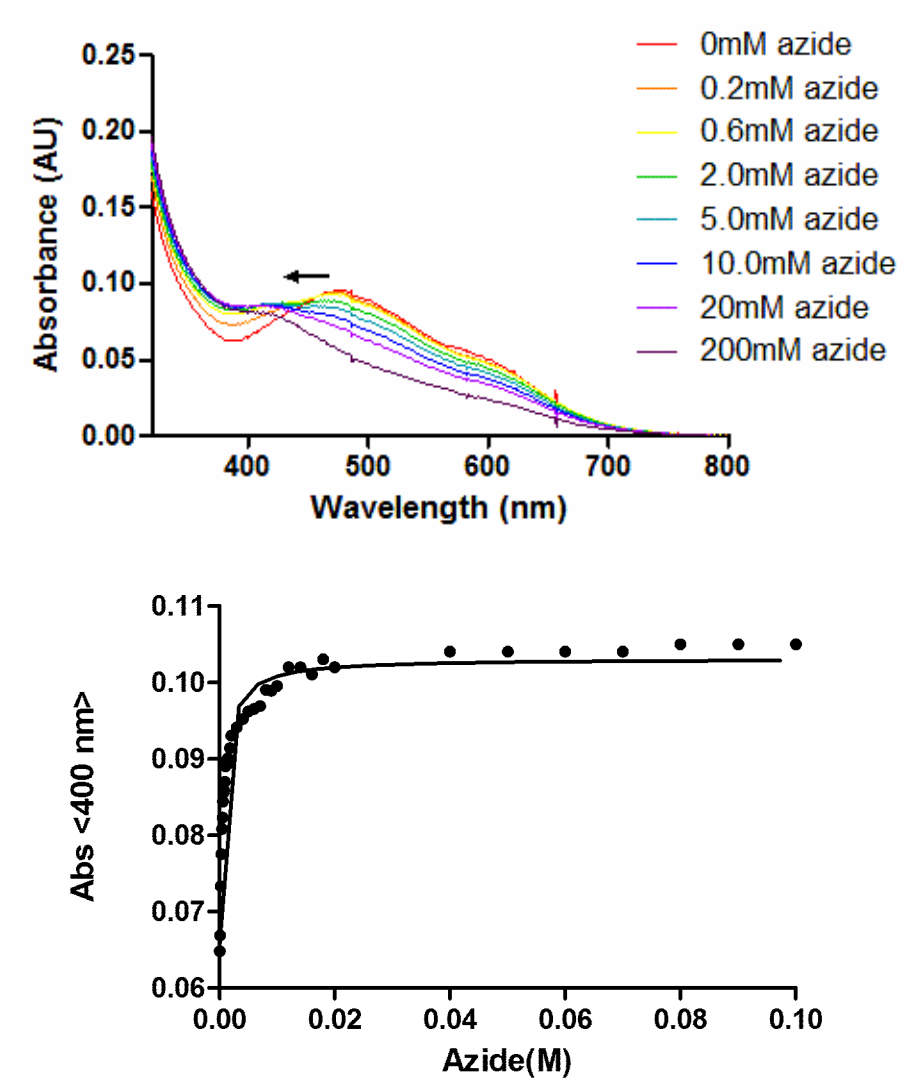


Figure 4-8: Effect of azide binding on the UV/Vis spectra of Mn-SOD.

UV/Vis spectra of Mn-SOD upon azide titration (top) and the nonlinear fitting analysis on data (bottom) are represented. The measurement of UV/Vis spectra of azide titration was performed at room temperature (25 ℃) in a buffer containing 5 mM potassium phosphate buffer pH 7.4. The absorbance was corrected by the absorbance of single wavelength at 800 nm. The nonlinear fit of data was analysis by user defined tight binding fitting of GraphPad Prism (equations 4.4) where the least square value is 0.97.The estimated Kd from the graph is 7.7 ± 1.0 mM.

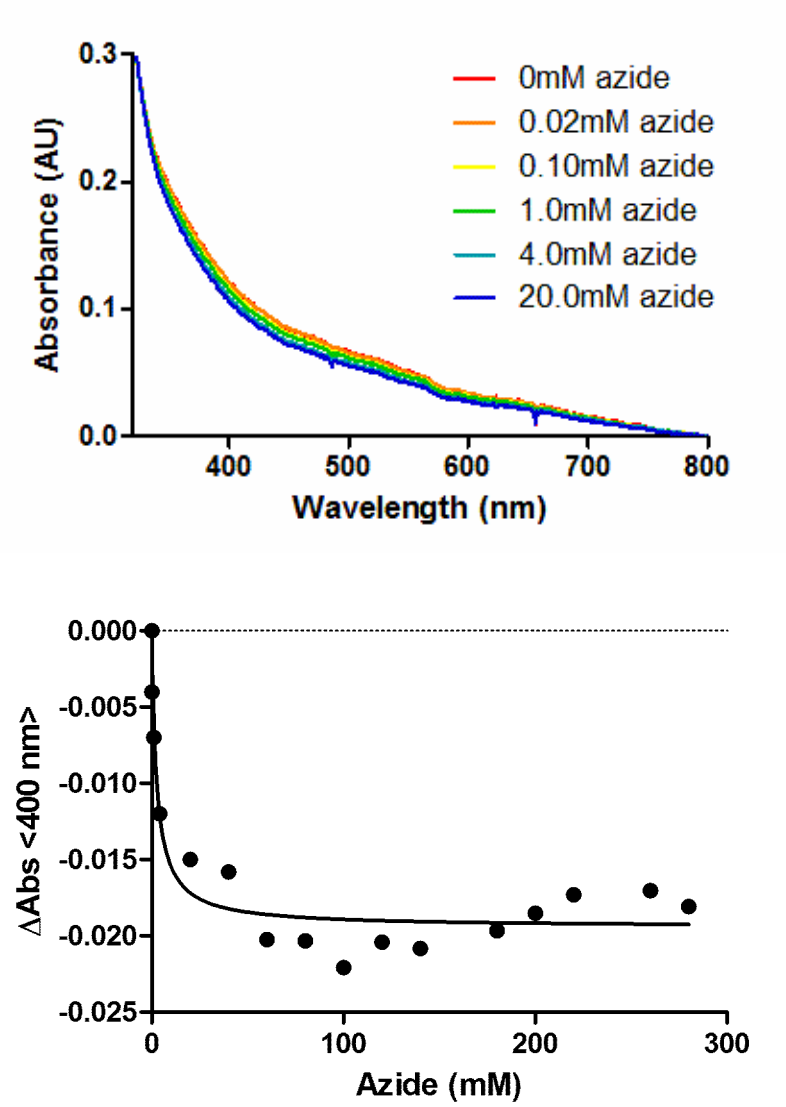


Figure 4-9: The effect of azide binding on the UV/Vis spectra of mutant Q146A-Mn-SOD.

The UV/Vis spectra of Q146A-Mn-SOD (top) were record from 200 to 1100 nm upon azide titration at 25 ºC in a buffer of 5 mM potassium phosphate pH 7.4. The absorbance was corrected by absorbance of single wavelength at 800 nm. Bottom is the difference of absorbance of Q146A-Mn-SOD at 400 nm upon azide titration by subtracting the spectrum of protein solution (0 mM azide) from absorption curve of each addition. The nonlinear fit of data was analysis by user defined tight binding fitting of GraphPad Prism (equation 4.4) where the least square value is 0.92.The estimated Kd from the graph is 3 ± 1 mM.

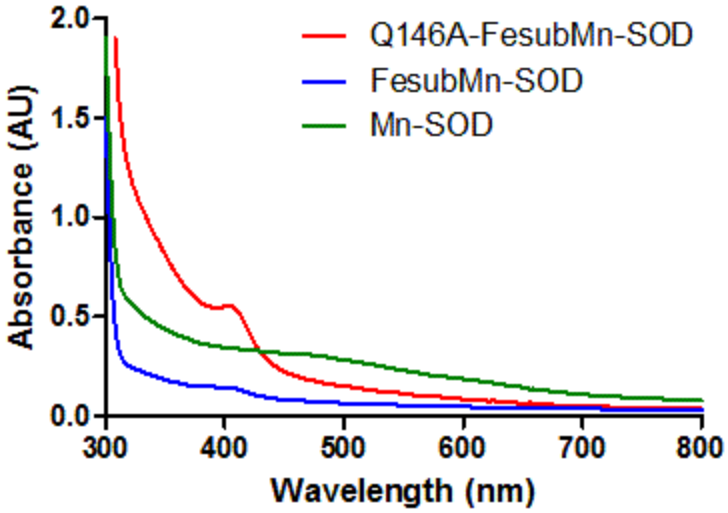


Figure 4-10: UV/Vis spectra of Mn-SOD, FesubMn-SOD and its mutants Q146A-FesubMn-SOD.

UV/Vis spectrum of protein sample as purified is measured at room temperature in 5 mM potassium phosphate buffer pH 7.4. A sharp radical absorption showed up at 420 nm for the signal of mutant Q146A-FesubMn-SOD and FesubMn-SOD.

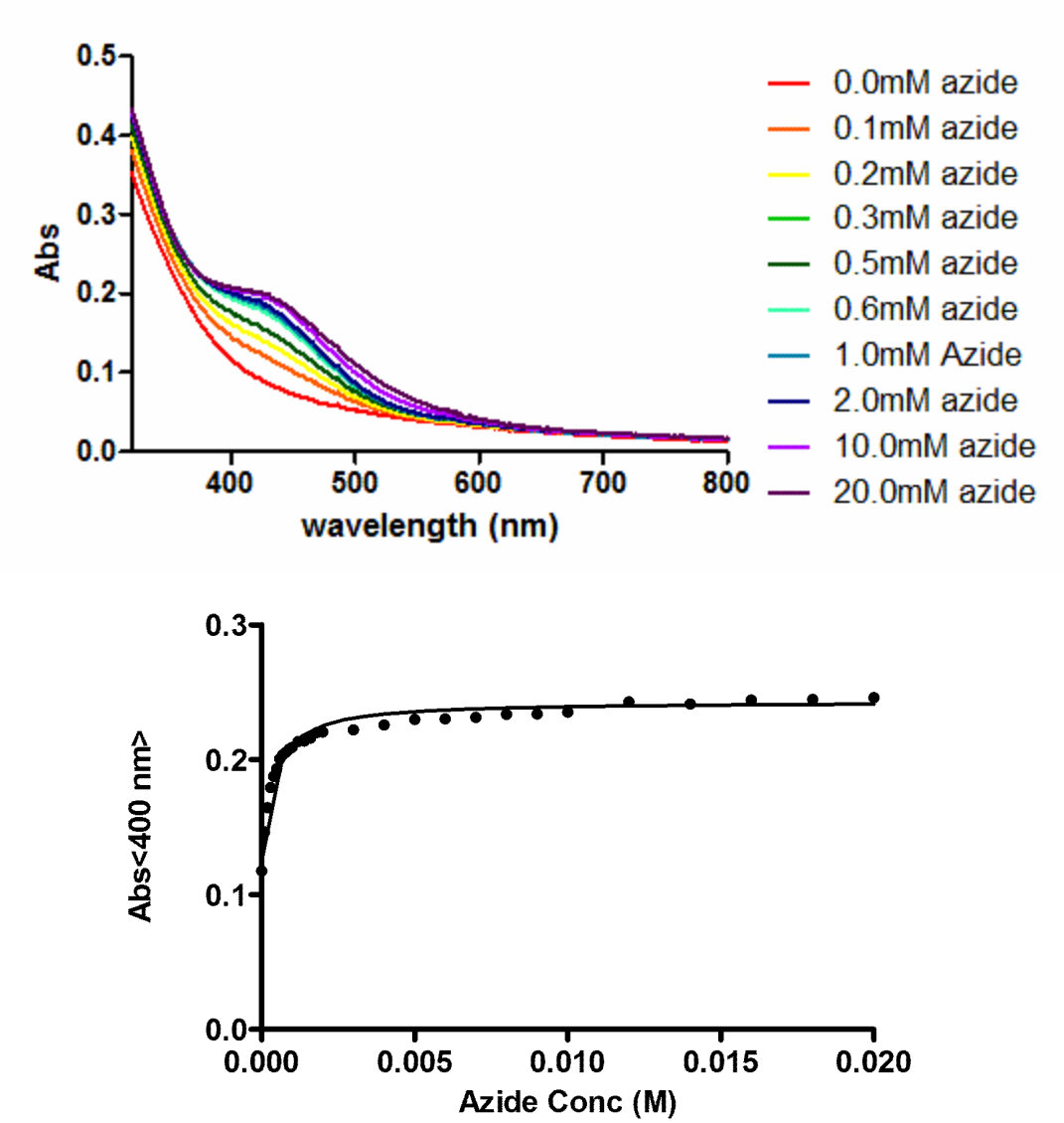


Figure 4-11: Effect of azide binding on the UV/Vis spectra of Q146A-FesubMn-SOD.

UV/Vis spectra of Q146A-FesubMn-SOD upon azide titration (top) and the nonlinear fitting analysis on data of 400 nm (bottom) are represented. The measurement of UV/Vis spectra of azide titration were performed at room temperature (25 ℃) in a buffer containing 5 mM potassium phosphate buffer pH 7.4. The absorbance was corrected by absorbance baseline between 800 – 1000 nm. The nonlinear fit of data was analysis by user defined tight binding fitting of GraphPad Prism (equation 4.4). The estimated Kd is the value of azide concentration at half the value of maximum of absorption, 0.33 ± 0.04 mM.

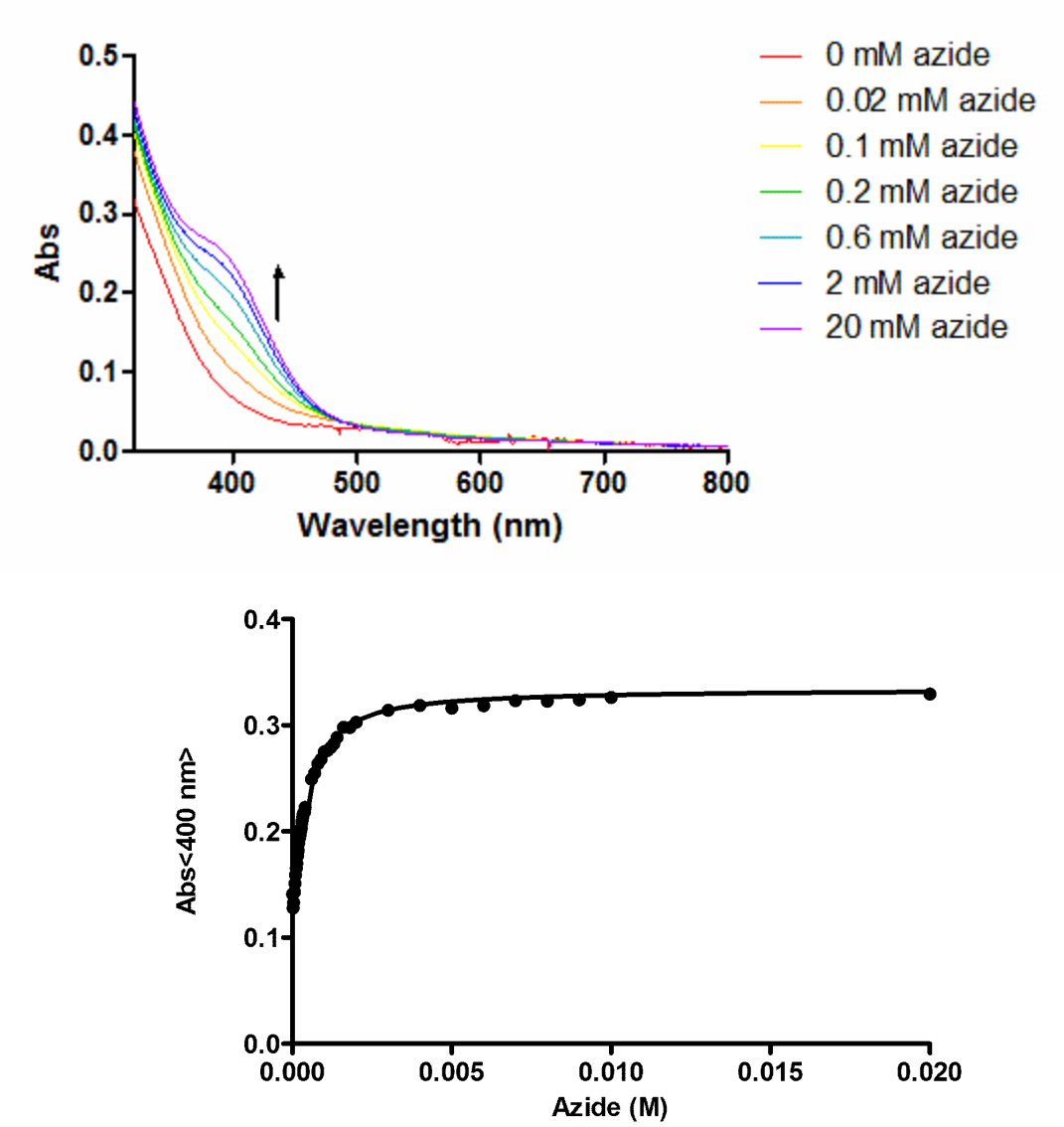


Figure 4-12: Effect of azide binding on the UV/Vis spectra of FesubMn-SOD.

UV/Vis spectra of FesubMn-SOD upon azide titration (top) and the nonlinear fitting analysis on collected data at 400 nm(bottom) are represented. The measurement of UV/Vis spectra of azide titration were performed at room temperature (25 ℃) in a buffer containing 5 mM potassium phosphate buffer pH 7.4. The absorbance was corrected by absorbance baseline between 800 – 1000 nm. The nonlinear fit of data was analysis by user defined tight binding fitting of GraphPad Prism (equations 4.4). Kd is the value of azide concentration at half the value of maximum absorption, 0.29 ± 0.02 mM.

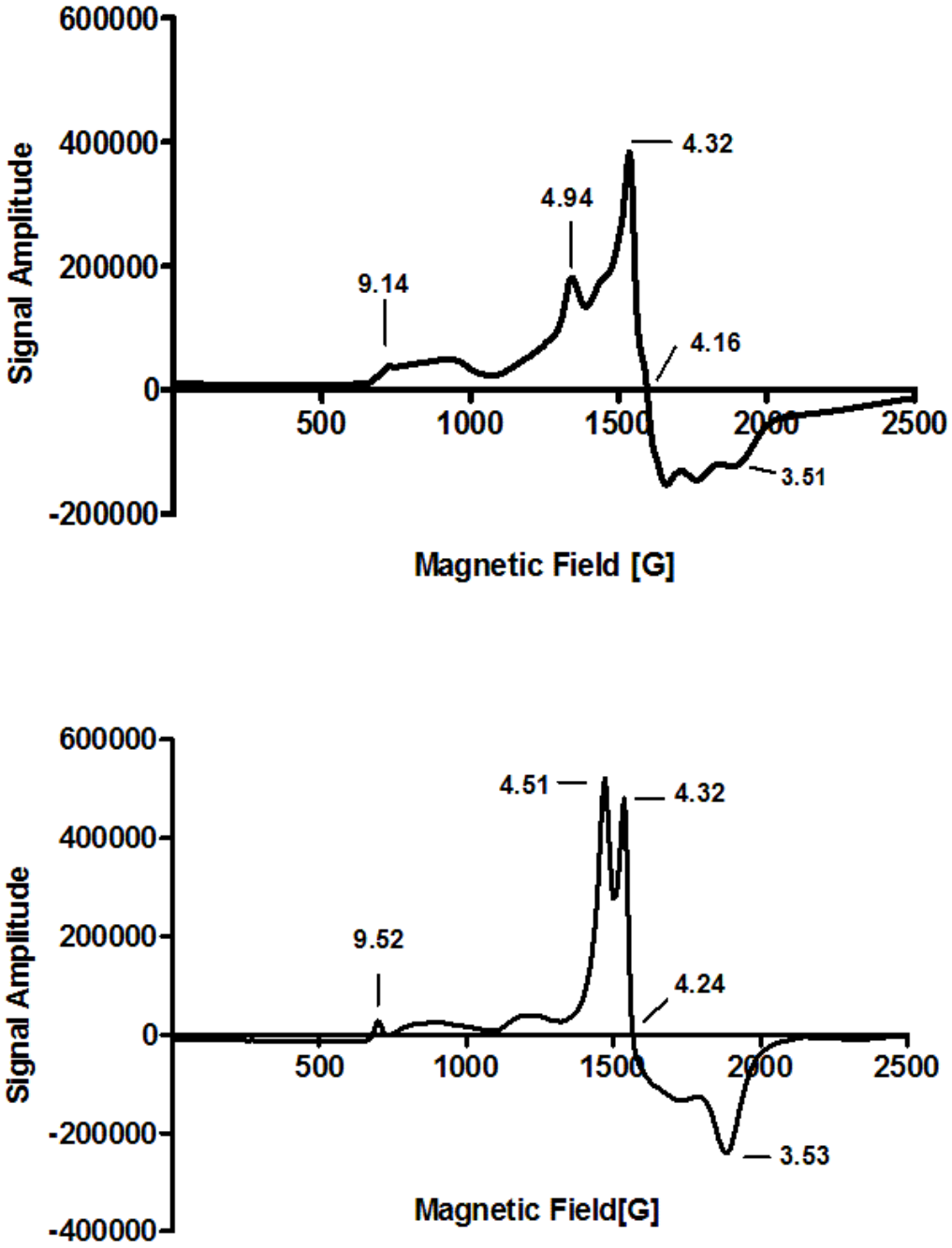


Figure 4-13: Effect of azide binding on the EPR spectra of Q146A-$Fe^{3+}$subMn-SOD.

EPR spectra of free Q146A-$Fe^{3+}$subMn-SOD in 50 % glycerol (top) and $N_3^-$ - bound Q146A-$Fe^{3+}$subMn-SOD (bottom) are shown. Sample contained about ~0.5 mM Q146A-FesubMn-SOD in a buffer of 5 mM potassium phosphate pH 7.4, with 50% (v/v) glycerol, with (bottom) or without (top) 10mM $NaN_3$. EPR spectra were collected on a Bruker 300MX at 114K with a cryostat taking liquid nitrogen flow as the coolant.

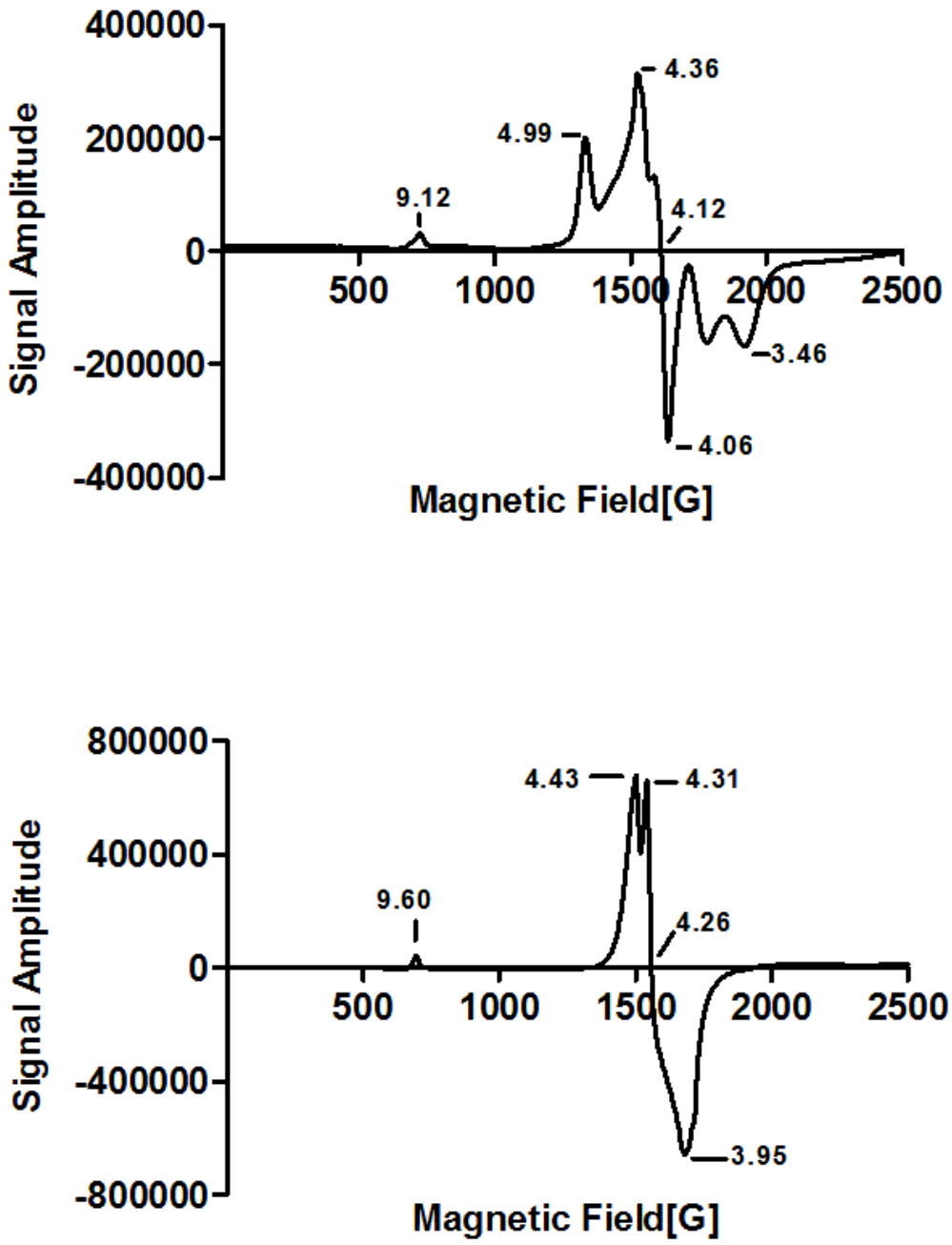


Figure 4-14: Effect of azide binding on the EPR spectra of $Fe^{3+}$subMn-SOD.

EPR spectra of free $Fe^{3+}$subMn-SOD in 50 % glycerol (top) and $N_3^-$-bound Q146A-$Fe^{3+}$subMn-SOD(bottom) are shown. Sample contained about ~0.5 mM Q146A-FesubMn-SOD in a buffer of 5 mM potassium phosphate pH 7.4, with 50% (v/v) glycerol, with (bottom) or without (top) 10mM $NaN_3$. EPR spectra were collected on a Bruker 300MX at 114K with a cytostat taking liquid nitrogen flow as the coolant.

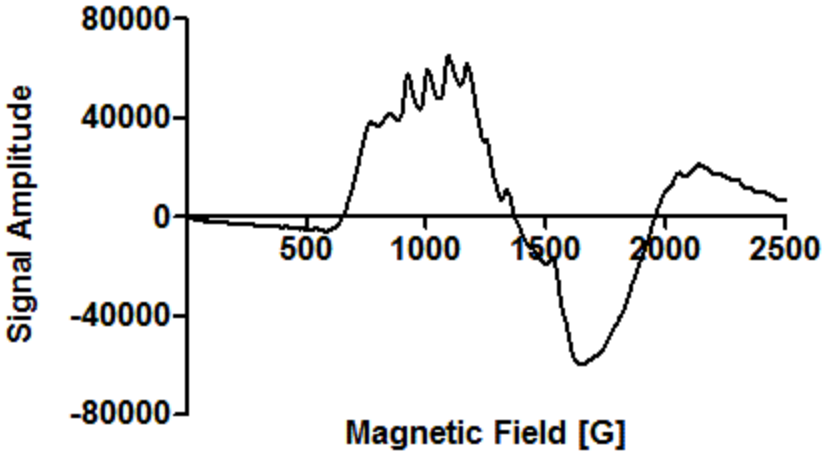


Figure 4-15: Effect of azide binding on the EPR spectra of Q146A-$Mn^{2+}$-SOD.

EPR spectra of free Q146A-Mn-SOD in 50 % glycerol. Sample contained about ~0.5 mM Mn-SOD in a buffer of 5 mM potassium phosphate pH 7.4, with 50% (v/v) glycerol. EPR spectra were collected on a Bruker 300MX at 114K with a cytostat taking liquid nitrogen as the coolant. Spectrum peak with the largest amplitude in the region of 1500G – 1600 G are due to those common amount of non-active site iron (NAS Fe) [31, 71]where g = 4.3. EPR spectra of $N_3^-$ - bound Q146A-Mn-SOD is exactly the same as this one.

# Chapter 5 Conclusions and Future Work

## 5.1 Conclusions

Extending from the buried metal ion to the outer sphere, the hydrogen bond network of MnSOD modulates the reduction midpoint potential (E°), participates in the proton transfer relay and optimizes the catalytic activity.[45, 79b] Within the hydrogen bound network, the mutations of His 30, [97a, 97c] Tyr 34,[50a, 116] Gln 143,[49] Try 161[117] and Tyr 166,[97a, 97c] which at the second shell of outer sphere of active site, would influence the protein catalytic activity significantly. Of all these five site, by site-directed mutagenesis, Gln143 is the one exerting the most significant effect on catalytic activity.[49] Equivalent to Gln143, Gln146 is a highly conserved second-sphere amino acid residue at the active site of *E. coli* MnSOD. It serves as a hydrogen bond donor for the solvent molecule and the conserved "gateway" amino acid residue Tyr34.[42b] In FeSOD, substitution of the analogous residue Gln 69 has large effects on the *E*°, the Q69E variant displaying a $Fe^{3+}/Fe^{2+}$ *E*° elevated by at least 660 mV.[42a] In MnSOD, the equivalent variant Q146E is always isolated as apo-protein[79a] displaying zero catalytic activity.

By observing the temperature induced unfolding transition and the corresponding metal content after applying different metallation methods in chapter 3, it is found that even without metal ion binding Q146E-apoMn-SOD is already thermally stable exceeding that of WT-Mn-SOD. The melting temperature ($T_m$) of apo protein Q146E-apoMn-SOD of ~ 88 °C is more than 35 ℃ higher than that of apoMn-SOD (53 ℃ ) and 20 ℃ higher than that of holoMn-SOD (metal ion-replete) (67 ℃). It is normally expected that mutation of a conserved residue should interrupt protein stability substantially. And more interesting we found that metal ion binding might actually compromises the stability and $T_m$ of this hyper-

stable apo protein Q146E-apoMn-SOD. The unfolding transition temperature ($T_m$) of metallated Q146E-MnSOD is estimated of ~ 51 ℃ which is much lower than that of MnSOD (67 ℃). The temperature dependence of metal ion binding indicates that Gln146 is crucial for partial unfolding of the protein and metal ion binding. Thus compromising of the thermal stability of apo protein actually provides enormous benefits of favoring metal ion binding. The hyper-thermal stability of the variant Q146E-apoMn-SOD requests the additional effect when shifting the equilibrium between apo- and holo- protein in favor of the former, which explains why Q146E-MnSOD is always isolated as apo protein and also demonstrates that naturally Gln146 of MnSOD evolved in a strategy to maintain its metal ion binding ability by sacrificing part of its thermal stability.

Introducing the Q146X (X- A, C, N, S, Y) variants of MnSOD increased Fe ion content at active site, decreased $Mn^{3+}$/Mn ratio, reduced catalytic activity, improved protein stability, compared to WT-Mn-SOD. The elevated $T_m$ of these mutants Q146X (X- A, C, N, S) apo protein perfectly agrees with the conclusion that the conserved Gln146 of MnSOD had been evolved towards its metal ion binding ability while sacrificing part of its structure stability. Q146A-Mn-SOD shows the best per-Mn activity but a much lower binding affinity to the substrate analogue azide. Q146Y with a bulk of the Tyr side chain, has the least metal content and most destabilizing structure among the mutants. The most conservative mutant Q146N reserves the preference of Mn ion over Fe ion. Overall the most striking alterations were caused by the Q146E variant, despite the fact that Glu provides an isosteric and isoelectronic replacement of Gln.

## 5.2 New Contributions

The importance of Gln146 in the function of SOD includes the following:

- We proposed and developed the hypothesis that the natural amino acid composition of a protein is not always the one that maximizes protein stability. It is demonstrated that the Q146E substitution substantially enhances thermal stability of protein but killing its metal binding ability at the same time. The hyper stable Q146E-apoMn-SOD requires additional effect when shifting the equilibrium between apo- and holo- protein in favor of the apo form.
- Thermal or chemical destabilization of apo SOD is found to be a must to enable metal ion access to the active site.[35, 86, 94] It has been proved that Q146E-apoMn-SOD is much more thermally stable than Q146E-MnSOD. Consequently metal uptake is being compromised by the hyper stability of Q146E-apoMn-SOD. In consistence with Q146E, although not as severe as complete depletion of metal binding, the other mutants at the same position, Q146A, Q146C, Q146N and Q146S also displayed an increased thermal stability and decreased metal ion content.
- It is also found that the WT identity of residue Gln146 is the one that actually contributes to metal binding by destabilizing the apo-Mn form of the SOD protein, in addition to influence the activity of metal ion by modulating its $E°$.[10, 42a, 45a, 88, 109] as an agent of proton delivery to the active site hydrogen bond network.[42b, 49] We now know that replacements of Gln146 by Glu, Ala, Cys, Asn, Ser increases the protein stability of apoMn-SOD substantially based on the thermal quantities determined by CD melting curve.
- To our further surprise, the metal bound mutant protein Q146E-Mn-SOD exhibited disturbed thermal stability. We didn't observe a separated melting state on the melting

curves of other amino acid substitutions, probably because the metal content for each protein sample is low and inhomogeneous (including apo, Fe and Mn). Or the influences of other amino acid substitutions might be too gentle on the thermal stability such that the difference between different metal binding states of other mutants are not as prominent as that between Q146E-MnSOD and Q146E-apoMn-SOD. Unfortunately we could not draw conclusions for other mutants confidently now because the amount of Mn ion incorporated was too low to permit accurate estimates.

## 5.3 Future Work

The amino acids at second shell of the active site are less well understood, because their effects can be subtler than those ligands with metal ion, despite their importance in determining the activity of metal ion centers. Although it may be more difficult to address their influence on the activity of metal ion, the fact that more features of the WT- may be retained in perturbed form, rather than altogether eliminated, can make second-sphere variants more informative than drastically-changed first-sphere variants. Here we note that there are several areas of opportunities for additional work related to the Gln146 of MnSOD.

Our first task is about protein preparation. Introducing the desired metal ion to the designated site is a challenging task particularly if had some of the critical residues been mutated. In chapter 2, the method has been developed to keep a high yield of protein with simplified purification procedure. To take control over the metal content and protein purity completely, the next step could be manipulating the overexpression cell line, the concentration of metal ion or the cell growing condition (aerobic or anaerobic).

Investigation on the structure of the partially folded intermediate of apoMn-SOD is worthwhile. Because it is proposed that the partially unfolding of apoMn-SOD is required for metal binding. But such a species structure is not expected to be well-defined, it is necessary to find out a buffer condition or pH value to induce and define the unfolding of protein for exploring the metal binding process.

For the catalytic activity part, the substrate accessing is also affected by mutation at Gln146. The catalytic activity of MnSOD is very sensitive to the proton transfer around the active site. To understand the influence of protein transfer on the substrate accessing and releasing, try different pH condition when measuring the substrate binding affinity and EPR spectrum of protein sample Q146A-MnSOD.

Last, the interesting area is about the possible function of Gln146 in the proton relay, hydrogen bonds and electrostatic interactions at the active site. Solving the X-ray crystal structure and proton NMR of Q146E will provide a lot of information to further clarify the role of Gln146 during the metal-uptake process and to learn how this single substitution of an amino acid in the second shell could have enhanced the stability of the protein by such a large degree, elevating the $T_m$ by 30 ºC.

## References


1. Valko, M.; Rhodes, C. J.; Moncol, J.; Izakovic, M.; Mazur, M., Free radicals, metals and antioxidants in oxidative stress-induced cancer. *Chemico-biological interactions* 2006, *160* (1), 1-40.
2. Moslen, M. T., *Free Radicals in Diagnostic Medicine*. Plenum Press: New York, 1994.
3. Häggström, M., Medical gallery of Mikael Häggström 2014. *Wikiversity Journal of Medicine* 2014, *1*, 8-18.
4. Fridovich, I., Superoxide anion radical (O2-.), superoxide dismutases, and related matters. *J Biol Chem* 1997, *272*, 18515-18517.
5. Sheng, Y.; Abreu, I. A.; Cabelli, D. E.; Maroney, M. J.; Miller, A. F.; Teixeira, M.; Valentine, J. S., Superoxide Dismutases and Superoxide Reductases. *Chemical Reviews* 2014, *114*, 3854-3918.
6. Fridovich, I., Superoxide racical and superoxide dismutases. *Annu Rev Biochem* 1995, *64*, 97-112.
7. McCord, J. M.; Fridovich, I., Superoxide Dismutase an enzymic function for erythropurein. *The Journal of Biological Chemistry* 1969, *224*, 6049-6055.
8. Zelko, I. N.; Mariani, T. J.; Folz, R. J., Superoxide dismutase multigene family: a comparison of the CuZn-SOD (SOD1), Mn-SOD (SOD2), and EC-SOD (SOD3) gene structures, evolution, and expression. *Free Radic Biol Med.* 2002, *33*, 337-349.
9. Melov, S.; Coskun, P.; Patel, M.; Tuinstra, R.; Cottrell, B.; Jun, A. S.; Zastawny, T. H.; Dizdaroglu, M.; Goodman, S. I.; Huang, T. T.; Miziorko, H.; Epstein, C. J.; Wallace, D. C., Mitochondrial disease in superoxide dismutase 2 mutant mice,. *Proc. Natl. Acad. Sci.* 1999, *96*, 846-851.
10. Miller, A. F., Fe superoxide dismutase. In *Handbook of Metalloproteins*, Messerschmidt, A.; Huber, R.; Poulos, T.; Wieghardt, K. E., Eds. John Wiley & Sons, Ltd,pp 668-682: Chichester, 2001.
11. Holley, A. K.; Bakthavatchalu, V.; Velez-Roman, J. M.; St Clair, D. K., Manganese Superoxide Dismutase: Guardian of the Powerhouse. *Int J Mol Sci* 2011, *12* (10), 7114-62.
12. Li, Y.; Huang, T. T.; Carlson, E. J.; Melov, S.; Ursell, P. C.; Olson, J. L.; Noble, L. J.; Yoshimura, M. P.; Berger, C.; Chan, P. H.; Wallace, D. C.; Epstein, C. J., Dilated cardiomyopathy and neonatal lethality in mutant mice lacking manganese superoxide dismutase. *Nat. Genet.* 1995, *11*, 376-381.
13. (a) Regelsberger, G.; Laaha, U.; Dietmann, D.; Ruker, F.; Canini, A.; Grilli-Caiola, M.; Furtmuller, P. G.; Jakopitsch, C.; Peschek, G. A.; Obinger, C., The iron superoxide dismutase from the filamentous cyanobacterium Nostoc PCC 7120. Localization, overexpression, and biochemical characterization. *J Biol Chem* 2004, *279* (43), 44384-93; (b) Mockett, R. J.; Orr, W. C.; Rahmandar, J. J.; Benes, J. J.; Radyuk, S. N.; Klichko, V. I.; Sohal, R. S., Overexpression of Mn-containing superoxide dismutase in transgenic Drosophila melanogaster. *Arch Biochem Biophys* 1999, *371*, 260-269; (c) Hu, D.; Cao, P.; Thiels, E.; Chu, C. T.; Wu, G. D.; Oury, T.; Klann, E., Hippocampal longterm potentiation, memory, and longevity in mice that overexpress mitochondrial superoxide dismutase. *Neurobiol Learn Mem* 2007, (87), 372-384.
14. Giedroc, D. P.; Arunkumar, A. I., Metal sensor protein: nature's metalloregulated allosteric switches. *Dalton Trans* 2007, 3107-3120.

15. Maret, W., Metalloproteomics, metalloproteomes, and the annotation of metalloproteins. *Metallomics* 2010, *2* (2), 117-25.
16. Eklund, H.; Uhlin, U.; Farnegardh, M.; Logan, D. T.; Nordlund, P., Structure and Function of the Radical Enzyme Ribonucleotide Reductase. *Prog Biophys Mol Biol* 2001, *77*, 177-268.
17. Hou, X. J.; Hou, J. M., Roles of manganese in photosystem II dynamics to irradiations and temperatures. *Frontiers in Biology* 2013, *8* (3), 312-322.
18. (a) Touati, D., iron and oxidation stress in bacteria. *Arch Biochem Biophys* 2000, *373*, 1-6; (b) Finney, L. A.; O'Hailoran, T. V., Transition metal speciation in the cell: insights from the chemistry of metal ion receptors. *Science* 2003, *300*, 931-936.
19. (a) Lill, R.; Muhlenhoff, U., Maturation of iron-sulfur proteins in eukaryotes: mechanisms, connected processes, and diseases. *Anne Rev Biochem* 2008, *77*, 669-700; (b) Holz, R. C.; Bzymek, K. P.; Swierczek, S. I., Co-catalytic metallopeptidases as pharmaceutical targets. *Curr. Opin. Chem. Biol.* 2003, *7*, 197-206; (c) Yamakura, F.; Kobayashi, K.; Furukawa, S.; Suzuki, Y., In vitro preparation of iron-substituted human manganese superoxide dismutase: possible toxic properties for mitochondria. *Free Radic Biol Med* 2007, *3* (43), 423-430.
20. Kuchar, J.; Hausinger, R. P., biosynthesis of metal sites. *Chem Rev* 2004, *104*, 509-525.
21. (a) McCord, J. M., Iron- and manganese-containing superoxide dismutases: structure, distribution and evolutionary relationships. *Adv Exp Med Biol* 1976, *74*, 540-550; (b) McCord, J. M.; Fridovich, I., The Biology and Pathology of Oxygen Radicals. *Ann Intern Med* 1978, *89*, 122-127; (c) Dennis, R. J.; Micossi, E.; McCarthy, J.; Moe, E.; Gordon, E. J.; Kozielski-Stuhrmann, S.; Leonard, G. A.; McSweeney, S., Structure of the manganese superoxide dismutase from Deinococcus radiodurans in two crystal forms. *Acta Crystallogr Sect F Struct Biol Cryst Commun* 2006, *63*, 325-9.
22. Carlioz, A.; Touati, D.; Ludwig, M. L.; Stallings, W. C.; Fee, J. A.; Steinman, H. M.; Touati, D., Iron superoxide dismutase: nucleotide sequence of the gene from Escherichia coli K12 and correlations with crystal structures. *J Biol Chem* 1988, *263*, 1555-1562.
23. Lah, M. S.; Dixon, M. M.; Pattrige, K. A.; Stalling, W. C.; Fee, J. A.; Ludwig, M. L., Structure-function in Escherichia coli iron superoxide dismutase: comparisons with the manganese enzyme from Thermus thermophilus, Biochemistry 34. *Biochemistry* 1995, *34*, 1646-1660.
24. Culotta, V. C.; Yang, M.; O'Halloran, T. V., Activation of superoxide dismutases: putting the metal to the pedal. *Biochimica et Biophysica Acta* 2006, *1763*, 747-758.
25. (a) Edwards, R. A.; Whittaker, M. M.; Whittaker, J. W.; Jameson, G. B.; Baker, E. N., Distinct Metal Environment in Fe-Substituted Manganese Superoxide Dismutase Provides a Structural Basis of Metal Specificity. *J. Am. Chem* 2001, *120*, 9684-9692; (b) Naranuntarat, A.; Jensen, L. T.; Pazicni, S.; Pazicni, S. E.; Panner-Hahn J., The Internation of Mitochondrial Iron with Manganese Superoxide Dismutase. *J Biol Chem* 2009, *284* (34).
26. Beyer, W. F. J.; Fridovich, I., In vivo competition between iron and manganese for occupancy of the active site region of the manganese superoxide dismutase of Escherichia coli. *J Biol Chem* 1991, *266*, 303-308.
27. (a) Rosenzweig, A. C.; O'Halloran, T. V., Structure and chemistry of the copper cheperon proteins. *Curr Opin Chem Biol* 2000, *4*, 140-147; (b) Rae, T. D.; J, S. P.; Pufahl,

R. A.; Culotta, V. C.; O'Halloran, T. V., Undetectable intracellular free copper: the requirement of a copper chaperone for superoxide dismutase. *Science* 1999, *284*, 805-808.
28. Whittaker, J. W., The Irony of Manganese Superoxide Dismutase. *Biochemical Society Transactions (2003) Volume 31, part 6* 2003, *31*, 1813-1821.
29. Maret, M., Metalloproteomics, metalloproteomes, and the annotation of metalloproteins. *Metallomics* 2010, *2*, 117-125.
30. Whittaker, J. W.; Whittaker, M. M., Active site spectral studies on manganese superoxide dismutase. *J Am Chem Soc* 1991, *113*, 5528-5540.
31. Vance, C. K., Miller, A.F., Spectroscopic Comparisons of the pH Dependencies of Fe-Substituted (Mn)Superoxide Dismutase and Fe-superoxide Dismutase. *Biochemistry 37: 5518-5517* 1998, 37, 5518-5527.
32. (a) Mizuno, K., Whittaker, M.M., Bächinger, H.P., Whittaker, J.W., Calorimetric studies on the tight binding metal interactions of Escherichia coli manganese superoxide dismutase. *J Bio Chem* 2004, 279, 277339-27344; (b) Whittaker, M. M.; Whittaker, J. W., Recombinant superoxide dismutase from a hyperthermophilic archaeon. pyrobaculum aerophilum. *JBIC* 2000, *5*, 402-408; (c) Whittaker, M. M.; Whittaker, J. W., Thermally triggered metal binding by recombinant Thermus thermophilus manganese superoxide dismutase, expressed as the apo-enzyme. *J Biol Chem* 1999, *274*, 34751-34757.
33. Whittaker, J. W., A model for local melting of metalloprotein structure. *J Phys Chem* 1997, *101*, 674-677.
34. Whittaker, M. M.; Whittaker, J. W., Low-temperature thermochromism marks a change in coordination for the metal ion in manganese superoxide dismutase. *Biochemistry* 1996, *21* (35), 6762-6770.
35. (a) Whittaker, M. M.; Whittaker, J. W., A Glutamate Bridge Is Essential for Dimer Stability and Metal Selectivity in Manganse Superoxide Dismutase. *The Journal of Biological Chemistry* 1998, *273* (35), 22188-22193; (b) Edwards, R. A.; Whittaker, M. M.; Whittaker, J. W.; Baker, E. N.; Jameson, G. B., Removing a hydrogen bond in the dimer interface of Escherichia coli manganese superoxide dismutase alters structure and reactivity. *Biochemistry* 2001, *40* (15), 4622-4632.
36. Whittaker, M. M.; Mizuno, K.; Bachinger, H. P.; Whittaker, J. W., Kinetic Analysis of the Metal Binding Mechanism of Escherichia coli Manganese Superoxide Dismutase. *Biophysical Journal* 2006, *90*, 598-607.
37. Whittaker, M. M., Lerchb, T.F., Kirillovab, O., Chapmanb, M.S., Whittaker, J.W.,, Subunit dissociation and metal binding by Escherichia coli apomanganese superoxide dismutase. *Arch Biochem biophys 505(2): 13.* 2011, 505, 13- 22.
38. Whittaker, M. M.; Whittaker, J. W., Conformationally Gated Metal Uptake by Apomanganese Superoxide Dismutase. *Biochemistry* 2008, *47*, 11625-11636.
39. Garrett, R. H.; Grisham, C. M., Why Are Coupled Processes Important To Living Things? In *Biochemistry*, McGahey, P.; Woods, E.; Weber, L.; Camp, S. V., Eds. Mary Finch: Belmont, CA, 2012; pp 68-69.
40. Barrette, J. W. C.; Sawyer, D. T.; Fee, J. A.; T, C. L., Potentiometric Titrations and Oxidation-Reductation Potentials of Several Iron Superoxide Dismutases. *Biochemistry* 1983, *22*, 624-627.
41. Imlay, J. A.; Fridovich, I., Assay of metabolic superoxide production in Escherichia coli. *J. Biol. Chem.* 1991, *266* (11), 6957–6965.

42. (a) Vance, C. K.; Miller, A. F., Novel Insights into the Basis for Escherichia coli Superoxide Dismutase's Metal Ion Specificity from Mn-Substituted FeSOD and Its Very High Em. *Biochemistry* 2001, *40* (43), 13079-113087; (b) Lévêque, V. J. P.; Stroupe, M. E.; Lepock, J. R.; Cabelli, D. E.; Tainer, J. A.; Nick, H. S.; Silverman, D. N., Multiple replacements of glutamine 143 in human manganeses superoxide dismutase: effects on structure, stability, and catalysis. *Biochemistry* 2000, *39*, 7131-7138.
43. Miller, A. F., Redox tuning over almost 1 V in a structurally conserved active site:Lessons from Fe-containing superoxide dismutase. *Accounts of Chemical Research* 2008, *41* (4), 501-510.
44. Dean, J. A., *Lange's Handbook of Chemistry*. McGraw-Hill: New York, 1985.
45. (a) Xie, J.; Yikilmaz, E.; Miller, A. F.; Brunold, T. C., Second-Sphere Contributions to Substrate-Analogue Binding in Iron(III) Superoxide Dismutase. *J AM CHEM SOC* 2002, *124*, 3769-3774; (b) Yikilmaz, E.; Porta, J.; Grove, L. E.; Vahedi-Faridi, A.; Bronshteyn, Y.; Brunold, T. C.; Borgstahl, G. E.; Miller, A. F., How can a single second sphere amino acid substitution cause reduction midpoint potential changes of hundreds of millivolts? *J Am Chem Soc* 2007, *129* (32), 9927-9940.
46. Yamakura, F.; Kobayashi, K.; Ue, H.; Konno, M., The pH-Dependent Changes of the Enzymic Activity and Spectroscopic Properties of Iron-Substituted Manganese Superoxide Dismutase. *Euro J Biochem* 1995, *227* (3), 700-706.
47. Fersht, A., *Structure and Mechanism in Protein Science*. W.H. Freeman and Company: New York, 1998.
48. Borgstahl, G.; Pokross, M.; Chehab, R.; Sekher, A.; Snell, E. H., Cryo-trapping the six-coordinate, distorted-octahedral active site of manganese superoxide dismutase. *J Mol Biol* 2000, *259*, 951-959.
49. Hsieh, Y.; Guan, Y.; Tu, C. K.; Bratt, P. J.; Angerhofer, A.; Lepock, J. R.; Hickey, M. J.; Tainer, J. A.; Nick, H. S.; Silverman, D. N., Probing the active site of Human Manganese Superoxide Dismutase: The Role of Glutamine 143. *Biochemistry* 1998, *37*, 4731-4739.
50. (a) Whittaker, M. M.; Whittaker, J. W., Mutagenesis of a Proton Linkage Pathway in Escherichia coli Manganese Superoxide Dismutase. *Biochemistry* 1997, *36*, 8923-8931; (b) Chockalingam, K.; Luba, J.; Nick, H. S.; Silverman, D. N.; Zhao, H., Engineering and characterization of human manganese superoxide dismutase mutants with high activity and low product inhibition. *The FEBS journal* 2006, *273* (21), 4853-61; (c) Schwartz, A. L.; Yikilmaz, E.; Vance, C. K.; Vathyam, S.; Koder, R. L.; Miller, A. F., Mutational and spectroscopic studies of the significance of the active site glutamine to metal ion specificity in superoxide dismutase. *J Inorg Biochem* 2000, *80* (3), 247-256; (d) Zheng, J.; Domsic, J. F.; Cabelli, D.; McKenna, R.; Silverman, D. N., Structural and kinetic study of differences between human and Escherichia coli manganese superoxide dismutases. *Biochemistry* 2007, *46* (51), 14830-14837.
51. Sawyer, D. T.; Valentine, J. S., How Super is Superoxide. *Acc. Chem. Res* 1981, *14*, 393-400.
52. Pugh, S. Y.; Fridovich, I., Induction of superoxide dismutases in Escherichia coli B by metal chelators. *J Bacteriol* 1985, *162* (1), 196-202.
53. Pettersen, E. F.; Goddard, T. D.; Huang, C. C.; Couch, G. S.; Greenblatt, D. M.; Meng, E. C.; Ferrin, T. E., UCSF Chimera--a visualization system for exploratory research and analysis. *Journal of computational chemistry* 2004, *25* (13), 1605-12.

54. Edwards, R. A.; Baker, H. M.; Whittaker, M. M.; Whittaker, J. W.; Jameson, G. B.; Baker, E. N., Crystal structure of Escherichia coli manganese superoxide dismutase at 2.1-angstrom resolution. *J Biol Inorg Chem.* 1998, *3*, 161-171.
55. Miller, A. F., Superoxide dismutases: Ancient enzymes and new insights. *FEBS Letters* 2012, *586*, 589-595.
56. (a) Ken, C. F.; Hsiung, T. M.; Huang, Z. X.; Juang, R. H.; Lin, C. T., Characterization of Fe/Mn superoxide dismutase from diatom Thallassiosira. *Journal. Agric. Food Chem* 2005, *53*, 1470-1474; (b) Santos, R.; Bocquet, S.; Puppo, A.; Touati, D., Characterization of an atypical superoxide dismutase from Sinorhizobium meliloti. *Journal Bacteriol.* 1999, *181*, 4509-4516.
57. Steinman, H. M., Construction of an Escherichia coli K-12 strain deleted for manganese and iron superoxide dismutase genes and its use in cloning the iron superoxide dismutase gene of Legionella pneumophila. *Mol. Gen. Genet.* 1992, *232*, 427-430.
58. Edelhoch, H., Spectroscopic Determination of Tryptophan and Tyrosine in Proteins. *Biochemistry* 1967, *6*, 1948 - 1954.
59. Beauchamp, C.; Fridovich, I., Superoxide dismutase: improved assays and an assay applicable to acrylamide gels. *Anal Biochem* 1971, *44*, 276-287.
60. Beauchamp, C.; Fridovich, I., Superoxide Dismutase - Improved Assays and an Assay Applicable to Acrylamide Gels. *Anal. Biochem* 1971, *44*, 276-278.
61. Manning, T. J.; Grow, W. R., In the classroom - Inductively Coupled Plasma-Atomic Emission spectrometry. *The Chemical Educator* 1997, *2*, 2741-2742.
62. (a) Koder, R. L.; Miller, A. F., Overexpression, Isotopic Labeling, and Spectral Characterization of Enterobacter cloacae Nitroreductase. *PROTEIN EXPRESSION AND PURIFICATION* 1998, *13*, 8; (b) Bryant, C.; Hubbard, L.; McElroy, W. D., Cloning, nucleotide sequence, and expression of the nitroreductase gene from Enterobacter cloacae. *J Biol Chem* 1991, *266* (7), 4126-30.
63. McCord, J. M., and Fridovich, I., Superoxide Dismutase an enzymic function for erythropurein. *The Journal of Biological Chemistry* 1969, 224. 6049-6055.
64. Beyer, J. W. F.; Fridovich, I., In vivo Competition between Iron and Manganese for Occupancy of the Active Site Region of the Manganese-Superoxide Dismutase of Escherichia coli. *The Journal of Biological Chemistry* 1991, 266, 303-308.
65. (a) Lee, B.; McKenna, K.; Bramhall, J., Kinetic studies of human erythrocyte membrane resealing. *Biochim Biophys Acta* 1985, *815* (1), 128-34; (b) Morris, G. J., Liposomes as a model system for investigating freezing injury. In *Effects of Low Temperatures on Biological Membranes*, Morris, G. J.; A, C., Eds. Academic: London, 1981; pp 241-262.
66. Johnson, B. H.; Hecht, M. H., Recombinant Proteins Can Be Isolated from E. coli Cells by Repeated Cycles of Freezing and Thawing. *Bio/Techonology* 1994, *12*, 1357-1360.
67. Sturtz, L. A.; Diekert, K.; Jensen, L. T.; Lill, R.; Culotta, V. C., A fraction of yeast Cu,Zn-superoxide dismutase and its metallochaperone, CCS, localize to the intermembrane space of mitochondria. A physiological role for SOD1 in guarding against mitochondrial oxidative damage. *J Biol Chem* 2001, *276* (41), 38084-9.
68. (a) Benov, L.; Sage, H.; Fridovich, I., The copper- and zinc-containing superoxide dismutase from Escherichia coli: molecular weight and stability. *Arch Biochem Biophys* 1997, *340* (2), 305-10; (b) St John, G.; Steinman, H. M., Periplasmic copper-zinc

superoxide dismutase of Legionella pneumophila: role in stationary-phase survival. *J Bacteriol* 1996, *178* (6), 1578-84.
69. Petersen, S. V.; Oury, T. D.; Ostergaard, L.; Valnickova, Z.; Wegrzyn, J.; Thogersen, I. B.; Jacobsen, C.; Bowler, R. P.; Fattman, C. L.; Crapo, J. D.; Enghild, J. J., Extracellular superoxide dismutase (EC-SOD) binds to type i collagen and protects against oxidative fragmentation. *J Biol Chem* 2004, *279* (14), 13705-10.
70. Carlioz, A.; Touati, D., Isolation of superoxide dismutase mutants in Escherichia coli: is superoxide dismutase necessary for aerobic life? *The EMBO Journal* 1986, *5*, 623 - 630.
71. Beauchamp, C.; Fridovic, I., Superoxide Dismutase - Improved Assays and an Assay Applicable to Acrylamide Gels. *Anal. Biochem* 1971, 44, 276 - 278.
72. Manning, T. J., Grow, W. R., In the classroom - Inductively Coupled Plasma-Atomic Emission spectrometry. *The Chemical Educator* 1997, 2, 2741-2742.
73. (a) Zelko, I. N., Mariani, T. J., Folz, R. J., Superoxide dismutase multigene family: a comparison of the CuZn-SOD (SOD1), Mn-SOD (SOD2), and EC-SOD (SOD3) gene structures, evolution, and expression. *Free Radic Biol Med.* 2002, 33, 337-349; (b) Youn, H. D., Kim, E. J., Roe, J. H., Hah, Y. C., Kang, S. O., A novel nickel-containing superoxide dismutase from Streptomyces spp. *Biochem. J.* 1996, 318, 889-896.
74. Jackson, S. M.; Cooper, J. B., An analysis of structural similarity in the iron and manganese superoxide dismutases based on known structures and sequences. *Biometals. 1998 Apr;11(2):159-73.* 1998, 11, 159- 173.
75. (a) Beyer, W. F. J.; Rosebrough, N. J.; Fridovich, I., Differences between the manganese- and the iron-containin superoxide dismutases of Escherichia coli detected through sedimentation equilibrium, hydrodynamic, and spectroscopic studies. *Biochemistry* 1989, *28*, 4403-4409; (b) Ose, D. E.; Fridovich, I., Manganese-containing superoxide dismutase from Escherichia coli: reversible resolution and metal replacements. *Arch. Biochem. Biophys.* 1979, *194*, 360-364.
76. Jackson, T. A.; Gutman, C. T.; Maliekal, J.; Miller, A. F.; Brunold, T. C., Geometric and electronic structures of manganese-substituted iron superoxide dismutase. *Inorganic chemistry* 2013, *52* (6), 3356-67.
77. Meier, B.; Scherk, C.; Schmidt, M.; Parak, F., pH-dependent inhibition by azide and fluoride of the iron superoxide dismutase from Propionibacterium shermanii. *Biochem J* 1998, *331* (2), 403-407.
78. Parker, M. W.; Blake, C. C. F., Iron- and Manganese- Containing Superoxide Dismutase can be Distinguished by Analysis of their Primary structure. *FEBS Lett* 1988, *229* (2), 377-382.
79. (a) Edwards, R. A.; Whittaker, M. M.; Whittaker, J. W.; Baker, E. N.; Jameson, G. B., Outer Sphere Mutations Perturb Metal Reactivity in Manganese Superoxide Dismutase *Biochemistry* 2001, *40* (1), 15-27; (b) Greenleaf, W. B.; Perry, J. J.; Hearn, A. S.; Cabelli, D. E.; Lepock, J. R.; Stroupe, M. E.; Tainer, J. A.; Nick, H. S.; Silverman, D. N., Role of hydrogen bonding in the active site of human manganese superoxide dismutase. *Biochemistry* 2004, *43* (22), 7038-45.
80. Miller, A.-F.; Padmakumar, K.; Sorkin, D. L.; Karapetian, A.; Vance, C. K., Proton-coupled electron transfer in Fe-superoxide dismutase and Mn-superoxide dismutase. *Journal of Inorganic Biochemistry* 2003, *93* (1-2), 71-83.

81. Bull, C.; Neiderhoffer, E. C.; Yoshida, T. A.; Fee, J., Kinetic-studies of Superoxide Dismutases Properties of the Manganese-containing Protein from Thermus thermophilus. *J. Am Chem soc* 1991, *113*, 4069-4076.
82. (a) Sreerama, N.; Woody, R. W., Estimation of protein secondary structure from circular dichroism spectra: comparison of CONTIN, SELCON, and CDSSTR methods with an expanded reference set. *Anal Biochem* 2000, *287* (2), 252-60; (b) Chen, Y. H.; Yang, J. T.; Chau, K. H., Determination of the helix and beta form of proteins in aqueous solution by circular chroism. *Biochemistry* 1974, *13*, 3350-3359.
83. Beyer, W. F. J.; Fridovich, I., An ultrasensitive colorimetric assay for manganese. *Biochemistry* 1987, *26*, 1252-1257.
84. Meinnel, T.; Lazennec, C.; Blanquet, S., Mapping of the active site zinc ligands of peptide deformylase. *J Mol Biol* 1995, *254* (2), 175-83.
85. Yamakura, F., Kazuo, K., Harumi, U.E., Konno, M., The pH dependent changes of the enzymic activity and spectroscopic properties of iron-substituted manganese superoxide dismutase A study on the metal-specific activity of Mn-containing superoxide dismutase. *Eur J Biochem 227(3): 700-706.* 1995, 227, 700-706.
86. Mizuno, K.; Whittaker, M. M.; Bachinger, H. P.; Whittaker, J. W., Calorimetric studies on the tight binding metal interactions of Escherichia coli manganese superoxide dismutase. *J Biol Chem* 2004, *279* (26), 27339-44.
87. Whittaker, J. W., Metal uptake by manganese superoxide dismutase. *Biochim Biophys Acta* 2010, *1804* (2), 298-307.
88. Vance, C. K.; Miller, A. F., A Simple Proposal That Can Explain the Inactivity of Metal-Substituted Superoxide Dismutases. *J Am Chem Soc* 1997, *120* (3), 461-467.
89. Kumar, S.; Tsai, C. J.; Nussinov, R., Factors enhancing protein thermostability. *Protein engineering* 2000, *13* (3), 179-91.
90. Sadeghi, M.; Naderi-Manesh, H.; Zarrabi, M.; Ranjbar, B., Effective factors in thermostability of thermophilic proteins. *Biophysical chemistry* 2006, *119* (3), 256-70.
91. Vetriani, C.; Maeder, D. L.; Tolliday, N.; Yip, K. S.; Stillman, T. J.; Britton, K. L.; Rice, D. W.; Klump, H. H.; Robb, F. T., Protein thermostability above 100 degreesC: a key role for ionic interactions. *Proceedings of the National Academy of Sciences of the United States of America* 1998, *95* (21), 12300-5.
92. Querol, E.; Perez-Pons, J. A.; Mozo-Villarias, A., Analysis of protein conformational characteristics related to thermostability. *Protein engineering* 1996, *9* (3), 265-71.
93. (a) Amo, T., Atomi, Haruyuki., Imanaka, Tadayuki., Biochemical Properties and Regulated Gene Expression of the Superoxide Dismutase from the Facultatively Aerobic Hyperthermophile Pyrobaculum calidifontis. *J Bacteriol* 2003, 21, 6340-6347; (b) Chambergoa, F. S., Valencia, Estela Y., Ferreira-Júniora, José Ribamar., Camiloc, César M.,, Conformational stability of recombinant manganese superoxide dismutase from the filamentous fungus Trichoderma reesei. *International Journal of Biological Macromolecules* 2012, 50, 19- 24; (c) Kardinahl, G. S. a. S., Iron superoxide dismutases: structure and function of an archaic enzyme. *Biochemical Society Transactions* 2003, 31, 1330-1334.
94. Edwards, R. A., Baker, H. M., Whittaker, M. M., Whittaker, J. W., Jameson, G. B., Baker, E. N., Crystal structure of Escherichia coli manganese superoxide dismutase at 2.1-angstrom resolution. *J Biol Inorg Chem.* 1998, 3, 161-171.

95. Bishop, E., *Indicators: International Series of Monographs in Analytical Chemistry*. Pergamon Press: Headington Hill Hall, Oxford, 2010; Vol. 51.
96. Hunter, T., Bannister, J. V., Hunter, G. J., Thermostability of manganese- and iron-superoxide dismutases from Escherichia coli is determined by the characteristic position of a glutamine residue. *Eur J Biochem* 2002, 269, 5137-5148.
97. (a) Hearn, A. S.; Fan, L.; Lepock, J. R.; Luba, J. P.; Greenleaf, W. B.; Cabelli, D. E.; Tainer, J. A.; Nick, H. S.; Silverman, D. N., Amino acid substitution at the dimeric interface of human manganese superoxide dismutase. *J Biol Chem* 2004, *279* (7), 5861-6; (b) Hearn, A. S.; Stroupe, M. E.; Cabelli, D. E.; Ramilo, C. A.; Luba, J. P.; Tainer, J. A.; Nick, H. S.; Silverman, D. N., Catalytic and structural effects of amino acid substitution at histidine 30 in human manganese superoxide dismutase: insertion of valine C gamma into the substrate access channel. *Biochemistry* 2003, *42* (10), 2781-9; (c) Ramilo, C. A.; Leveque, V.; Guan, Y.; Lepock, J. R.; Tainer, J. A.; Nick, H. S.; Silverman, D. N., Interrupting the hydrogen bond network at the active site of human manganese superoxide dismutase. *J Biol Chem* 1999, *274* (39), 27711-6.
98. Li, W.; Wang, H.; Wang, Q.; Tan, X., Structural, spectroscopic and functional investigation into Fe-substituted MnSOD from human pathogen Clostridium difficile. *Metallomics* 2014, *6* (8), 1540-8.
99. Sheng, Y.; Butler, G. E.; Schumacher, M.; Cascio, D.; Cabelli, D. E.; Valentine, J. S., Six-coordinate manganese(3+) in catalysis by yeast manganese superoxide dismutase. *Proc Natl Acad Sci USA* 2012, *109* (36), 14314-14319.
100. Hearn, A. S.; Tu, C.; Nick, H. S.; Silverman, D. N., Characterization of the product-inhibited complex in catalysis by human manganese superoxide dismutase. *J Biol Chem* 1999, *274* (35), 24457-60.
101. Carter, P., Spectrophotometric determination of serum iron at the submicrogram level with a new reagent (ferrozine). *Anal Biochem* 1971, *40* (2), 450-8.
102. Lippard, S. J.; Berg, J. M., *Principles of bioinorganic chemistry*. University Science Books: Mill Valley, CA, 1994.
103. Tomter, A. B.; Zoppellaro, G.; Bell, C. B.; Barra, A. L.; Andersen, N. H.; Solomon, E. I., Spectroscopic Studies of the Iron and Manganese Reconstituted Tyrosyl Radical in Bacillus Cereus Ribonucleotide Reductase R2 Protein. *Plos one* 2012, *7* (3), 33436-33447.
104. Miller, A. F.; Sorkin, D. L.; Padmakumar, K., Anion binding properties of reduced and oxidized iron-containing superoxide dismutase reveal no requirement for tyrosine 34. *Biochemistry* 2005, *44* (16), 5969-5981.
105. (a) Blaber, M.; Zhang, X. J.; Matthews, B. W., Structural basis of amino acid alpha helix propensity. *Science* 1993, *260*, 1637 - 1640; (b) Tripet, B.; Wagschal, K.; Lavigne, P.; Mant, C. T.; Hodges, R. S., Effects of side-chain characteristics on stability and oligomerization state of a de novo-designed model coiled-coil: 20 amino acid substitutions in position "d". *J Mol Biol* 2000, *300*, 377-402.
106. Han, W. G.; Lovell, T.; Noodleman, L., Coupled redox potentials in manganese and iron superoxide dismutases from reaction kinetics and density functional/electrostatics calculations. *Inorganic chemistry* 2002, *41* (2), 205-18.
107. Matthew, W. V.; Ohlendorf, D. H., The 1.8 Å crystal structure of catechol 1,2-dioxygenase reveals a novel hydrophobic helical zipper as a subunit linker. *Structure* 2000, *8* (4), 429-440.

108. Sawyer, D. T., and Valentine, J.S., How Super is Superoxide. *Acc. Chem. Res* 1981, 14, 393-400.
109. Maliekal, J.; Karapetian, A.; Vance, C.; Yikilmaz, E.; Wu, Q.; Jackson, T.; Brunold, T. C.; Spiro, T. G.; Miller, A. F., Comparison and contrasts between the active site PKs of Mn-superoxide dismutase and those of Fe-superoxide dismutase. *J Am Chem Soc* 2002, *124* (50), 15064-15075.
110. Narayana, P. A.; Suryanarayana, D.; Kevan, L. J., Electron spin-echo Studies of the Solvation Structure of O2- in water *J. Am. Chem. Soc* 1982, *104*, 3552-3566.
111. Bielski, B. H.; Cabelli, D. E.; Arudi, R. L.; Ross, A. B., Reactivity of HO2/O2-Radicals in Aqueous Solution. *J. Phys. Chem.* 1985, *14*, 1041-1101.
112. Silverman, D. N.; Nick, H. S., Catalytic pathway of manganese superoxide dismutase by direct observation of superoxide. *Methods Enzymol* 2002, *349*, 61-74.
113. Touati, D., The molecular genetics of superoxide dismutase in E. coli. An approach to understanding the biological role and regulation of SODS in relation to other elements of the defence system against oxygen toxicity. *Free Radic Res commun* 1989, *8* (1), 1-9.
114. Viggiani, A.; Siani, L.; Notomista, E.; Birolo, L.; Pucci, P.; Di Donato, A., The role of the conserved residues His-246, His-199, and Tyr-255 in the catalysis of catechol 2,3-dioxygenase from Pseudomonas stutzeri OX1. *J Biol Chem* 2004, *279* (47), 48630-9.
115. (a) Cavadini, P.; Biasiotto, G.; Poli, M.; Varardi, R.; Zanelia, I.; Derosas, M.; Ingrassia, R.; Corrado, M.; Arosio, P., RNA silencing of ABCB7 transporter in Hela cells causes and iron-deficient phenotype with mitochondrial ion overload. *Blood* 2007, *109*, 3552-3560; (b) Duttaroy, A.; Paul, A.; Kundu, M.; Belton, A., A sod2 null mutation confers severely reduced adult life span in Drosophila. *Genetics* 2003, *165*, 2295-2299.
116. Guan, Y.; Hickey, M. J.; Borgstahl, G. E.; Hallewell, R. A.; Lepock, J. R.; O'Connor, D.; Hsieh, Y.; Nick, H. S.; Silverman, D. N.; Tainer, J. A., Crystal structure of Y34F mutant human mitochondrial manganese superoxide dismutase and the functional role of tyrosine 34. *Biochemistry* 1998, *37* (14), 4722-30.
117. Cabelli, D. E.; Guan, Y.; Leveque, V.; Hearn, A. S.; Tainer, J. A.; Nick, H. S.; Silverman, D. N., Role of tryptophan 161 in catalysis by human manganese superoxide dismutase. *Biochemistry* 1999, *38* (36), 11686-92.

**Vita**

Ting Wang

Chemistry Department, Room 106
Chem-physics building
University of Kentucky
Lexington, Kentucky, 40506
twa222@uky.edu

**Research interests**

Protein structure and metalloprotein thermal stability
Interactions between metal ion and protein in metal ion assimilation and reactivity
Energetic of metal ion binding via biophysical characterization in SOD

**Education**

PhD candidate in Chemistry Dept
University of Kentucky, Lexington, KY
Thesis: Role of Gln 146 to the stability and activity of manganese superoxide dismutase.
Advisor: Dr. Anne-Frances Miller

M.Sc in Genetics, Dec 2007.
Wuhan University, Wuhan, Hubei, China
Thesis: The effects about inhibitors of electron transfer chain on the function and expression of related genes of mitochondria in suspension cultures of rice
Advisor: Dr.Yingguo Zhu

B.Sc. in Biological Science, June, 2005.
Hubei University, Wuhan, Hubei, China
Thesis: The growth property of the allopolypoid rice
Advisor: Dr.Detian Cai

**Professional Experience**

As research Assistant:
Fall 2008 – 2015, Department of Chemistry, University of Kentucky, Lexington, KY
Optimization of methods on overexpression and purification of the target protein MnSOD (manganese superoxide dismutases).
Characterization of metalloprotein MnSOD and its mutant Q146E in metal content and corresponding enzymetic activity.
Compare the protein stability of MnSOD and Q146E via finding out the temperature dependence of the secondary structure and metal binding ability of MnSOD and its mutant Q146E.

Introduce a series of amino acid substitutions at position Gln 146 of MnSOD. By characterizing the mutants, explore the function of Gln146 at MnSOD in the redox tuning, enzyme activity, substrate binding and metal content.

**Teaching Experience**

As Teaching Assistant:

General chemistry Lab 1 (CHE 111). Fall 2008, 2013, 2014 & 2015. U. of Kentucky, Lexington, KY.

General chemistry Lab 2 (CHE 113). Fall 2009, Summer 2013 & 2014. U. of Kentucky, Lexington, KY.

Biochemistry Lab (CHE 554). Spring 2010, 2013 & 2014. U. of Kentucky, Lexington, KY.

Analytical chemistry Lab (CHE 226). Spring 2011. U. of Kentucky, Lexington, KY.

**Association Memberships:**

American Chemical Society (ACS)

**Skills:**

Languages: Chinese (native), English (fluent).

Operating system: Windows, Linux (Ubuntun).

Computer languages: Python, MATLAB, C

Biological techniques: Cultivation of plant tissue, extraction of mitochondrion, extraction of DNA, RNA, DNA primer design, clone vector, RT-PCR, SDS-PAGE, Western blot, fluorescence microscope, gene gun, EPR, Elisa, site-directed mutagenesis, Circular Dichroism, chromatograph, enzyme kinetics analysis, ICP-OES.

**Posters:**

Role of Gln146 to the stability and activity of MnSOD, 246$^{th}$ American Chemical Society National Meeting & Exposition, Indianapolis, 2013

Investigation of the Q146E mutant of MnSOD: The differences between Mn-Superoxide Dismutase and its mutant Q146E, 1$^{st}$ South East Enzyme Conference, Atlanta, 2011

The differences between Mn-superoxide Dismutase and its mutant Q146E, 30$^{th}$ Midwest Enzyme Chemistry Conference. Chicago, 2010

Purification of Fe-Superoxide Dismutase and Mn-Superoxide Dismutase from Escherichia coli, 29$^{th}$ Midwest Enzyme Chemistry Conference. Chicago, 2009